

**Water and CO<sub>2</sub> solubilities in rhyolitic to basaltic melts:  
experimental determination and calibration for IR  
spectroscopy**

**Wasser und CO<sub>2</sub> Löslichkeiten in rhyolitischen bis  
basaltischen Schmelzen: experimentelle Bestimmung und  
Kalibration für IR Spektroskopie**

Vom Fachbereich Geowissenschaften und Geographie der Universität Hannover

zur Erlangung des Grades

DOKTOR DER NATURWISSENSCHAFTEN

Dr. rer. Nat.

genehmigte Dissertation

von

**Dipl. Min. Susanne Ohlhorst**

geboren am 15.04.1971 in Braunschweig

**2002**

Referent: Prof. Dr. François Holtz

Korreferenten: Dr. PD Harald Behrens

Dr. Penelope King

Tag der Promotion: 05.06.2002

**TABLE OF CONTENTS**

<i>Danksagung</i>	<hr/>	5
<i>Abstract</i>	<hr/>	6
<i>Zusammenfassung</i>	<hr/>	8
<i>Introduction</i>	<hr/>	11
<b>1</b>	<b><i>Compositional dependence of molar absorptivities of near - infrared OH - and H<sub>2</sub>O bands in rhyolitic to basaltic glasses</i></b>	<b>14</b>
1.1	<b>Introduction</b>	<b>14</b>
1.2	<b>Experimental Techniques</b>	<b>15</b>
1.3	<b>Analytical</b>	<b>16</b>
1.3.1	Karl - Fischer Titration	16
1.3.2	Densities	17
1.3.3	IR spectroscopy	18
1.4	<b>Results and analysis of the IR - spectra</b>	<b>19</b>
1.4.1	Band assignment and peak positions	19
1.4.2	Procedure for baseline correction of the combination bands	21
1.4.3	Determination of molar absorption coefficients	24
1.5	<b>Discussion</b>	<b>27</b>
1.5.1	Compositional dependence of molar absorption coefficients	27
1.5.2	Comparison with data of other authors	28
1.5.3	Comparison of two spectrometer setups	29
1.5.4	Water speciation in glasses	32
<b>2</b>	<b><i>Water and CO<sub>2</sub> solubilities in dacitic melts</i></b>	<b>35</b>
2.1	<b>Introduction</b>	<b>35</b>
2.2	<b>Methodology</b>	<b>36</b>
2.3	<b>Experimental</b>	<b>37</b>
2.3.1	Starting material	37
2.3.2	Solubility experiments	38
2.3.3	Synthesis of standards for the Secondary Ion Mass Spectrometry (SIMS)	38
2.3.4	Experimental apparatus	39
2.4	<b>Analytical</b>	<b>39</b>
2.4.1	Determination of the fluid composition after the experiment	39
2.4.2	Karl - Fischer - Titration (KFT)	40
2.4.3	CO <sub>2</sub> - Titration	41
2.4.4	IR-Spectroscopy	41
2.4.5	Secondary Ion Mass Spectrometry (SIMS)	43
2.4.5.1	Measurement conditions	43

<b>2.5 Results</b>	<b>44</b>
2.5.1 Description of run products and water solubilities	44
2.5.2 NIR spectroscopic determination of water contents	45
2.5.3 MIR spectroscopic investigation of CO <sub>2</sub>	47
2.5.4 Determination of CO <sub>2,total</sub> contents with secondary ion mass spectrometry	49
2.5.4.1 Evolution of the <sup>12</sup> C/ <sup>28</sup> Si ratio with time	49
2.5.4.2 Calculation of the relative sensitivity factor from standard glasses	51
2.5.4.3 Determination of the C content and uncertainty	52
<b>2.6 Discussion</b>	<b>55</b>
2.6.1 Water solubility	55
2.6.1.1 Comparison of water solubilities in the dacitic with a rhyolitic composition	55
2.6.1.2 Empirical water solubility model	55
2.6.2 Speciation of CO <sub>2</sub>	57
2.6.3 CO <sub>2</sub> solubility	61
2.6.3.1 First model	64
2.6.3.2 Second model	67
2.6.3.3 Third model	71
2.6.3.4 Comparison of CO <sub>2</sub> solubilities in the dacitic with a rhyolitic composition	74
<b>2.7 Implication (Degassing)</b>	<b>74</b>
<b>3 The effect of the composition on the water solubility and applications to degassing</b>	<b>76</b>
<b>3.1 Introduction</b>	<b>76</b>
<b>3.2 Experimental and analytical</b>	<b>76</b>
<b>3.3 Results and Discussion</b>	<b>77</b>
3.3.1 Description of run products	77
3.3.2 NIR spectroscopic determination of water contents	78
3.3.3 Water solubilities $x_{H_2O}^{fluid} = 1$	79
3.3.4 Water solubilities $0 \leq x_{H_2O}^{fluid} \leq 1$	80
<b>3.4 Discussion</b>	<b>80</b>
<b>3.5 Implications</b>	<b>83</b>
3.5.1 Pre-eruptive volatile contents	83
3.5.2 Degassing of ascending magma	86
<b>References</b>	<b>89</b>
<b>Appendix: Tables</b>	<b>101</b>
<b>Lebenslauf</b>	<b>109</b>

## DANKSAGUNG

Die vorliegende Arbeit wurde am Institut für Mineralogie der Universität Hannover unter der Leitung von Dr. PD Harald Behrens und Prof. Dr. François Holtz angefertigt. Beiden danke ich für die intensiven Diskussionen, die zahlreichen Anregungen und die Unterstützung besonders in schwierigen Phasen der Arbeit.

Frau Dr. Penelope King danke ich für die Übernahme des Koreferates.

Für die technische Unterstützung geht ein großes Dankeschön an Willi Hurkuck, Bettina, Lars, Manuel, Florian und Christiana. Bei Otto Diedrich bedanke ich mich für die hervorragende Präparation zahlreicher Proben. Danken möchte ich auch Michel Champenois für die technische Betreuung bei den Messungen mit der SIMS in Nancy.

Für die Unterstützung bei Arbeiten an der Gasdruckanlage danke ich besonders Max und Frank. Markus Freise möchte ich für die Hilfe bei Computer-Problemen danken. Dieter Ziegenbein danke ich für seine „Allround“-Hilfe. Jürgen Koepke möchte ich für die Unterstützung an der Mikrosonde danken.

Vanessa Kunde danke ich für die Herstellung einiger wasserhaltiger Gläser.

Ein großer Dank geht an Brigitte Arens-Meyenbörg und Dirk Arens für die emotionale Unterstützung während der Promotion.

Weiterhin danke ich Frank, Max, Achim, Karsten, Marilia, Nathalie, Jürgen, Jens, Matthi, Jasper, Marcus, Astrid, Kevin, Melli, Antje, Lesslie, Antje und Dörte und alle die ich vergessen habe.

Zu guter Letzt möchte ich mich bei meinen Eltern für die Finanzierung meines Studiums sowie die moralische Unterstützung bedanken.

**ABSTRACT**

I have undertaken a series of experiments to understand the incorporation of water and CO<sub>2</sub> in basaltic to rhyodacitic glasses with particular attention to compositions relevant to the Unzen volcano in Japan.

First, molar absorption coefficients (molar absorptivities) of the near infrared combination bands at 4500 and 5200 cm<sup>-1</sup> assigned to OH groups and H<sub>2</sub>O molecules, respectively, were determined for glasses of dacitic, andesitic and basaltic compositions. This work was necessary to determine water contents by IR spectroscopy. Different combinations of baseline types and intensity measure (peak height / area) were applied to investigate the effect of evaluation procedure on infrared spectroscopic determination of apparent species concentrations and total water. The best reproducibility of total water was obtained by modeling the baseline of the combination bands by two gaussians at ~5700 cm<sup>-1</sup> and ~4000 cm<sup>-1</sup> and evaluating peak heights (maximum deviation of ± 0.17 wt.% water). A parabolic equation is proposed to predict the molar linear and integrated absorption coefficients as a function of the SiO<sub>2</sub> content of the glass within the range of water contents used in the calibration. At a given water content and quench rate, OH concentrations are higher in andesitic than in dacitic glasses which is consistent with higher fictive temperatures of hydrous andesitic glasses containing more than 1.5 wt.% water.

Second, water and CO<sub>2</sub> solubilities in a dacitic melt (Unzen volcano, Japan) in equilibrium with H<sub>2</sub>O-CO<sub>2</sub> fluids were determined at 100, 200 and 500 MPa and 1250°C. Molecular CO<sub>2</sub> was determined by MIR spectroscopy, but total CO<sub>2</sub> (carbonate and CO<sub>2,mol</sub>) was determined by SIMS, because the weak carbonate IR bands at 1430 and 1530 cm<sup>-1</sup> could not be reliably separated from background features in the spectra. The ratio of CO<sub>2,mol</sub>/carbonate decreases with increasing water content.

At 100 and 200 MPa, the water solubility changes from a square root dependence on mole fraction of H<sub>2</sub>O in the fluid phase ( $x_{H_2O}^{fluid}$ ) at low  $x_{H_2O}^{fluid}$  to a linear dependence above  $x_{H_2O}^{fluid}=0.2$ . Up to about 6 wt.% dissolved water in the melt (corresponding to  $x_{H_2O}^{fluid} \sim 0.5$ ), a similar trend is observed at 500 MPa. At higher  $x_{H_2O}^{fluid}$  the dependence of the water solubility on  $x_{H_2O}^{fluid}$  is more pronounced. An empirical model was derived to

predict the water solubility in dacitic melts in the pressure range 100 – 500 MPa at 1250°C. The model reproduces our data within  $\pm 0.31$  wt.% water.

At 100-500 MPa, the dependence of CO<sub>2</sub> solubility on  $x_{CO_2}^{fluid}$  shows a positive deviation from linearity. The CO<sub>2</sub> solubility is almost constant at  $x_{H_2O}^{fluid}$  up to 0.2 although  $x_{CO_2}^{fluid}$  is decreasing. This indicates that dissolved water strongly enhances the solubility of CO<sub>2</sub>. The maximum CO<sub>2</sub> solubilities are 795 $\pm$ 41, 1376 $\pm$ 73 and 2949 $\pm$ 166 ppm at 100, 200 and 500 MPa, respectively. I developed two thermodynamic models to describe the dependence of the CO<sub>2</sub> solubility in dacitic melts on the pressure,  $f_{CO_2}^{fluid}$  and the water content in the melt (one assuming that dissolved water stabilizes exclusively carbonate in the melt, one assuming that the CO<sub>2,mol</sub>/carbonate ratio remains constant). Both models reproduce our CO<sub>2</sub> solubility data within  $\pm 14$  % relative.

Third, the effect of the melt composition on the water solubility of basaltic to rhyolitic melts which were equilibrated at 50 to 500 MPa and 1000 to 1250°C with pure water or with mixed H<sub>2</sub>O-CO<sub>2</sub> fluids were investigated. The water solubility increases from the basaltic to the dacitic composition at 50-200 MPa and  $x_{H_2O}^{fluid} = 1$  but decreases from the dacitic to the rhyolitic composition at 50-200 MPa and  $0 \leq x_{H_2O}^{fluid} \leq 1$ . The same trend is observed at 500 MPa and  $x_{H_2O}^{fluid} < 0.8$  for dacitic to rhyolitic melts. However, at 500 MPa and  $x_{H_2O}^{fluid} \geq 0.8$  the water solubility increases from the dacitic to the rhyolitic composition.

The combined H<sub>2</sub>O-CO<sub>2</sub> solubility data obtained in this work were used to model possible degassing paths of the pre-eruptive melt of the Unzen volcano. Both the open and closed system degassing calculation show that at the beginning of degassing CO<sub>2</sub> partitions strongly into the fluid phase, whereas the water content in the melt remains nearly constant. Decompression of a crystal bearing magma with an almost constant water content will lead to decompression melting.

Keywords: water, CO<sub>2</sub>, solubility, dacitic melt , IR spectroscopy

**ZUSAMMENFASSUNG**

Ich habe eine Serie von Experimenten durchgeführt, um den Einbau von Wasser und CO<sub>2</sub> in basaltischen bis rhyodazitischen Gläsern und Schmelzen zu untersuchen. Dabei lag der Schwerpunkt auf Zusammensetzungen, die relevant sind für den Unzen-Vulkan in Japan.

(1) Es wurden molare Absorptionskoeffizienten für die infrarot -OH und -H<sub>2</sub>O Banden bei 4500 und 5200 cm<sup>-1</sup>, in dazitischen, andesitischen und basaltischen Zusammensetzungen bestimmt. Unterschiedliche Kombinationen von Basislinien - Typen und Intensitätsmessungen (Peakhöhe/-fläche) wurden angewendet, um den Effekt der Auswertungsprozedur auf die infrarotspektroskopische Bestimmung von scheinbaren Spezieskonzentrationen und Gesamtwassergehalten zu untersuchen. Die beste Reproduzierbarkeit des Gesamtwassergehaltes wurde erhalten durch Anpassung der Basislinie der Kombinationsbanden durch zwei Gaußfunktionen bei ~5700 cm<sup>-1</sup> und ~4000 cm<sup>-1</sup> und Auswertung der Peakhöhen (maximale Abweichung von ± 0.17 Gew.% Wasser). Zur Vorhersage von molaren und integralen Absorptionskoeffizienten als Funktion vom SiO<sub>2</sub> - Gehalt des Glases wird eine parabolische Gleichung vorgeschlagen. Bei einem gegebenen Wassergehalt und gegebener Abkühlrate sind die OH Konzentrationen in andesitischen Gläsern höher als in dazitischen. Dies ist konsistent mit höheren fiktiven Temperaturen in wasserhaltigen andesitischen Gläsern mit mehr als 1.5 Gew.% Wassergehalt.

(2) Wasser- und CO<sub>2</sub> - Löslichkeiten wurden bei 100 - 500 MPa und 1250°C in dazitischen Schmelzen (Unzen Vulkan, Japan) im Gleichgewicht mit H<sub>2</sub>O-CO<sub>2</sub> - Fluiden bestimmt. Der Gehalt von molarem CO<sub>2</sub> wurde mit IR-Spektroskopie bestimmt, aber der Gesamt - CO<sub>2</sub> - Gehalt mit SIMS (Sekundärionen-Massenspektroskopie), weil die schwachen IR-Carbonatbanden bei 1430 und 1530 cm<sup>-1</sup> nicht zuverlässig vom Untergrund der Spektren separiert werden konnten. Das CO<sub>2,mol</sub>/Carbonat Verhältnis nimmt mit steigendem Wassergehalt ab.

Bei 100 und 200 MPa wechselt die Abhängigkeit der Wasserlöslichkeit vom Molenbruch der Fluidphase ( $x_{H_2O}^{fluid}$ ) von einer exponentiellen Abhängigkeit bei kleinen  $x_{H_2O}^{fluid}$  zu einer linearen Abhängigkeit oberhalb von  $x_{H_2O}^{fluid}=0.2$ . Bis zu ca. 6 Gew.% Wasser in der Schmelze (was einem  $x_{H_2O}^{fluid} \sim 0.5$  entspricht) wurde der gleiche Trend bei



500 MPa beobachtet. Bei größeren  $x_{H_2O}^{fluid}$  ist die Abhängigkeit der Wasserlöslichkeit vom  $x_{H_2O}^{fluid}$  ausgeprägter. Es wurde ein empirisches Modell entwickelt um die Wasserlöslichkeit in dazitischen Schmelzen im Druckbereich von 100-500 MPa und 1250°C vorauszusagen. Das Modell reproduziert unsere Daten mit einem relativen Fehler von  $\pm 14\%$ .

Bei 100 - 500 MPa, zeigt die Abhängigkeit der CO<sub>2</sub> - Löslichkeit vom  $x_{H_2O}^{fluid}$  eine positive Abweichung von einem linearen Kurvenverlauf. Die CO<sub>2</sub> - Löslichkeit ist fast konstant bis zu einem  $x_{H_2O}^{fluid}=0.2$ , obwohl das  $x_{CO_2}^{fluid}$  abnimmt. Dies weist darauf hin, daß gelöstes Wasser die CO<sub>2</sub> - Löslichkeit stark erhöht. Die maximalen CO<sub>2</sub> - Löslichkeiten sind  $795\pm 41$  ppm bei 100 MPa,  $1376\pm 73$  ppm bei 200 MPa und  $2949\pm 166$  ppm bei 500 MPa. Ich habe zwei thermodynamische Modelle entwickelt, mit denen die Abhängigkeit der CO<sub>2</sub> Löslichkeit in dazitischen Schmelzen vom Druck, der CO<sub>2</sub> Fugazität ( $f_{CO_2}^{fluid}$ ) und dem Wassergehalt beschrieben werden können (das eine Modell beruht auf der Annahme, daß der gelöste Wassergehalt ausschließlich das Carbonat in der Schmelze stabilisiert, im zweiten Modell wird angenommen, daß das CO<sub>2,mol</sub>/Carbonat-Verhältnis konstant bleibt). Beide Modelle reproduzieren unsere CO<sub>2</sub>-Löslichkeitsdaten mit einem relativen Fehler von  $\pm 14\%$ .

(3) Es wurde der Effekt der Schmelzzusammensetzung auf die Wasserlöslichkeit in basaltischen bis rhyolitischen Schmelzen, die bei 50 bis 500 MPa und 1000-1250°C mit reinem Wasser oder mit gemischten H<sub>2</sub>O-CO<sub>2</sub> - Fluiden equilibriert wurden, untersucht. Die Wasserlöslichkeit nimmt von der basaltischen zur dazitischen Zusammensetzung bei 50-200 MPa und einem  $x_{H_2O}^{fluid}=1$  zu, nimmt aber von der dazitischen zur rhyolitischen Zusammensetzung bei 50-200 MPa und  $0\leq x_{H_2O}^{fluid}\leq 1$  ab. Derselbe Trend wurde bei 500 MPa und einem  $x_{H_2O}^{fluid}<0,8$  für dazitische bis rhyolitische Schmelzen beobachtet. Bei einem  $x_{H_2O}^{fluid}>0.8$  und 500 MPa steigt jedoch die Wasserlöslichkeit von der dazitischen zu rhyolitischen Zusammensetzung an.

Die kombinierten H<sub>2</sub>O-CO<sub>2</sub> - Löslichkeitsdaten, die in dieser Arbeit gewonnen worden sind, wurden verwendet um mögliche Entgasungspfade der präeruptiven Schmelze des Unzen - Vulkans (Japan) zu modellieren. Die Berechnungen zeigen, daß bei Druckentlastung sowohl im offenen System, als auch im geschlossenen System

zunächst fast ausschließlich CO<sub>2</sub> entgast, während der Wassergehalt in der Schmelze nahezu konstant bleibt. Eine Druckentlastung eines kristallhaltigen Magmas bei fast gleichbleibendem Wassergehalt führt zu einer Aufschmelzung der Kristalle (decompression melting).

Schlagwörter: Wasser, CO<sub>2</sub>, Löslichkeit, dazitische Schmelze, IR-Spektroskopie

## INTRODUCTION

Volatile components such as H<sub>2</sub>O and CO<sub>2</sub> which are dissolved in melts and their degassing processes are of essential importance for the development of volcanic eruptions. For example, three major recent eruptions, Pinatubo (Phillipines) in 1991, Mount St. Helens (USA) in 1980, and Unzen (Japan) in 1990-95, were caused by felsic magmas with chemical compositions similar to each other, including similar concentrations of the volatile components that account for explosive activity (Cashman, 1992; Pallister et al., 1992; Nakada and Motomura, 1999). However styles of eruption among the three are very different. Whereas Pinatubo produced almost only large-scale plinian explosions, Mount St. Helens' eruptions began explosively, but produced more and more dome lavas as the episode progressed (Nakada and Motomura, 1999). Only one explosive eruption, a Vulcanian eruption in June 1991, occurred during the recent activity at Unzen volcano. The eruptive activity of Unzen volcano is characterized by the formation of a dacite dome, associated with frequent pyroclastic flows generated by dome collapse, due to high excess pore gas pressure (Sato et al., 1992). Explosive versus effusive eruption of felsic magma has been explained by a difference of changes in the efficiency of degassing (Jaupart and Allegre, 1991). Explosive eruptions result from rapid ascent of volatile-rich magma (Jaupart and Allegre, 1991). The eruptive style of the Unzen is related to slow ascent rates and an extensive degassing of the magma before the eruption. Degassing processes are directly related to the amount and nature of volatile components which can be dissolved in the magmas during ascent.

The aim of my Ph.D. thesis is to investigate experimentally the evolution of the solubility of mixed H<sub>2</sub>O-CO<sub>2</sub> volatiles during the ascent of magmas on the example of the Unzen volcano in Japan. This work is part of a DFG project in which solubilities of mixed C-H-O-S-Cl fluids are examined (Botcharnikov et al., 2002), and pre-eruptive conditions in the magma chamber are investigated by phase relations and determination of composition of glass inclusions (Holtz et al., revised). The Unzen volcano was selected because it will be investigated by drilling in the frame of the ICDP program (international continental scientific drilling program). The results of our work can be directly compared with the gained insights of the drilling. The most important question about Unzen and similar volcanoes is: How did the hydrous

(volatile bearing) magma degas effectively so that it erupted non-explosively? Among other factors the gas permeability of the wall rock and the conduit size which is necessary to calculate the ascent rate will be explored during drilling (Nakada et al., 2002).

To be able to model the degassing processes, knowledge of solubilities of the volatile species which are released during degassing are of fundamental importance. Until now predominantly solubilities of pure fluids (e.g., H<sub>2</sub>O, CO<sub>2</sub>, S, Cl) have been investigated in silicate melts (e.g., Hamilton et al., 1964; Brey, 1976; Stolper et al., 1987; Fogel and Rutherford, 1990; Pawley et al, 1992; Blank and Brooker, 1994; Carroll and Holloway, 1994; Holtz et al, 1995; Moore et al, 1998; Yamashita, 1999). But in the nature complex mixed fluids exist and solubilities of the pure fluids are only rarely applicable. H<sub>2</sub>O and CO<sub>2</sub> solubilities in melts equilibrated with mixed H<sub>2</sub>O-CO<sub>2</sub> fluids were investigated only in a few studies (e.g.: rhyolitic melts: Tamic et al., 2001; Blank et al, 1993; andesitic melts: King and Holloway, 2002; basaltic melts Dixon et al., 1995).

To my knowledge there are only three models for the prediction of H<sub>2</sub>O-CO<sub>2</sub> solubilities in silicate melts (Holloway and Blank, 1994; Dixon and Stolper, 1995; Papale, 1999). As Tamic et al. (2002) have shown for rhyolitic compositions the model of Holloway and Blank (1994) underestimates the water solubility by 15 % relative at 500 MPa and 800°C. This is probably because this model is based on the water solubility model of Burnham (1979) which underestimates water solubilities at higher pressures (Holtz et al., 1995). The model of Dixon and Stolper is developed only for the basaltic composition and is not applicable to intermediate compositions such as those found at the Unzen volcano. The model of Papale (1999) is based on the largest data set, but data are included which have been reported to be wrong, e.g. water solubility data by Oxtoby and Hamilton (1978a, 1978 b), which have been determined by weight loss method, which underestimates the water solubility at pressures higher than 300 MPa (Holtz et al., 1995), and more than 60 % of the CO<sub>2</sub> solubility database are from Mysen and co-workers (Mysen, 1976; Mysen et al., 1994; Mysen and Virgo 1980a, 1980b) whose results have been criticized by many authors (for example Lange, 1994) as having low accuracy because of the <sup>14</sup>C β-track mapping technique. The applicability of this model to compositions of the Unzen volcano is

doubtful because no (reliable) CO<sub>2</sub> solubility data in intermediate compositions are included in their database.

In this Ph.D. study the solubility of H<sub>2</sub>O and CO<sub>2</sub> in various melt compositions (rhyolitic to basaltic) in equilibrium with mixed H<sub>2</sub>O-CO<sub>2</sub> fluids was investigated in the P-T range 50-500 MPa and 1000-1250°C. The focus was made on the dacitic composition which corresponds to the bulk composition of the volcanic rocks at Unzen volcano. To quantify the water concentration by NIR spectroscopy in glass compositions which are applicable to the Unzen volcano, a new calibration was performed to determine the compositional dependence of molar absorption coefficients for the OH- and H<sub>2</sub>O bands at 4500 and 5200 cm<sup>-1</sup>. On the basis of the new solubility data an empirical model was developed to calculate the water solubility in dacitic melts as a function of the mole fraction of H<sub>2</sub>O in the fluid phase ( $x_{H_2O}^{fluid}$ ) and the pressure. I propose two thermodynamic models to describe the dependence of the CO<sub>2</sub> solubility in dacitic melts on pressure, the CO<sub>2</sub> fugacity ( $f_{CO_2}^{fluid}$ ) and the water content in the melt. The development of such models is of importance to predict the conditions at which magmas start to degas and the evolution of the amount and composition of the fluid release during decompression.

# 1 COMPOSITIONAL DEPENDENCE OF MOLAR ABSORPTIVITIES OF NEAR - INFRARED OH - AND H<sub>2</sub>O BANDS IN RHYOLITIC TO BASALTIC GLASSES

## 1.1 Introduction

In the last decades, infrared (IR) spectroscopy has become a powerful analytical tool to study water in volcanic glasses (e.g., Pandya et al., 1992; Johnson et al., 1994; Dixon et al., 1995; Zhang et al., 1995; Barclay et al., 1996; Jakobsson, 1997; Yamashita et al., 1997; Bureau et al., 1998). Beside the fundamental OH vibration band at 3550 cm<sup>-1</sup> the combination bands at ~4500 cm<sup>-1</sup> and at ~5200 cm<sup>-1</sup> are widely used for water determination in geoscience. The combination bands are not only useful for total water determination, but also allow to distinguish quantitatively between hydrous species (OH - groups and molecular H<sub>2</sub>O). The absorption peak heights of these bands obey the Lambert - Beer law and hence are useful to determine water concentrations in volcanic glasses (e.g., Stolper, 1982; Newman et al., 1986; Silver et al., 1990; Jendrzewski et al., 1996; Withers and Behrens, 1999). The intensities of the combination bands are about two orders of magnitude lower than that of the fundamental OH vibration band. Thus, for a sample thickness in the range of several tenths to hundreds of micrometer the combination bands are suitable to determine water contents in the wt.% range, whereas the fundamental band is more sensitive in the range of several hundreds to thousand ppm water. Quantitative evaluation of the water content from the IR spectra requires the knowledge of the molar absorption coefficients for the IR bands as well as of the density - water content relationship. Both are strongly dependent on anhydrous glass composition (Silver et al., 1990; Behrens et al., 1996). The density of the glass often can be estimated reasonably well (within 1 or 2 %) from its composition using experimental determinations or empirical calculations. The molar absorption coefficients for the combination bands at ~4500 cm<sup>-1</sup> and ~5200 cm<sup>-1</sup>, however, are only known for selected natural compositions (rhyolitic glass: Newman et al., 1986; Ihinger et al., 1994; Zhang et al., 1997; Withers and Behrens, 1999, etc.; dacitic glass: Yamashita et al., 1997; islanditic glass: Jakobsson, 1997; basaltic glass: Dixon et al., 1995; Yamashita et al., 1997) and for limited ranges of water contents. Application of absorption coefficients outside of their experimental calibration range may lead to a high error. For example, the calibration of Zhang et al. (1997) for rhyolitic glasses can be used for total water

## 1. Compositional dependence of molar absorptivities of near-infrared water bands

---

contents in the range of 0.8 - 2.7 wt.%. However, using this calibration for glasses with higher water contents leads to an underestimation of the total water content (Withers and Behrens, 1999). The discrepancy increases with water content and reaches up to 0.55 wt.% at 6.2 wt.% total water.

A systematic variation of the absorption coefficients with composition is difficult to extract from the published data because different evaluation methods, especially in fitting the baseline of the absorption bands, were applied. Thus, the determination of water contents in compositions for which the absorption coefficients have not been specifically calibrated is associated with a high uncertainty.

In this study I present new determinations of molar absorption coefficients for the OH and H<sub>2</sub>O combinations bands at ~4500 and ~5200 cm<sup>-1</sup>, respectively, for hydrous glasses of dacitic, andesitic and basaltic compositions. The data are combined with data of rhyolitic glasses from Withers and Behrens (1999) to illustrate the variation of the absorption coefficients from a basaltic to a rhyolitic composition. Possible applications of my results to natural glasses of intermediate compositions are discussed.

### 1.2 Experimental Techniques

Starting materials were synthetic glasses with compositions close to a dacite of the Unzen Volcano (DC, Chen et al., 1993), a Pre - Unzen andesite (PU, Chen et al., 1993) and an averaged primitive MOR basalt (B1, Berndt, 2002). Homogeneous dry glasses were synthesized by melting oxides and carbonates at 1600°C for more than four hours, grinding and remelting for additional four hours at the same temperature. The compositions measured with the electron microprobe are given in table 1.

The synthesis of hydrous glasses were performed in two different ways:

- a) To obtain large homogeneous glass bodies (200 - 500 mg), water and glass powder were filled in several portions into Pt or Au<sub>80</sub>Pd<sub>20</sub> capsules, which subsequently were welded shut. Syntheses were performed at 1250 - 1350 °C and 500 MPa. The amounts of water initially introduced in the capsules (1.5 - 6.3 wt.%) are lower than the water solubility under these P - T conditions. To reduce loss of iron to the capsule, duration of experiments in Pt - capsules was short (60 min for DC, 30 min for PU). The duration of experiments in Au<sub>80</sub>Pd<sub>20</sub>-capsules was 4 hours.

## 1. Compositional dependence of molar absorptivities of near-infrared water bands

---

b) Small glass samples (20 - 50 mg) were obtained in water solubility experiments by using DC and B1 glass blocks and excess water. Runs were performed at different pressures (50 - 300 MPa), at 1200°C for 15 - 52 hours in Au<sub>80</sub>Pd<sub>20</sub> capsules.

All experiments were performed in internally heated pressure vessels (IHPV) orientated vertically and pressurized with argon. A detailed description of the IHPV used at Hannover is given by Becker et al. (1998). The temperatures were recorded with two thermocouples placed in the vicinity of the samples and the temperature variation along the capsules was always less than 20°C, except for one experiment (DC 77, see table 2). Intrinsic redox conditions during synthesis was close to the MnO-Mn<sub>3</sub>O<sub>4</sub> solid oxygen buffer for water saturated conditions (Berndt, 2002). The oxygen fugacity  $f_{O_2}$  shifts to more reducing conditions at reduced water activities (1 log unit for  $a_{H_2O}^{fluid}=0.3$ , Berndt, 2002). To avoid quench crystals I have used a rapid quench device similar to that described by Berndt et al. (2002). Quench rates of the samples are supposed to be >150 K/s.

### 1.3 Analytical

#### 1.3.1 Karl - Fischer Titration

Water concentrations in the synthesized glasses were determined by pyrolysis and subsequent Karl - Fischer titration (KFT). KFT is based on the quantitative reaction of water with iodine:  $I_2 + SO_2 + H_2O = 2 HI + SO_3$ . The amount of iodine necessary for this reaction is generated electrolytically (coulometric titration):  $2 I^- = I_2 + 2 e^-$ . Samples of 10 - 30 mg were loaded into the sample chamber and flushed by dried argon. Then water was extracted by heating the samples from room temperature to 1100 - 1300°C (typical duration of extraction: 7 - 10 min). Because hydrous glasses sometimes dehydrate explosively, leading to a sputtering of the glass out of the heating zone, the samples were wrapped in platinum foil. The extracted gas is transported by the argon stream through an oxidation furnace, where H<sub>2</sub> is oxidized to H<sub>2</sub>O, into the titration cell (for more details see Behrens et al., 1996). Uncertainties in measured water contents were calculated on the basis of  $\pm 0.02 \mu g s^{-1}$  uncertainty in titration rate (Behrens et al., 1996). After the titration the samples are foamed and compact glass volumes are often very small. Only in one dacitic sample I found glass volumes large enough for IR - microspectroscopic determination of residual water after KFT. Using the peak height of the mid infrared absorption band at  $3550 cm^{-1}$  and



## 1. Compositional dependence of molar absorptivities of near-infrared water bands

---

the calibration of Yamashita et al. (1997), residual water contents of 0.02 wt.% were obtained in two regions of the sample. These values are similar to residual water contents in the rhyodacitic glass (GMS, residual water 0.02 - 0.03 wt.%) but significantly lower than in polymerized samples such as quartzofeldspathic glasses ( $0.10 \pm 0.05$  wt.%, Behrens 1995). Based on these results I suggest that residual water contents in depolymerized glasses are not sensitive on the glass composition and always  $\sim 0.02$  wt.%. All water contents determined in this study were corrected by adding this value to the measured KFT values. I assume that the error in this correction is in the order of the correction itself.

For the a - type glasses two KFT - analyses were performed using fragments from the two opposite ends. The relative difference between the two measured water contents is always  $< 5\%$ . For the b - type glasses only one KFT measurement was made for each sample.

### 1.3.2 Densities

Densities of the a - type products were determined by weighing the single glass pieces in air and in water. For glass pieces of  $>100$  mg the uncertainty in density determination is  $<1\%$ . The densities show a linear relationship with water content (figure 1.1).

Using the density data given in table 2 the following equations were obtained:

$$\rho = -18.4 (\pm 2.0) * c_{\text{water}} + 2661 (\pm 7) \text{ for andesite} \quad (1.1)$$

(standard deviation of  $\rho$ : 6.2 g/l) and

$$\rho = -11.8 (\pm 2.0) * c_{\text{water}} + 2515 (\pm 6) \text{ for dacite} \quad (1.2)$$

(standard deviation of  $\rho$  : 6.6 g/l) ( $\rho$  = density in g/l,  $c_{\text{water}}$  = wt.% water determined by KFT).

Densities of b - type dacitic glasses were calculated using the density - water content relationship given above. Based on data from Yamashita et al (1997, composition #43gm) a density - water content relationship

$$\rho = -20.8 (\pm 6.6) * c_{\text{water}} + 2819 (\pm 13.5) \quad (1.3)$$

(standard deviation of  $\rho$ : 8.8 g/l)

was derived for basaltic glasses for water contents between 0.7 and 3.1 wt.%. I have used this relationship to estimate the density for the basaltic composition used in this study.

## 1. Compositional dependence of molar absorptivities of near-infrared water bands

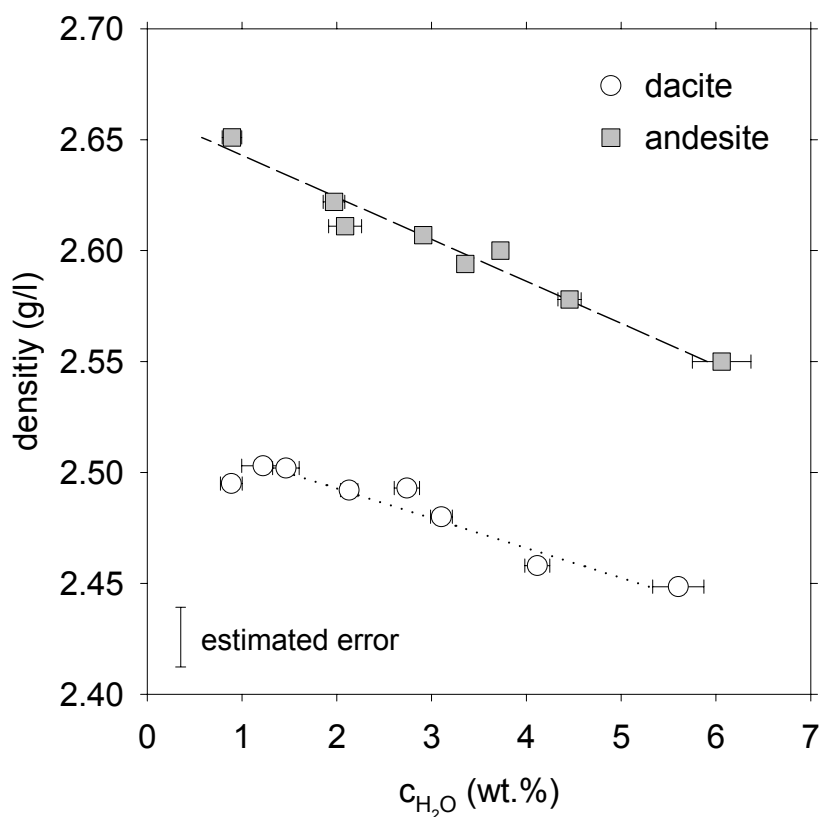


**Figure 1.1:** Density - water content relationships of dacitic and andesitic glasses.

The densities of the dry dacitic (2467 g/l) and andesitic (2600 g/l) glasses which were synthesized at one atmosphere are 2% lower than the dry densities calculated by equations (1.1) and (1.2). This may be explained by an effect of pressure (hydrous glasses are synthesized at high pressure). The calculated density of anhydrous basaltic glass is 1% higher than an experimentally determined value (2782 g/l) for the basaltic starting material. This indicates that the density - water content relationship for basaltic glasses is a good approximation for the basaltic composition used in this study. However, there may be a systematic error of 1 - 2 % in the derived absorption coefficients for the basaltic composition resulting from the uncertainty of the glass density.

### 1.3.3 IR spectroscopy

Doubly polished glass plates of 0.3 - 0.5 mm thickness were prepared for IR analysis. For the large a - type samples slices were cut directly adjacent to the pieces analyzed by KFT. For the b - type samples slices were cut from the center of glass pieces. The thickness of each IR section was measured with a digital micrometer (Mitutoyo; precision  $\leq 2 \mu\text{m}$ ).

## 1. Compositional dependence of molar absorptivities of near-infrared water bands

---

IR spectra were recorded using an IR microscope A590 attached to a FTIR spectrometer Bruker IFS88. Measurement conditions were: tungsten white light source, CaF<sub>2</sub> beamsplitter, cassegranian 15x objective, narrow band HgCdTe detector with NIR equipment (600 - 10000 cm<sup>-1</sup>). The analyzed spot was typically 100 μm in diameter, and the spectra resolution was 4 cm<sup>-1</sup>. For each spectrum 100 scans were accumulated. Because of iron loss to the platinum capsule, only spectra measured in the middle of the sample were used. Errors in peak heights ( $\pm 0.003$  absorbance units for the OH peak and  $\pm 0.002$  for the H<sub>2</sub>O peak) and peak areas ( $\pm 1$  integrated absorbance unit for the OH peak and  $\pm 0.7$  for the H<sub>2</sub>O peak) are based on the reproducibility of intensity measure (repeated measures at different points of the sample).

### 1.4 Results and analysis of the IR - spectra

All the experimental products were crystal and bubble - free glasses. The experimental conditions, the water content determined by KFT, the thickness and density of the samples and the absorbances at  $\sim 4500$  and  $\sim 5200$  cm<sup>-1</sup> are listed in table 2.

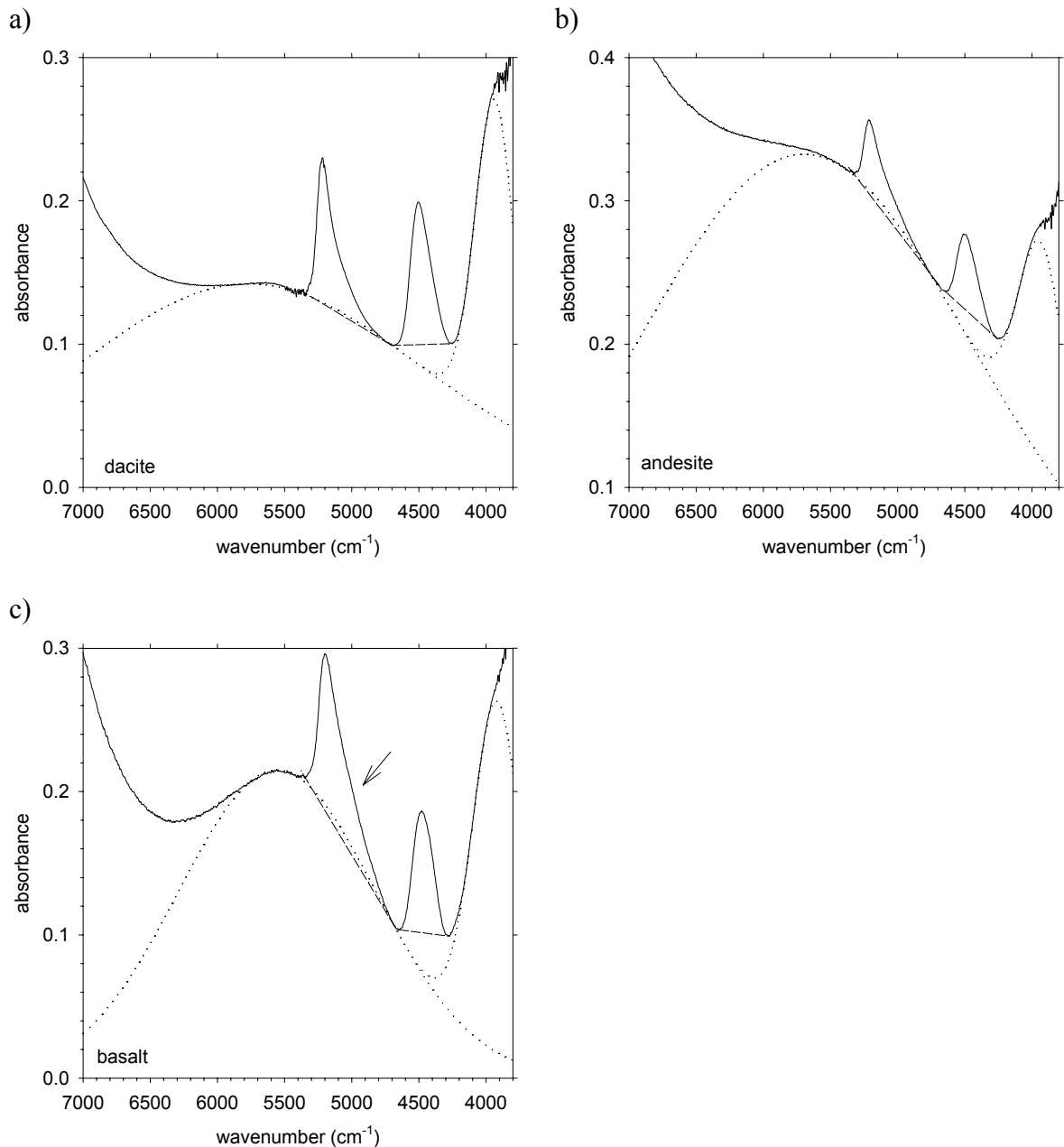
#### 1.4.1 Band assignment and peak positions

Figure 1.2 a, b, c shows typical near - infrared spectra of dacitic, andesitic and basaltic glasses. In the range 3800 - 7000 cm<sup>-1</sup> the spectra display broad intense bands at  $\sim 5700$  cm<sup>-1</sup> and higher wavenumbers which are attributed to crystal field transitions of divalent iron. Moreover, Fe<sup>2+</sup> - Fe<sup>3+</sup> - intervalence charge transfer bands may extend down to the near infrared range. (Rossmann, 1988; Burns, 1993; Dixon et al., 1995). At least three water - related bands at around 4000, 4500 and 5200 cm<sup>-1</sup> are visible in the spectra. The peak at  $\sim 4000$  cm<sup>-1</sup> is an unassigned band related to total water (Stolper, 1982; Withers and Behrens, 1999). The band at 4500 cm<sup>-1</sup> is assigned to the combination of stretching + bending mode of structurally bonded OH and the band at 5200 cm<sup>-1</sup> to the combination of stretching + bending mode of H<sub>2</sub>O molecules (Scholze, 1960, 1966; Bartholomew et al., 1980, Stolper, 1982).

In the range of water contents used in this study the positions of the maxima of the combination bands are independent on total water within analytical error ( $\pm 2$  cm<sup>-1</sup>) for dacitic to basaltic glasses. The maximum of the OH combination band shifts with increasing SiO<sub>2</sub> content from 4471 cm<sup>-1</sup> (basalt) over 4488 cm<sup>-1</sup> (andesite) to 4500 cm<sup>-1</sup> (dacite). The same trend is observed for the H<sub>2</sub>O combination band (basalt:

## 1. Compositional dependence of molar absorptivities of near-infrared water bands

5195  $\text{cm}^{-1}$ , andesite: 5209  $\text{cm}^{-1}$ , dacite: 5218  $\text{cm}^{-1}$ ). The dependence of peak positions on  $\text{SiO}_2$  content is consistent with data for rhyolitic glasses (Withers and Behrens, 1999). However, in the case of the rhyolitic glass the position of the combination bands depends also on total water.



**Figure 1.2 a-c:**

Near infrared spectra of three hydrous glasses (a) DC 58A = dacitic, 3.14 wt.% water, 0.0458 cm thickness (b) PU 73A = andesitic, 3.37 wt.% water, 0.0277 cm thickness (c) B1 23 = basaltic, 4.91 wt.% water, 0.0453 cm thickness. Two types of baselines are used for evaluation of the OH combination band at 4500  $\text{cm}^{-1}$  and the  $\text{H}_2\text{O}$  combination band at 5200  $\text{cm}^{-1}$ . The GG type baseline is composed of two gaussians (dotted lines) fitted under the iron - related band at  $\sim 5700 \text{ cm}^{-1}$  and the water - related band at  $\sim 4000 \text{ cm}^{-1}$ . The TT type baselines (dashed lines) are straight line fits through the minima on both sides of the combination bands (for details of baseline fitting see text).

### ***1.4.2 Procedure for baseline correction of the combination bands***

To determine total water and water speciation from peak heights or peak areas, an appropriate baseline under the 4500 and 5200  $\text{cm}^{-1}$  bands must be defined. I have tested three types of baselines: (1) simple straight lines under the 4500 and 5200  $\text{cm}^{-1}$  bands, (2) combinations of gaussians to account for the effects of the other bands influencing the spectra and (3) a flexicurve (or French curve) technique. The methods are described in detail in the following paragraphs. In analogy to Withers and Behrens (1999) I denoted the methods as TT, GG and FC, respectively. A basic assumption for all types of baselines is that the bands at 4500  $\text{cm}^{-1}$  and 5200  $\text{cm}^{-1}$  do not overlap. As the discrete shape of the near - infrared bands is unknown and the spectra can not be deconvoluted in a set of distinct peaks this assumption is essential for a reproducible evaluation of the spectra.

#### **1) Straight line (TT):**

The easiest baseline correction is to fit simple straight lines to the base of the 4500 and 5200  $\text{cm}^{-1}$  bands (see figure 1.2). In iron - poor systems such as rhyolites, the straight lines are unambiguously defined as tangents through the minima on both sides of each band (Withers and Behrens, 1999). Due to the superimposed iron - related bands in dacitic to basaltic compositions the linear baseline under the  $\text{H}_2\text{O}$  combination band intersects the absorbance curve on the high frequency side at around 5400  $\text{cm}^{-1}$  (figure 1.2).

It is obvious that the TT baseline is a rough approximation and it is likely that the area and height of the OH band is underestimated. Thus, systematic errors of the OH/ $\text{H}_2\text{O}$  ratio might be introduced in the calibration and therefore, the TT method is not recommended to determine species concentrations. On the other hand, fitting of linear baselines leads to a high reproducibility of the determination of total water content (from the peak heights or areas). However, because the shape of superimposed bands is not specifically considered in this baseline correction, it might be expected that the TT calibration is very sensitive to the iron content and the oxidation state of iron. Therefore the determination of water contents in natural samples using the absorption coefficients from the TT calibration in this study is recommended only for samples displaying spectra similar to those presented in figure 1.2.

### 2) Two gaussians (GG):

In a second approach the background of the OH and the H<sub>2</sub>O combination bands is modeled using two gaussians fitted to the iron - related band at  $\sim 5700\text{ cm}^{-1}$  and the water - related band at  $\sim 4000\text{ cm}^{-1}$  (figure 1.2). This method is slightly different from the GG type baseline of Withers and Behrens (1999) for rhyolitic glasses, who fitted only one gaussian to the  $\sim 4000\text{ cm}^{-1}$  band. The baseline correction for the H<sub>2</sub>O combination band was made using a tangent under this band. Because of the very low iron content of the rhyolitic composition of Withers and Behrens (1999), it was not necessary to fit the background by a gaussian in the high frequency range (above  $5200\text{ cm}^{-1}$ ) in this composition. Using the GG type of baseline, water species concentrations derived from IR spectra were shown to be in an excellent agreement with NMR spectroscopic determination for simple alkali-aluminosilicate glasses (Schmidt et al., 2001).

The GG baseline is defined in two steps: first a gaussian is manually fitted to the  $\sim 5700\text{ cm}^{-1}$  band, then the gaussian to the  $\sim 4000\text{ cm}^{-1}$  band is fitted. The  $\sim 5700\text{ cm}^{-1}$  band was fitted using following criteria: (1) punctual overlap of the spectrum with the gaussian curve between the two bands at  $4500\text{ cm}^{-1}$  and  $5200\text{ cm}^{-1}$  and (2) overlap of the spectrum with the gaussian over  $100 - 600\text{ cm}^{-1}$  on the high frequency side of the  $5200\text{ cm}^{-1}$  band (figure 1.2). To fit the gaussian at  $\sim 4000\text{ cm}^{-1}$  I always used the spectral region between  $4000 - 4150\text{ cm}^{-1}$ .

Due to changing measurement conditions as well as to scattering of light in the sample, the background in the spectra typically differs from the zero line of the absorbance axis and varies from spectrum to spectrum. Fitting a gaussian to the iron - related band, however, is very sensitive to the position of the spectrum relative to the zero point of the absorbance axis. For instance if the spectrum is shifted towards higher absorbance the half width of the gaussian will significantly decrease. The subsequent change in the baseline of the combination bands has only a small effect on the band at  $5200\text{ cm}^{-1}$  but a relatively large effect on the band at  $4500\text{ cm}^{-1}$  which apparently increases in both, peak height and peak area. As a constraint for a reproducible fitting procedure, the deepest point of the spectrum (usually on the right side of the  $4500\text{ cm}^{-1}$  band, sometimes left side of this band) was arbitrary moved to 0.2 absorbance units for andesite and to 0.1 absorbance units for dacite and basalt. These are the lowest heights at which the spectra could be fitted adequately by gaussians.

## 1. Compositional dependence of molar absorptivities of near-infrared water bands

---

The second constraint required for a reproducible GG baseline fitting procedure is to fix the position of the gaussians at  $\sim 5700\text{ cm}^{-1}$  and  $\sim 4000\text{ cm}^{-1}$ . The following procedure was used: (1) all spectra were first manually fitted without constraints of the band positions. In doing so the spectra of the andesitic glasses were the most difficult to fit, because the band at  $\sim 5700\text{ cm}^{-1}$  is superimposed by a very intensive second iron - related band at around  $10000\text{ cm}^{-1}$  (Rossmann, 1988; Dixon et al., 1995); (2) in a second step, all the spectra were refitted using a constant position for the maxima of the bands at  $\sim 4000$  and  $\sim 5700\text{ cm}^{-1}$  as a constraint. The position of each band was chosen so that all spectra of a given bulk composition could be adequately fitted. The positions of the maxima that were used are:  $5770$  and  $3937\text{ cm}^{-1}$  for dacite,  $5700$  and  $3931\text{ cm}^{-1}$  for andesite and  $5556$  and  $3917\text{ cm}^{-1}$  for basalt.

### 3) Flexicurve (FC):

Another method which has been widely used to fit a curved baseline is the flexicurve technique (Stolper, 1982; Newman et al., 1986; Silver et al., 1990; Zhang et al., 1997). I have tested this baseline fitting technique for several samples. Most of the baseline corrected spectra were similar for FC type baseline and GG type baseline. Because a major problem is to define unambiguously the FC baseline below the  $4500\text{ cm}^{-1}$  band, I performed no independent calibration for this baseline.

Another approach for baseline correction is to subtract the spectrum of an anhydrous glass of the same composition to the sample. This method has been successfully used for deconvolution of mid IR bands (Behrens and Schmidt, 1998). However, the positions and relative intensities of the iron - related bands may be strongly dependent on synthesis conditions, i.e. the oxygen fugacity and the water content. For instance in the spectrum of the anhydrous dacitic glass no discrete absorption band at  $\sim 5700\text{ cm}^{-1}$  is resolved, and if spectra are normalized to the same thickness the iron - related absorbance in the NIR region is much higher in the anhydrous glass than in the hydrous glasses. Thus, subtracting the spectrum of the anhydrous to the hydrous dacitic glass shown in figure 1.2a overcompensates the effect of iron. Even in iron free glasses an anhydrous spectrum alone cannot adequately describe the baseline of the combination bands, because the baseline for the  $4500\text{ cm}^{-1}$  band (and, to some extent, the  $5200\text{ cm}^{-1}$  band) contains components of the water - related bands at  $4000$  and  $3550\text{ cm}^{-1}$ .

### 1.4.3 Determination of molar absorption coefficients

The concentration of OH and H<sub>2</sub>O can be determined from the intensities of the NIR absorption bands by using the Lambert - Beer law:

$$c_{H_2O} = \frac{1802 \cdot A_{H_2O}}{d \cdot \rho} \cdot \frac{1}{\varepsilon_{H_2O}} \quad (1.4)$$

$$c_{OH} = \frac{1802 \cdot A_{OH}}{d \cdot \rho} \cdot \frac{1}{\varepsilon_{OH}} \quad (1.5)$$

were A denotes the absorbance (peak height), d the thickness in cm, ρ the density in g/l, ε the linear molar absorption coefficient in l mol<sup>-1</sup> cm<sup>-1</sup> and c<sub>OH</sub> and c<sub>H<sub>2</sub>O</sub> the concentrations of OH groups and molecular H<sub>2</sub>O, respectively in wt.%. If peak areas are used instead of absorbances, A is replaced by A\* (integrated intensity in cm<sup>-1</sup>) and ε by ε\* (integral molar absorption coefficient in l mol<sup>-1</sup> cm<sup>-2</sup>). All absorption coefficients are given in terms of mole H<sub>2</sub>O component in this study.

If no other water species are present besides OH and H<sub>2</sub>O the concentration of total water (c<sub>water</sub>) is given as

$$c_{water} = c_{H_2O} + c_{OH} \quad (1.6)$$

Inserting equations (1.4) and (5) in equation (1.6) and rearrangement gives

$$\left[ \frac{1802 \cdot A_{H_2O}}{d \cdot \rho \cdot c_{water}} \right] = \varepsilon_{H_2O} - \frac{\varepsilon_{H_2O}}{\varepsilon_{OH}} \cdot \left[ \frac{1802 \cdot A_{OH}}{d \cdot \rho \cdot c_{water}} \right] \quad (1.7)$$

This equation can be used for determination of the molar absorption coefficients. Plotting the normalized absorbances (given in parenthesis in equation (1.7)) against each other, a straight line will be obtained provided the absorption coefficients are independent on total water and quench rate. In this case the absorption coefficients can be directly determined from the intercepts of the line with both axes.

As shown recently for simple alkalialuminosilicate glasses (Schmidt et al., 2001) the assumption of concentration independent absorption coefficients is in excellent agreement with results of low temperature static <sup>1</sup>H NMR measurements at least for water contents > 1.5 wt.%. However, at low water contents there may be a compositional dependence of the absorption coefficients as indicated by the IR spectroscopic study of Zhang et al. (1997) on rhyolitic glasses.

Normalized absorbances and normalized integrated intensities are plotted in figure 1.3. The scatter of the data is generally larger in plots of normalized integrated intensities,



# 1. Compositional dependence of molar absorptivities of near-infrared water bands

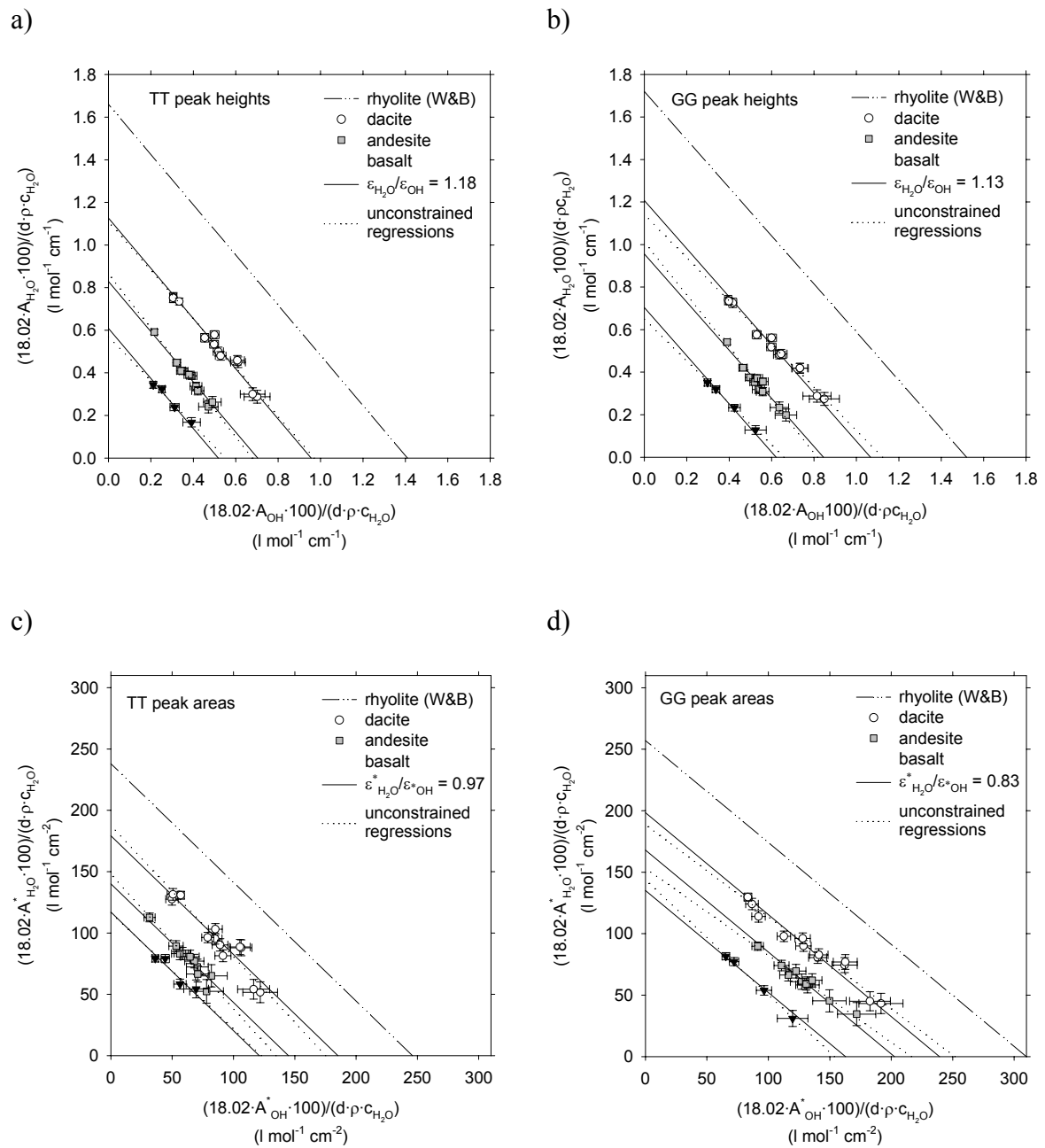


**Figure 1.3 a-d:**

Normalized absorbances of the OH - and H<sub>2</sub>O - bands for basaltic to rhyolitic glasses using TT (Figs. 3 a + c) and GG type (Figs. 3 b + d) baselines. Dashed dotted lines correspond to data for rhyolitic glasses from Withers and Behrens (1999). Solid lines are linear regressions assuming a constant  $\epsilon_{H_2O} / \epsilon_{OH}$  for all glasses. Dotted lines are unconstrained regressions. The molar absorption coefficients for H<sub>2</sub>O and OH are given by the intercepts on the y and x - axes, respectively. For details see text.

## 1. Compositional dependence of molar absorptivities of near-infrared water bands

---

especially at low total water contents. This is a direct consequence of the lower precision in measuring peak areas as compared to measuring peak heights. The highest reproducibility of the total water content is obtained with the GG / peak height combination (maximum deviation  $\pm 0.17$  wt.% water) and, therefore, I recommend this method for total water determination.

As the precision of the TT / peak height method is also high in terms of total water (maximum deviation  $\pm 0.19$  wt.% water) this method may be a useful alternative for rapid evaluation of spectra displaying similar iron - related absorption features as shown in figure 1.2 without complicated baseline fitting procedure.

For both types of baselines (TT and GG) and for both evaluation methods of the absorption (A and A\*) the data obtained for the dacitic, andesitic and basaltic glasses are aligned on straight lines which are almost parallel to the lines defined by the absorption coefficients of rhyolitic glasses (Withers and Behrens, 1999; figure 1.3). There is no indication for a dependence of absorption coefficients on the total water content. Molar absorption coefficients of dacite, andesite and basalt were determined by weighted linear regressions of each data set. These linear regressions were made without constraints as well as with the assumption that the ratio of the absorption coefficients is identical to that determined by Withers and Behrens (1999) for rhyolitic glasses (GG:  $\epsilon_{\text{H}_2\text{O}}/\epsilon_{\text{OH}} = 1.13$ ,  $\epsilon^*_{\text{H}_2\text{O}}/\epsilon^*_{\text{OH}} = 0.83$ ; TT:  $\epsilon_{\text{H}_2\text{O}}/\epsilon_{\text{OH}} = 1.18$ ,  $\epsilon^*_{\text{H}_2\text{O}}/\epsilon^*_{\text{OH}} = 0.97$ ). In both cases the normalized data are reproduced within experimental error by the fitted lines. I have chosen the rhyolitic composition as reference, because this composition has a very low iron content, so that the error in fitting the iron - related bands is small.

The  $\epsilon$  values obtained from linear regression are listed in table 3. The mean deviation of total water determined by IR and KFT is  $\leq 0.06$  wt.% for all baseline / intensity measure combinations except TT / peak areas (0.09 wt.%). The deviation is only slightly higher assuming constant  $\epsilon_{\text{H}_2\text{O}}/\epsilon_{\text{OH}}$  ratios (0.060 - 0.065 wt.%) than using an unconstrained linear regression (0.046 - 0.057 wt.%). In both cases the mean deviation between KFT and IR data is significantly smaller than the mean error of KFT ( $\pm 0.11$  wt.%). The unconstrained linear regression does not significantly improve the reproducibility of total water contents. Thus, the calibration using a constant  $\epsilon_{\text{H}_2\text{O}}/\epsilon_{\text{OH}}$  ratio is preferred, which allows the compositional dependence of the absorption coefficients to be modeled in a simple way.

## 1. Compositional dependence of molar absorptivities of near-infrared water bands

---

Using the GG / peak area fitting procedure, which is recommended for species determination (see below), the differences in species concentrations ( $c_{\text{OH}}$  and  $c_{\text{H}_2\text{O}}$ ) between the two regression lines (with and without fixed  $\varepsilon_{\text{H}_2\text{O}}/\varepsilon_{\text{OH}}$ ) are less than 5.3 %, 9.8 % and 5.8 % relative for dacitic, andesitic and basaltic compositions, respectively. As long as I do not have independent information about species concentrations in these types of glasses (e.g. from NMR spectroscopy) it is difficult to favor one of the two regression methods.

### 1.5 Discussion

#### 1.5.1 Compositional dependence of molar absorption coefficients

The  $\varepsilon$  values systematically increase from basaltic over andesitic to dacitic and rhyolitic compositions. Previous studies have shown that the absorption coefficients of the OH and H<sub>2</sub>O combination bands in silicate glasses might depend on various compositional parameters, e.g. SiO<sub>2</sub> content, the ratio of Na/K, the excess of alkali to aluminum or the concentration of alkaline earth elements (e.g., Stolper, 1982; Silver et al., 1990; Behrens et al., 1996). In complex multicomponent natural systems ranging from rhyolite to basalt a direct correlation between the absorption coefficients and the anhydrous composition is almost impossible. Because the SiO<sub>2</sub> content is often used as a differentiation index, I have used SiO<sub>2</sub> as a proxy to describe the compositional dependence of the absorption coefficients from rhyolitic to basaltic glasses (figure 1.4). My data are well reproduced by a simple parabolic equation

$$\varepsilon = a + b x^2 \quad (1.8)$$

with  $x = \text{wt.}\% \text{ SiO}_2$ . However, a straight line would also be suitable to describe the compositional dependence within experimental error.

Two sets of parameters  $a$  and  $b$  for  $\varepsilon_{\text{OH}}$ ,  $\varepsilon_{\text{OH}}^*$ ,  $\varepsilon_{\text{H}_2\text{O}}$  and  $\varepsilon_{\text{H}_2\text{O}}^*$  are given in table 4. The two sets result from the different procedures used to define the baselines of the spectra (TT and GG). Equation (1.8) allows to predict absorption coefficients for glasses of intermediate compositions such as rhyodacite. However, if the chemical compositions of the glasses of interest deviate strongly from the compositions used in the calibration, extrapolation or interpolation may be very uncertain. It is emphasized that if the constant value  $\varepsilon_{\text{H}_2\text{O}}/\varepsilon_{\text{OH}}$  holds for intermediate compositions, a single experiment

## 1. Compositional dependence of molar absorptivities of near-infrared water bands

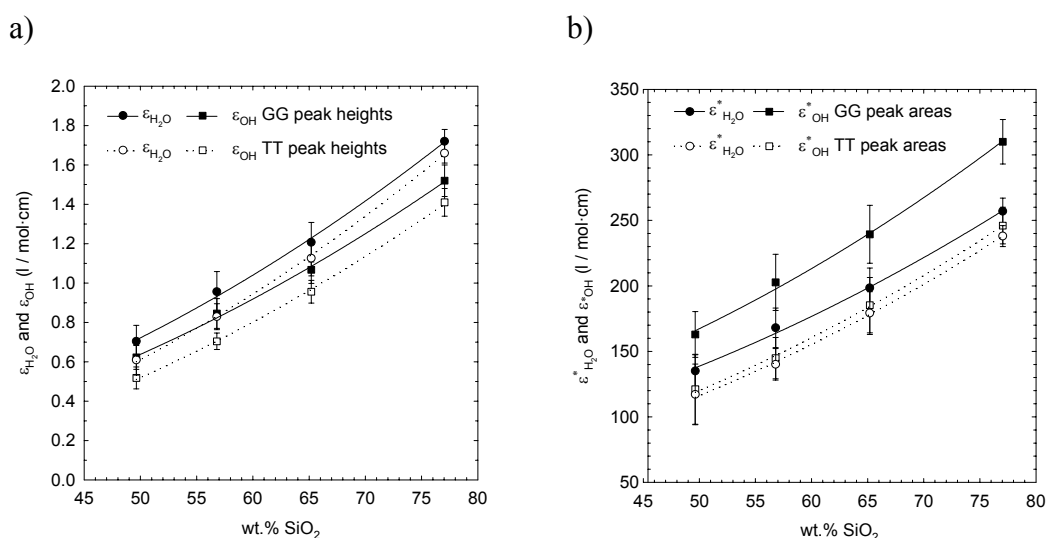


**Figure 1.4 a+b:**

Compositional dependence of molar linear (Fig 1.4 a) and integral (Fig 1.4 b) absorption coefficients for molecular H<sub>2</sub>O (5200 cm<sup>-1</sup> band) and OH groups (4500 cm<sup>-1</sup> band). Lines are fitted using an equation  $\epsilon = a + b x^2$ , with  $x = \text{wt. \% SiO}_2$ . Parameters  $a$  and  $b$  for different baseline / intensity measure combinations are given in Table 4.

may be sufficient to determine the absorption coefficients for the combination bands, which considerably reduces the work of calibration.

### 1.5.2 Comparison with data of other authors

Our absorption coefficients for basalt (GG, peak heights) are identical within errors to those from Dixon et al. (1995), see table 3. Dixon et al. (1995) corrected their spectra with 3 gaussians with maxima at  $\sim 4000$ ,  $5500$  and  $9500$  cm<sup>-1</sup> and two gaussians to fit the high - energy shoulder of the  $3530$  cm<sup>-1</sup> absorption band. The good agreement between the data of Dixon et al. (1995) and my study suggests that additional fits of the bands at  $3550$  and  $\sim 10000$  cm<sup>-1</sup> to characterize the baseline do not have a noticeable effect on the baseline - corrected OH and H<sub>2</sub>O bands. Therefore, fitting two gaussians (our study) instead of five (Dixon et al., 1995) might be sufficient to define the intensity of the baseline corrected OH and H<sub>2</sub>O bands. It is emphasized that the composition used by Dixon et al. (1995) differs slightly in FeO, MgO, Al<sub>2</sub>O<sub>3</sub> and TiO<sub>2</sub> contents (differences of 3.8, 3.1, 2.4 and 0.9 wt.%, respectively) when compared to composition B1. Thus, the identical absorption coefficients found in both studies may result from a fortuitous combined effect of the difference in fitting procedure and in anhydrous composition. On the other hand, it may also indicate that small variations in basaltic compositions do not affect the molar absorption coefficients. The latter

## 1. Compositional dependence of molar absorptivities of near-infrared water bands

---

interpretation is supported by results of Yamashita et al. (1997) who found no difference in molar absorptivity between a high - Al and a tholeiite basalt (note however that the  $\epsilon$  values differ from those in my study due to different fitting procedures, see below).

Yamashita et al. (1997) have published  $\epsilon$  values for a dacite and basalts (table 3). The  $\epsilon_{\text{H}_2\text{O}}/\epsilon_{\text{OH}}$  of the dacite composition differs strongly from my data, which may in part be due to the small range of water contents (1.4 - 3.0 wt.%) and therefore small range of H<sub>2</sub>O/OH ratios used by Yamashita et al. (1997; see table 3). The  $\epsilon$  values for basalt determined by Yamashita et al. (1997) are significantly higher than those of Dixon et al. (1995) and my study, whereas the  $\epsilon_{\text{H}_2\text{O}}/\epsilon_{\text{OH}}$  ratios are similar in the three studies. Yamashita et al. (1997) explain the difference to Dixon et al. (1995) by a substantial compositional dependence of  $\epsilon$  values of the OH and H<sub>2</sub>O bands. To determine the baseline below the OH and H<sub>2</sub>O bands, Yamashita et al. (1997) fitted the bands at  $\sim 5700 \text{ cm}^{-1}$  and  $\sim 10000 \text{ cm}^{-1}$  with two gaussians. However, the contribution of the water - related band at  $\sim 4000 \text{ cm}^{-1}$  was not taken into account, which has strong consequences on the estimation of the  $4500 \text{ cm}^{-1}$  peak intensity (see figure 1.2). Because of the different fitting procedures, it is possible that the strong compositional dependence of  $\epsilon$  value in basaltic glasses suggested by Yamashita et al. (1997) has to be reconsidered. The different fitting procedures may also explain in part the deviation in  $\epsilon$  values observed for the dacite composition.

### ***1.5.3 Comparison of two spectrometer setups***

In the course of this study, the spectrometer setup has been modified: the microscope with a new objective, a condenser lens instead of a mirror, a slit aperture instead of an aperture hole and a new HgCdTe detector with a better signal/noise ratio has been replaced. In addition a new CaF<sub>2</sub> beamsplitter is used. Thus, the whole optical path changed.

Using the absorption coefficients for the dacitic composition given in table 3 the measured water contents are apparently 2 - 10 % relatively higher, than water contents determined by KFT. Absorption coefficients are different for samples measured with the new spectrometer setup (see chapter 2.5.2 for the new calibration). To illustrate this effect the absorbances of the OH and the H<sub>2</sub>O band normalized for peak height, density and water content are shown in figure 1.5. The discrepancy is higher for lower

## 1. Compositional dependence of molar absorptivities of near-infrared water bands

water contents which can be attributed to a higher error on the OH band (the OH/H<sub>2</sub>O ratio in glasses increases with decreasing water content).

Most of the samples measured with the new spectrometer setup are different from those measured with the old spectrometer setup: (1) they are CO<sub>2</sub> bearing, (2) have a slightly different bulk composition (compare DC and DC2 in table 1) and (3) have been synthesized in another IHPV, which might have a slightly different intrinsic oxygen fugacity (these samples are listed in table 6). However, these variations can not explain the discrepancy between the datasets obtained with the two spectrometer setups.

(1) No systematic variation of the discrepancy between water contents measured using KFT and IR with the CO<sub>2</sub> content was observed. CO<sub>2</sub> can have an effect on the density of the glass. The density of CO<sub>2</sub> bearing glasses is expected to be lower than the density of CO<sub>2</sub> free glasses (see also chapter 2.5.2). The density calculation base on measurements of CO<sub>2</sub> free water bearing samples. The effect of an apparently higher

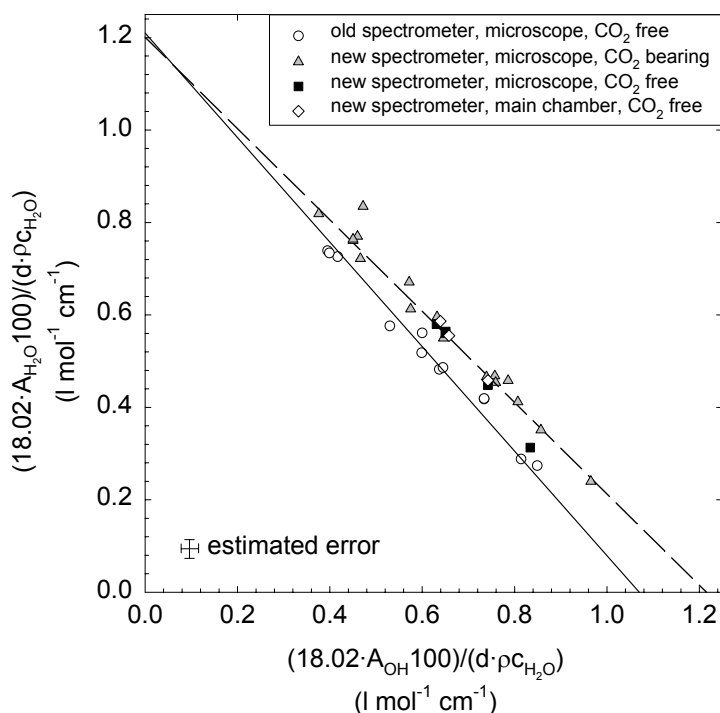


**Figure 1.5:**

Normalized absorbances of the OH and H<sub>2</sub>O bands for dacitic glasses using the GG type baselines, measured with two different spectrometer setups (see text for more detail).

The solid line is a linear regression (constant  $\epsilon_{\text{H}_2\text{O}}/\epsilon_{\text{OH}}$ ) for dacites measured with the old spectrometer (compare figure 1.3b). The dashed line is a linear regression for CO<sub>2</sub> bearing dacites measured with the new spectrometer setup.

## 1. Compositional dependence of molar absorptivities of near-infrared water bands

---

density would lead to a calculation of lower water contents in the sample. Hence, this cannot be an explanation for the deviation.

(2) It is unlikely, that the deviation is due to the changes in the bulk composition, because for a glass with a lower SiO<sub>2</sub> content than the composition for which the absorption coefficients have been calibrated, I would expect to obtain apparently lower water contents (3% relative, calculated after equation 1.8).

(3) Changes of the oxygen fugacity would have an effect on the speciation of iron. That would lead to changes in the background features in the range of 5500 cm<sup>-1</sup> and higher wavelength. But there are no systematic variations in the iron related NIR bands between the samples analyzed with the old and the new spectrometer setup.

To check if the deviation in apparent water contents is due to the spectrometer setup or due to the composition of the glasses, samples used for the calibration (samples DC55 - DC58, see table 2) were remeasured with the new spectrometer setup. These samples show higher normalized absorbances too, which results in apparently 4-7 % relatively higher water contents when evaluated with the absorption coefficients given in table 3.

Therefore, I assume that the deviation in the calculated water content must be due to changes of the optical path of the spectrometer. Behrens et al. (1996) also observed that spectra of the same sample collected by four different FTIR micro spectrometers vary by up to 10% relative in peak intensities. They explained these deviations by different specific measurement conditions such as the magnification of the objectives, spectral ranges of the system (due to different beamsplitters) and characteristics of the detectors. They mentioned that an unambiguous explanation of the differences is not possible due to the complexity of FTIR spectroscopy.

Behrens et al. (1996) stated, that the band intensities measured in the main chamber of the spectrometer and with the IR microscope attached to this spectrometer (old spectrometer setup) agreed within error. Measurements of samples DC56 to DC58 in the main chamber of the new spectrometer show within error the same absorbances when measured in the main chamber or with the microscope (new spectrometer setup). These results confirm the statement of Behrens et al. (1996). This implies, that the variation of the absorption coefficients are not due to the replaced microscope, but due to the new beamsplitter (or due to an enhanced formation of dust, which appeared

during the changes of the spectrometers because of construction works. Dust can change the dispersion of the IR radiation in the optical path of the spectrometer).

In order to reduce the uncertainty in determination of water species and total water content by FTIR spectroscopy a calibration of spectrometers against a reference system should be performed. If the setup of the spectrometer is changed, the calibration must be checked with standards.

### ***1.5.4 Water speciation in glasses***

We suggest that the GG baseline is more suitable to determine species concentrations than the TT baseline, because superimposition of bands resulting in a curved baseline is taken into account. Using the TT baseline the OH species concentrations are lower by 5 to 34 % relative for peak height and 9 to 51 % for peak area evaluation, when compared to the GG baseline.

In figure 1.6 concentrations of OH and H<sub>2</sub>O calculated using the GG baseline fitting procedure are plotted against the total water content. For dacite and andesite the species concentrations are identical within error if peak heights and peak areas are used. For the glasses of basaltic composition the evaluation of peak heights leads to a significantly higher apparent concentration of OH groups at a given total water content when compared to the evaluation of peak areas (e.g., the apparent concentration of OH groups in basalt is 19.3 % higher for peak heights when compared to peak areas, at 6.3 wt.% total water content). This discrepancy may have different causes. (1) The shape of the 5200 cm<sup>-1</sup> band is slightly different in basaltic composition than in rhyolitic to andesitic compositions. There seems to be a higher contribution of the low frequency part in the H<sub>2</sub>O band compared to the other compositions (see arrow in figure 1.2 c). Therefore, at a given total water content of the glass the relative proportion of H<sub>2</sub>O is lower if it is determined using peak heights rather than using peak areas. (2) The baseline is only an approach to separate the combination bands from other bands in the near infrared region. Depending on water content and relative intensities of the iron - related bands this approach may have systematic deviations to the “true” baseline. Such a misfit will not only affect the determination of peak height and peak areas (see above, chapter 1.4.2) but also the whole calibration and the resulting species concentrations. It is interesting to note that Withers and Behrens (1999) found an opposite effect for the rhyolitic composition. Using the GG type



## 1. Compositional dependence of molar absorptivities of near-infrared water bands

baseline the OH concentrations are up to 10% relative larger if peak areas are evaluated instead of peak heights.

Because the coefficients of determination ( $r^2$ ) are similar for the linear regressions of GG / peak height and GG / peak area data and because the species concentration is not known from an independent method it is difficult to recommend one method over the other. As the band shape varies with temperature and species concentrations (Withers and Behrens, 1999) it can be argued that peak areas provide a better description of the band intensity than peak heights since changes over the entire band width are considered. This is supported by NMR measurements on hydrous alkali-aluminosilicate glasses by Schmidt et al. (2001). Water species concentrations derived from static NMR spectra measured at temperatures low enough to freeze out the rotation of H<sub>2</sub>O molecules were found to be in better agreement with IR data if peak areas are evaluated than if peak heights are evaluated. However, this result may be not directly transferable to complex natural glasses.

The interpretation of the water speciations in figure 1.6 requires the fictive temperatures  $T_f$  of the glasses to be known.  $T_f$  is the temperature at which the

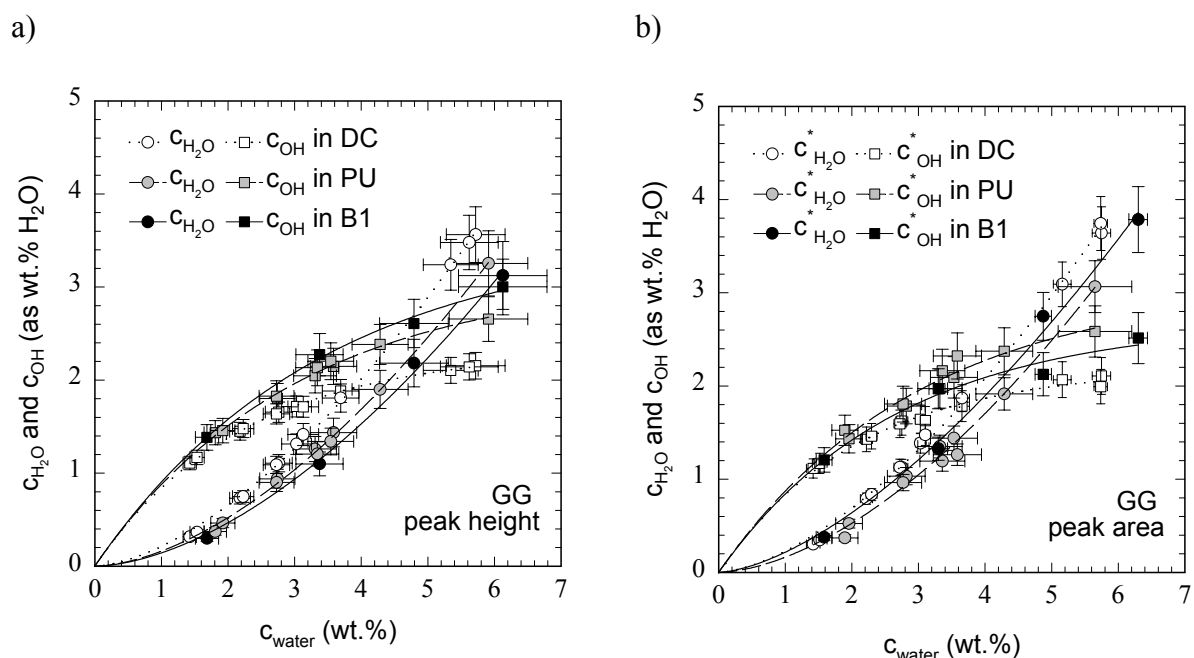


**Figure 1.6 a+b:**

Measured concentrations of H<sub>2</sub>O and OH (expressed as H<sub>2</sub>O) versus total water content in dacitic (DC), andesitic (PU) and basaltic (B1) glasses determined using the GG type baseline. Fig. 6 a: evaluation of peak height, Fig. 6 b: evaluation of peak area. Note that species concentrations are identical for evaluation from heights and areas in the cases of dacitic and andesitic glasses, but are different in the case of basaltic glasses (for details see text).

## 1. Compositional dependence of molar absorptivities of near-infrared water bands

---

quenched - in structure of the glass corresponds to the melt structure at equilibrium. This temperature is dependent on the quench - rate, the anhydrous composition, and the water content of the melt (Dingwell and Webb, 1990; Romano et al., 1995). The quenched - in temperatures are not well known for my samples as well as for those from most other IR spectroscopic studies. It is therefore difficult to compare the data sets on water speciation.

Nevertheless, some systematic effects are evident comparing my speciation data and those for rhyolitic glasses from Withers and Behrens (1999). In two of their experiments Withers and Behrens (1999) have used a rapid - quench device and the quench rates are assumed to be similar to those applied in my study. The OH concentrations of 1.64 and 2.13 wt.% recalculated from their data for rhyolitic glasses with 3.19 wt.% and 5.08 wt.% water, respectively, are close to my data for dacitic glasses. Thus, at high water content, the OH concentration in glasses obtained from rapid quench experiments decreases from andesitic to dacitic / rhyolitic melts (compare curves for andesite and dacite in figure 1.6). This trend is in general accordance with viscosity determinations for andesitic and rhyolitic compositions (Richet et al., 1996; Hess and Dingwell, 1996). The viscosity data indicate that the glass transition temperature  $T_g$  which is close to the fictive temperature is higher in dry rhyolite than in dry andesite. The opposite effect is observed for hydrous compositions containing more than 1.5 wt.% water. Because the water content in all investigated samples (this study and Withers and Behrens, 1999) is higher than 1.5 wt.%,  $T_g$  is expected to be lower in the rhyolitic samples than in the andesitic samples at a given water content. In situ determinations in hydrous aluminosilicate compositions have shown that the OH/H<sub>2</sub>O ratio increases with temperature (Shen and Keppler, 1995; Nowak and Behrens, 1995). Thus, the observed higher OH concentrations in andesitic glasses than in the rhyolitic glasses are consistent with higher fictive temperatures in the former ones. The trend of water speciation from andesitic to basaltic glasses is difficult to rationalize because of the discrepancy in water speciation between peak height and peak area evaluation and because of the so far unknown viscosity - water content relationship of basaltic glasses. Direct conclusions on relative stability of water species in melts of different anhydrous compositions are not possible on the basis of my experiments.

## 2 WATER AND CO<sub>2</sub> SOLUBILITIES IN DACITIC MELTS

### 2.1 Introduction

Volatiles (especially water) dissolved in silicate melts dramatically influence the chemical and physical properties of magmas. Because of its high solubility in silicate melts, water is of particular interest for understanding properties of magmas. Whereas water solubilities in rhyolitic melts coexisting with pure water fluid have been investigated by several authors in the last decades using different techniques (see Ihinger et al., 1994; Zhang, 1999; Kohn, 2000; Behrens and Jantos, 2001; Holtz et al., 2001), water solubility in more depolymerized natural melts are poorly known and water solubilities in dacitic melts have not been investigated so far.

CO<sub>2</sub> is the second most abundant volatile in natural magmas. Although the CO<sub>2</sub> is usually subordinate in concentration, it is often the first component to reach saturation due to its low solubility in the melt. Even small amounts of dissolved CO<sub>2</sub> in water bearing melts shift the fluid saturation limit to higher pressures and thus greater depth (Holloway, 1976). Because vesiculation initiated by exsolution of CO<sub>2</sub> from the melt is the driving force in many eruptive situations, it is important to investigate the saturation limit of fluids in the system C-H-O.

Raman-, NMR-, and IR measurements have shown that both H<sub>2</sub>O and CO<sub>2</sub> are dissolved in silicate glasses and melts in form of at least two different species, an unreacted molecular species (H<sub>2</sub>O and CO<sub>2</sub> molecules) and a species formed by reaction between molecular species and the silicate solvent (hydroxyl and carbonate groups). Whereas water speciation in glasses depends mainly on the total water content but only weakly on anhydrous composition (Silver et al., 1990; Behrens et al. 1996), the speciation of CO<sub>2</sub> is independent on total CO<sub>2</sub> concentration but varies strongly with anhydrous composition of the glass (Fine and Stolper, 1985; Blank and Brooker, 1994; Brooker et al., 2001). In highly polymerized rhyolitic glasses CO<sub>2</sub> is incorporated exclusively as molecular CO<sub>2</sub> (e.g., Tamic et al., 2001), whereas only carbonate is present in depolymerized basaltic glasses (Blank and Brooker, 1994). Glasses of intermediate compositions such as dacite, andesite and phonolite contain both types of species (Blank and Brooker, 1994; Morizet et al., 2001).

H<sub>2</sub>O and CO<sub>2</sub> solubility in melts equilibrated with mixed H<sub>2</sub>O-CO<sub>2</sub> fluids was investigated only in a few studies. In the pioneering work of Mysen et al. (1976) on albite, jadeite and nepheline compositions the highest CO<sub>2</sub> solubility were not found for the pure CO<sub>2</sub> fluid but at  $x_{CO_2}^{fluid} < 1$ . Their interpretation was that dissolved water enhances the solubility of CO<sub>2</sub> in the melt. However, as discussed by Blank and Brooker (1994), there may be substantial errors with the <sup>14</sup>C β-track autoradiography which was used by Mysen et al. (1976) as the analytical method for carbon determination. In more recent studies, IR and NMR spectroscopy was used to measure CO<sub>2</sub> speciation and concentration in glasses. Rhyolitic compositions (contain only molecular CO<sub>2</sub>) have been examined by Blank et al. (1993) and Tamic et al. (2001), and basaltic compositions (contain only carbonate) have been examined by Dixon et al., (1995). To my knowledge, Kohn and Brooker (1994) were the only authors so far, who have investigated the effect of water on CO<sub>2</sub> speciation in silicate glasses containing both CO<sub>2,mol</sub> and carbonate groups. Using <sup>13</sup>C MAS NMR spectroscopy, they found a maximum in the ratio of CO<sub>2,mol</sub>/carbonate at a water content of 1-2 wt.% in albitic and jadeitic glasses.

In this study, the solubility of H<sub>2</sub>O and CO<sub>2</sub> in dacitic melts in equilibrium with mixed fluids was investigated at 100, 200 and 500 MPa and 1250°C. On the basis of the new solubility data, an empirical model is developed to calculate the water solubility in the melt as a function of  $x_{H_2O}^{fluid}$  and pressure. Additionally, I propose two thermodynamic models to describe the dependence of the CO<sub>2</sub> solubility in dacitic melts on pressure,  $f_{CO_2}^{fluid}$  and the water content in the melt. To understand the solubility behavior of CO<sub>2</sub> in the melts, I also have examined the effect of water on the speciation of CO<sub>2</sub> in dacitic glasses.

### 2.2 Methodology

To determine H<sub>2</sub>O and CO<sub>2</sub> solubility, melts were equilibrated with CO<sub>2</sub>- and H<sub>2</sub>O-bearing fluids. After the run, the fluid composition was measured by gravimetry. The water content in the glasses (quenched melts) was determined by Karl-Fischer-Titration (KFT), the molecular CO<sub>2</sub> content by middle infrared (MIR) spectroscopy and the total CO<sub>2</sub> content by secondary ion mass spectrometry (SIMS).

To calibrate the SIMS method I used standards with known water and CO<sub>2,total</sub> contents. The CO<sub>2,total</sub> content in the standards was determined by CO<sub>2</sub> titration and the water content by near infrared (NIR) spectroscopy. For CO<sub>2</sub> titration large homogeneous samples of more than 100 mg are needed. Such samples only can be produced in acceptable run times when glass powder is used as starting material. On the other hand, solubility experiments cannot be performed with powder, because the melt viscosity is too high to remove bubbles (in the synthesis of the standards the fluid is completely dissolved because the volatile content in the capsule is below the saturation limit). Therefore, starting materials in solubility experiments were small glass pieces. The carbon concentration in the quenched glasses was measured with microtechniques (MIR and SIMS).

### 2.3 Experimental

#### 2.3.1 *Starting material*

The starting composition was a synthetic dry glass with a composition close to a dacite of the Unzen Volcano, Japan (Chen et al., 1993). The homogenous dry glass was synthesized by melting oxides and carbonates at 1600°C for more than 4 h, grinding and remelting for additional 4 h at the same temperature. The composition was determined by electron microprobe analysis, using a Cameca CAMEBAX microprobe, with 15 kV accelerating voltage, 5 nA beam current and a defocused beam with a 20 µm diameter (table 1).

The water content of the dacitic glass was measured by IR spectroscopy. A water content of 0.02 wt.% was determined from the peak height of the fundamental OH vibration band at 3550 cm<sup>-1</sup> using a linear molar absorption coefficient of 68 l mol<sup>-1</sup> cm<sup>-1</sup> for dacitic glasses (Yamashita et al., 1997). No CO<sub>2</sub> was detected by IR spectroscopy on polished fragments of the anhydrous glass. On the other hand, CO<sub>2</sub> titration of the pulverized glass yields a carbon content of 22-39 ppm. The carbon contamination can be attributed to CO<sub>2</sub> adsorbed on the surface of the glass powder. However, the amount of CO<sub>2</sub> is small and I think, that it has a negligible effect on the results.

### 2.3.2 *Solubility experiments*

For solubility experiments, small glass pieces (0.75-2 \* 2-3 \* 4-13 mm, 18-75 mg) were loaded with oxalic acid dihydrate as a combined CO<sub>2</sub> and H<sub>2</sub>O source (H<sub>2</sub>C<sub>2</sub>O<sub>4</sub>\*2H<sub>2</sub>O) or anhydrous oxalic acid (H<sub>2</sub>C<sub>2</sub>O<sub>4</sub>) as a CO<sub>2</sub> source and doubly distilled water into an Au<sub>80</sub>Pd<sub>20</sub> capsule. The anhydrous oxalic acid was produced by dehydration of H<sub>2</sub>C<sub>2</sub>O<sub>4</sub>\*2H<sub>2</sub>O in a drying oven at 105°C for more than one hour. Au<sub>80</sub>Pd<sub>20</sub> was used as a capsule material because it has been shown, that no iron diffuses into this alloy at the experimental conditions of this study (Berndt, 2002). Using Au<sub>80</sub>Pd<sub>20</sub> as capsule material also prevents loss of CO<sub>2</sub> during the experiments (Sierralta et al., 2002). During welding, the capsules were wrapped in a tissue which was water-soaked and frozen in liquid nitrogen to prevent any loss of water or CO<sub>2</sub>. After welding the oxalic acid was decomposed in an oven at 200°C. The amount of fluid was calculated, so that the CO<sub>2</sub> pressure was 20 bar at ambient conditions. For solubility experiments with pure water, the amount of water added was always >1 wt.% higher than the expected water solubility in the melt. Experiments were performed at 1200 - 1250°C and 100 - 500 MPa for 47 -140h (see table 5).

### 2.3.3 *Synthesis of standards for the Secondary Ion Mass Spectrometry (SIMS)*

The standards for the ion microprobe were synthesized using glass powder (400 - 500 mg), water and silver oxalate as a CO<sub>2</sub> source. To avoid problems of the silver alloying with the Au<sub>80</sub>Pd<sub>20</sub> capsule, which can lead to a leakage, the silver oxalate was isolated from the external capsule wall by wrapping it in an additional Au<sub>80</sub>Pd<sub>20</sub> foil. Water and glass powder were filled in two portions into the Au<sub>80</sub>Pd<sub>20</sub> capsules, which subsequently were welded shut (also with cooling the capsules with a water-soaked and frozen tissue to avoid water or CO<sub>2</sub> loss). To decompose the silver oxalate and to ensure a homogeneous CO<sub>2</sub> and water distribution, the capsules were stored horizontally for more than 8 hours at 200°C in an oven. Syntheses were performed at 1250°C and 500 MPa. The amounts of water and CO<sub>2</sub> introduced into the capsules were lower than the expected water and CO<sub>2</sub> - solubilities in rhyolitic melts at the P-T - conditions of the syntheses.

### **2.3.4 Experimental apparatus**

All experiments and syntheses of standards were performed at the University in Hannover in internally heated pressure vessels (IHPV) orientated vertically and pressurized with argon. A detailed description of the IHPV used in Hannover is given by Berndt et al. (2002). To avoid quench crystals I used a rapid quench device described by Bernd et al. (2002). One capsule or packages of up to 5 capsules wrapped into a Au<sub>80</sub>Pd<sub>20</sub> foil were fixed to a Pt-wire in the hot spot zone. Quenches were made by fusing the Pt-wire electrically. The capsule or capsule package dropped down on a copper block unit with high thermal conductivity.

The temperatures were recorded with four thermocouples. Two of them, connected to a Eurotherm unit, were used to control the power supply of the two furnace windings, two additional thermocouples were positioned inside the sample holder in which the samples were hanging and at about 2 mm next to the capsules. The temperature variation along the capsules/capsule packages (4-5 cm) was always less than 20°C. The cooling rate of rhyolite melts quenched with this device has been determined by Benne (2000, unpublished diploma thesis) using the geospeedometer of Zhang et al. (2000). Results show a quench rate of 150°C/s with a factor of two uncertainty. Intrinsic redox conditions during synthesis was equivalent to the MnO-Mn<sub>3</sub>O<sub>4</sub> solid oxygen buffer at water saturated conditions (Berndt, 2002). Note, that the oxygen fugacity  $f_{O_2}$  shifts to more reducing conditions at reduced water activities (1 log unit for  $a_{H_2O}^{fluid}=0.3$ , Berndt, 2002).

## **2.4 Analytical**

### **2.4.1 Determination of the fluid composition after the experiment**

The fluid composition after the experiment was determined by weighing the capsule using following procedure: (1) the capsule was weighed; (2) the water from the fluid phase was frozen using liquid nitrogen; (3) the capsule was punctured with a needle; (4) after heating the capsule to room temperature, the capsule was weighed to determine the mass of CO<sub>2</sub> (+ N<sub>2</sub> from air enclosed during loading the capsule); and (5) the capsule was placed into a drying oven and subsequently weighed to determine the mass of water. The weight loss was periodically checked (interval: approximately 10 minutes) until the weight remained constant. At this point, the water from the fluid

phase was considered to be extracted entirely. The temperature of the drying oven was 110°C, except for glass samples with expected water concentrations exceeding 6 wt.% H<sub>2</sub>O. For these glasses, the oven temperature was between 50 and 70°C.

In the calculation of  $x_{H_2O}^{fluid}$  and  $x_{CO_2}^{fluid}$  (mole fractions of water and CO<sub>2</sub> in the fluid phase, respectively), I take into account that atmospheric N<sub>2</sub> was trapped in the experimental charge during preparation of the capsule. Using the gravimetric method (described above), the individual weights of CO<sub>2</sub> and N<sub>2</sub> can not be distinguished. Therefore, the enclosed N<sub>2</sub> represents the main source of error in the determination of  $x_{CO_2}^{fluid}$  and  $x_{H_2O}^{fluid}$ . To account for N<sub>2</sub>, I used the value of  $x_{N_2}^{fluid} = 0.02 \pm 0.02$  determined by Tamic et al. (2001) for all experiments, except for experiments with pure water where  $x_{N_2}^{fluid}$  is negligible (<0.01, Tamic et al, 2001).

Only minor amounts of CO were detected (<0.6 mol% of total C-H-O) in CO<sub>2</sub> rich fluids with gas chromatography in sample DC156 and 5 more samples not further used in this study. As the concentrations of additional components are low at this f<sub>O<sub>2</sub></sub>, I consider the fluid phase as a two-component gas mixture composed of CO<sub>2</sub> and H<sub>2</sub>O.

#### 2.4.2 Karl - Fischer - Titration (KFT)

The water contents in the glasses obtained from the solubility experiments were determined by pyrolysis and subsequent Karl-Fischer-Titration (KFT). KFT is a coulometric method based on the quantitative reaction of water with iodine:  $I_2 + SO_2 + H_2O = 2HI + SO_3$ . Samples of 7-25 mg were loaded into a sample chamber and flushed by dried argon (or dried air, see below). Then water was extracted by heating the samples from room temperature to 1200-1300°C (typical duration of extraction: 7-12 min). Because hydrous glasses sometimes dehydrate explosively, leading to a sputtering of the glass out of the heating zone, the samples were wrapped in a platinum foil. The extracted gas is transported by the argon stream through an oxidation furnace, where H<sub>2</sub> is oxidized to H<sub>2</sub>O, into the titration cell (for more details see Behrens et al., 1996). Hydrogen might be formed by a redox reaction between ferric iron and water. Three additional analyses were made with a flux of dried air instead of an argon flux. This ensures, that hydrogen is oxidized directly on the sample. The results of analyses performed with argon and dried air are identical within analytical error (table 6). Uncertainties in measured water contents were calculated on



the basis of  $\pm 0.02 \mu\text{g/s}$  uncertainty in titration rate (Behrens et al, 1996), also taking into account a residual (unextracted) water content of  $0.02 \pm 0.02 \text{ wt.}\%$  (chapter 1.3.1).

### 2.4.3 CO<sub>2</sub> - Titration

The concentration of CO<sub>2</sub> in glasses used as SIMS standards was determined by pyrolysis and subsequent coulometric titration (Deltromat 500, Deltronic). The principle of the coulometric CO<sub>2</sub> titration is similar to that of the KFT. The method is based on the quantitative reaction of CO<sub>2</sub> with an alkaline (pH ~10) barium perchlorate solution:  $\text{Ba}^{2+} + \text{CO}_2 + 2 \text{OH}^- = \text{BaCO}_3 + \text{H}_2\text{O}$ . The pH value is lowered by this reaction. The consumed amount of hydroxyl ions is generated by electrolysis (coulometric titration), until the starting pH is reached:  $2\text{H}_2\text{O} + 2 \text{e}^- = 2\text{OH}^- + \text{H}_2$ . One mole of CO<sub>2</sub> reacts quantitatively with one mole Ba<sup>2+</sup> and 2 moles of hydroxyl groups and, therefore, 1 mg of CO<sub>2</sub> is equivalent to 4.39 coulombs.

The sample is heated in a combustion tube to 1200°C in order to extract CO<sub>2</sub>. This CO<sub>2</sub> is transported by a purified air stream to the titration cell connected with the coulometer electronics. The air stream was previously purified by oxidizing hydrocarbons in a gas purification oven and adsorbing all CO<sub>2</sub> in a trap with soda lime pellets.

For a typical measurement duration of 90 s the background CO<sub>2</sub> value is  $5.5 \pm 2.2 \mu\text{g}$ . Based on 30 repeated measurements of a rock powder with a known carbon content, the maximum uncertainty was estimated to be  $\pm 12.8 \mu\text{g CO}_2$  for an amount of 180 - 540  $\mu\text{g CO}_2$  determined. Tamic (2002) determined the same background CO<sub>2</sub> value, but a lower uncertainty of  $\sim \pm 7 \mu\text{g CO}_2$ . To obtain measurements with a precision better than 5 % relative, sample weights of more than 100 or 250 mg for 2500 or 1000 ppm CO<sub>2</sub>, respectively are needed.

### 2.4.4 IR-Spectroscopy

Doubly polished glass plates of 300 - 500  $\mu\text{m}$  (for NIR) and  $\sim 130 - 230 \mu\text{m}$  thickness (for MIR spectroscopy) were prepared. The thickness of each glass plate was measured with a digital micrometer (Mitutoyo; precision  $\leq 2 \mu\text{m}$ ). The glass fragments used for IR spectroscopy were directly adjacent to pieces analyzed by SIMS.

IR spectra were recorded with a Bruker IFS 88 FTIR spectrometer coupled with a microscope IR-Scope II. The spot size used in the measurements (typically 100  $\mu\text{m}$ ) was limited by a slit aperture placed in the plane of the real intermediate image of the sample. The detector was for both NIR and MIR a narrow band MCT detector with NIR equipment (range 600-10000  $\text{cm}^{-1}$ ) and a cassegranian 15x objective. The microscope and the spectrometer were flushed by air purified with a drying column with molecular sieve, to minimize disturbances due to changes in the H<sub>2</sub>O and CO<sub>2</sub> content in the air. Operation conditions for NIR were: a tungsten light source, a CaF<sub>2</sub> beamsplitter and 30-50 accumulated scans with a spectral resolution of 2  $\text{cm}^{-1}$ . Operation conditions for MIR were: a global light source, a KBr beamsplitter and 20-30 accumulated scans with a spectral resolution of 1  $\text{cm}^{-1}$ .

Twenty scans are sufficient to obtain good spectra with a good signal/noise ratio. Short times between measurement of background spectra and sample spectra lower the error due to changes of CO<sub>2</sub> concentrations in the air stream. Longer measurements up to 500 scans do not enhance the precision of the spectra. Only one or two sample measurements were performed after one background measurement.

To quantify the variation of CO<sub>2</sub> in the beam path, I have compared 150 spectra collected without sample. These spectra were recorded in two ways over a period of several days: (1) series of 10-110 spectra without sample were successively recorded without opening the sample chamber of the IR microscope; (2) one or several spectra without sample were directly collected after the IR measurement performed on a glass sample. The variation in peak intensity was found to be random, suggesting rapid changes of atmospheric CO<sub>2</sub> concentrations with time. For the measurement conditions used in this study the average of the peak intensity of the atmospheric CO<sub>2</sub> doublet at  $\sim 2350 \text{ cm}^{-1}$  is zero with an error of  $\pm 0.008$  linear absorbance units and  $\pm 0.40$  integral absorbance units. These values, which correspond to an equivalent CO<sub>2</sub> content of 10 ppm (peak height, absorption coefficients by Blank, 1993 and Tamic, 2002, see 2.5.3) or 35 ppm (peak area, absorption coefficient by Nowak et al., 2003, see 2.5.3) for a 130  $\mu\text{m}$  thick sample, are considered to be the precision of CO<sub>2</sub> absorbance measurements.

### 2.4.5 Secondary Ion Mass Spectrometry (SIMS)

SIMS is an analytical method whereby a beam of ions is accelerated and focussed onto the surface of a sample, and sputtered secondary ions are analyzed in a mass spectrometer (Finch et al., 2001). The absolute intensities of the measured ions are not very reproducible; hence it is usual to measure the ratio of the peak intensity of the isotope of interest to that of another isotope, the concentration of which is known (Si in silicates, e.g. Reed, 1989). Relative sensitivity factors are dependent not only upon the properties of the isotopes concerned (mainly the ionization potential) but also on the matrix (e.g. Reed, 1989). To avoid matrix effects I used standards close in composition to the samples from the solubility experiments. In addition, as already reported earlier, water has an effect on the ion yield of trace elements relative to Si (Brenan et al., 1995; Wiedenbeck et al., 2001). Because of the variation of dissolved water concentrations in my samples, I synthesized standards with various water contents.

Standards with 0.5 to 6.5 wt.% H<sub>2</sub>O and 1300 - 2600 ppm CO<sub>2</sub> and samples of the solubility experiments were mounted with a resin in object slides previously prepared with holes. Polishing the slices with diamond (=C) paste can lead to a carbon contamination on the surface. To avoid this contamination the slices were cleaned with distilled water in an ultrasonic bath and repolished with an alumina paste (a layer of ~ 2 µm thickness was removed). After the first test measurements I repolished the sample again with a cerium oxide paste (see chapter 2.5.4.1). After polishing the samples were coated with gold.

#### 2.4.5.1 Measurement conditions

The total <sup>12</sup>C concentration in the glasses was measured with the ims 1270 ion microprobe at the CRPG in Nancy. Carbon forms negative ions readily and SIMS is an effective method for <sup>12</sup>C isotope measurement (e.g. McKeegan et al., 1985, Zinner et al., 1989). A primary beam of <sup>133</sup>Cs<sup>+</sup> ions, which enhances the secondary ion yield of electronegative isotopes (Storms et al., 1977), was used to sputter secondary ions from the sample. The use of a positive primary beam and extraction of negative secondary ions causes a positive charge build-up on the surface of insulating samples, which has a significant effect on the yield of secondary ions (Harte et al., 1999). In the case of negative secondary ions a positive surface potential will inhibit or totally

suppress their emission (Vickermann, 1989). Other unwanted effects of charging include migration of small ions (e.g. Na<sup>+</sup>) in the host matrix, deflection of primary and secondary beams, and even sample movement when using fine powders (Eccles, 1989). Thus, a charge build-up causes a non-representative SIMS spectrum (Eccles, 1989). A NEG (Normal incidence Electron Gun) which produced an electronic cloud just in front of the sample is used to compensate the positive charge of the sample. The entry slit of the secondary beam was 150 μm, the exit slit was 300 μm, the field aperture was 3000 μm and the energy window was open at 60 eV. The mass resolution power ( $M/\Delta M$ ) was around 5000-6000.

Before the measurement the samples were presputtered for 2 minutes with a scanning beam of 50 μm size and 20 nA. The measurements were performed with a point beam of 50 μm diameter and 5 nA centered in the pre-sputtered region. The secondary <sup>12</sup>C - ions were counted with an electron multiplier (counting time 5 s) and the <sup>28</sup>Si - ions were measured with a Faraday cup (counting time 3 s), the counting time on the background was 1s. Counts were corrected for the deadtime of the electron multiplier and the background. 20 cycles were measured with a total analysis time of ~8 min.

## 2.5 Results

### 2.5.1 *Description of run products and water solubilities*

Most of the samples were bubble and crystal free. Exceptions are samples 101, 102 and 103 synthesized at 500 MPa which contain inhomogeneously distributed bubbles for example along cracks. These samples have bubble free regions which are large enough to be measured by IR spectroscopy. IR spectroscopic measurements on regions with bubbles give the same or slightly lower (up to 1.5 % relative) water contents than bubble free regions. I assume that these bubbles are quench bubbles which are water free or poor and have a negligible effect on the KFT measurements. This is supported by the good agreement of the water contents determined with IR and with KFT (0.8-1.5% relative deviation). The estimated fluid volume in bubbles is much smaller, than in the free fluid. Therefore I assume, that the quench bubbles have no effect on the fluid composition. The bubble bearing samples were not used for the IR calibration (see chapter 2.5.2).

Fluid compositions and the corresponding water and CO<sub>2</sub> contents of the quenched glasses are presented in tables 5 and 6, respectively, and in figures 2.5, 2.6 and 2.8. All samples analyzed by IR spectroscopy and SIMS show a homogeneous distribution of water and CO<sub>2,total</sub> with no detectable difference between rim and core of glasses within analytical error.

Water solubilities in dacitic melts measured by KFT increase with increasing pressure and  $x_{H_2O}^{fluid}$  (full symbols in figure 2.6). At all pressures (100, 200 and 500 MPa) a square root dependence of water solubility on  $x_{H_2O}^{fluid}$  is observed at low  $x_{H_2O}^{fluid}$  ( $x_{H_2O}^{fluid} < 0.2$ ). At 100 and 200 MPa an almost linear dependence on  $x_{H_2O}^{fluid}$  is observed for higher  $x_{H_2O}^{fluid}$  ( $x_{H_2O}^{fluid} > 0.2$ ). At 500 MPa, the water solubility shows a non-linear dependence on  $x_{H_2O}^{fluid}$  in the whole  $x_{H_2O}^{fluid}$  range. The 500 MPa data indicate a point of inflexion at around  $x_{H_2O}^{fluid} \sim 0.5$ .

### 2.5.2 *NIR spectroscopic determination of water contents*

The NIR spectroscopy was mainly used to determine the water content in the standards for the SIMS. Water contents of solubility samples were determined by KFT, because the NIR absorption coefficients changed (see below) and water determination was more exact by KFT. From the SIMS standards most sample material was consumed for CO<sub>2</sub> titration, so that KFT measurements were not possible.

The concentrations of H<sub>2</sub>O and OH were determined from the heights of the baseline corrected absorption bands at  $\sim 5200$  and  $\sim 4500$  cm<sup>-1</sup>, which are attributed to the combination stretching + bending mode of molecular H<sub>2</sub>O and the combination of stretching + bending mode of OH groups (Scholze, 1960; Bartholomew et al., 1980; Stolper, 1982) by using the Lambert-Beer law.

Densities (in g/l) of the samples were calculated using the linear relationship:

$$\rho = (-11.8 \pm 2.0) \cdot c_{\text{water}} + (2515 \pm 6),$$

where  $c_{\text{water}}$  is the total water content in wt.% (chapter 1.3.2, standard deviation of  $\rho$ : 6.6 g/l). This relationship is based on density measurements of CO<sub>2</sub>-free hydrous glasses with dacitic composition. Density data of Tamic et al. (2001) in CO<sub>2</sub>-bearing

hydrous rhyolite glasses are systematically lower (up to 2 % relative) than density data of Withers and Behrens (2000) in hydrous CO<sub>2</sub>-free glasses of the same bulk composition. Tamic et al., explained this deviation by the difference in synthesis pressure (Withers and Behrens, 1999: 500 MPa; Tamic et al., 2001: 150-500 MPa), sample size (higher uncertainty due to smaller sample size in Tamic et al., 2001) and by a possible effect of dissolved CO<sub>2</sub> in the glasses. I assume that the systematic error due to dissolved CO<sub>2</sub> and lower pressures should be in the same order in dacitic glasses.

I used the combination of two gaussians fitted to the iron-related band at ~5700 cm<sup>-1</sup> and the water-related band at ~4000 cm<sup>-1</sup> as the baseline for the bands at 4500 and 5200 cm<sup>-1</sup> (see chapter 1.4.2 for more detail). In chapter 1.4.2 I fitted the gaussians with fixed peak positions at 5770 and 3937 cm<sup>-1</sup> for the dacitic composition. In contrast to chapter 1.4.2, I fitted the gaussian at ~5700 cm<sup>-1</sup> without fixing the peak position in this chapter. The reason for this is that in some samples the band at ~5700 cm<sup>-1</sup> is more pronounced showing a discrete maximum at a lower wavenumber and it is not possible to fit this band accurately with a gaussian centered at 5770 cm<sup>-1</sup>. However, fits with constrained and unconstrained peak position differs only by ± 1.3 % relative in the total water content.

In the course of this study, the spectrometer setup has been modified: the microscope with a new objective, a condensor lens instead of a mirror, a slit aperture instead of an aperture hole and a new HgCdTe detector with a better signal/noise ratio has been replaced. In addition a new CaF<sub>2</sub> beamsplitter is used. Thus, the whole optical path changed.

Behrens et al. (1996) observed that spectra of the same sample collected by four different FTIR micro spectrometers vary by up to 10% relative in peak intensities. They explained these deviations by different specific measurement conditions as the magnification of the objectives, spectral ranges of the system (due to different beamsplitters) and characteristics of the detectors. They mentioned, that however, an unambiguous explanation of the differences is not possible due to the complexity of FTIR spectroscopy.

I calibrated the new spectrometer setup with the bubble free samples of my solubility experiments. The determined linear absorption coefficients for the H<sub>2</sub>O band at ~5200

cm<sup>-1</sup> and the OH band at ~4500 cm<sup>-1</sup> are  $\epsilon_{\text{H}_2\text{O}} = 1.18 \pm 0.06 \text{ l mol}^{-1} \text{ cm}^{-1}$  and  $\epsilon_{\text{OH}} = 1.22 \pm 0.06 \text{ l mol}^{-1} \text{ cm}^{-1}$ , respectively. These absorption coefficients are 2.5 % lower ( $\epsilon_{\text{H}_2\text{O}}$ ) and 14% higher ( $\epsilon_{\text{OH}}$ ), than those obtained in chapter 1. These values were used to determine the water content in the SIMS standard glasses.

The error on total water contents measured with IR is composed of the error on the density (3 % relative, see chapter 2.5.2), the thickness (2  $\mu\text{m}$ , see chapter 2.4.4), the absorbance (0.003 for OH peak and 0.002 for H<sub>2</sub>O peak) and the absorption coefficient (0.06 for both  $\epsilon_{\text{OH}}$  and  $\epsilon_{\text{H}_2\text{O}}$ , see above).

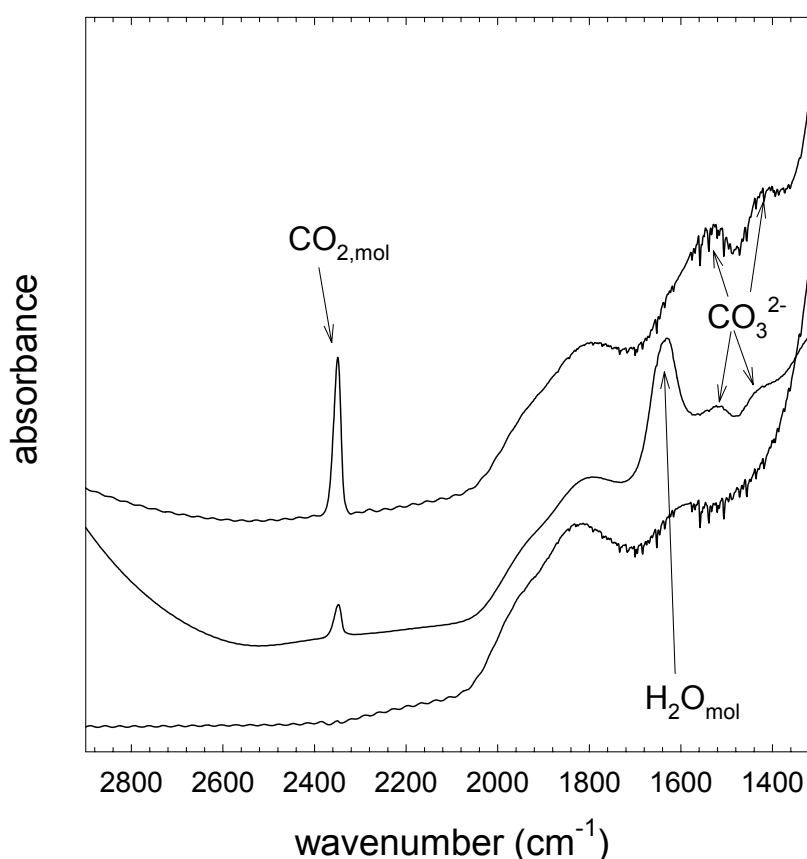
### 2.5.3 *MIR spectroscopic investigation of CO<sub>2</sub>*

Figure 2.1 shows IR spectra of CO<sub>2</sub> bearing hydrous (top) and anhydrous (bottom) dacitic glasses. In contrast to rhyolitic glasses in which CO<sub>2</sub> is incorporated as CO<sub>2,mol</sub> only and basaltic glasses in which CO<sub>2</sub> is incorporated only as carbonate, both C-species CO<sub>2,mol</sub> and carbonate are present in dacitic glasses.

The sharp absorption band at ~2350 cm<sup>-1</sup> is attributed to the  $\nu_3$  antisymmetric stretching vibration of CO<sub>2,mol</sub> dissolved in the glass (Fine and Stolper, 1985). This peak is distinct from that for free gaseous molecular CO<sub>2</sub>, which would rise to a doublet of unresolved rotational structure centered at ~2350 cm<sup>-1</sup> (Brooker et al., 1999). The band system at ~1530 cm<sup>-1</sup> and ~1430 cm<sup>-1</sup> is due to CO<sub>2</sub> dissolved as distorted carbonate (Blank and Brooker, 1994). Broad features with a maximum intensity at around 1800 cm<sup>-1</sup> are overtones related to the aluminosilicate framework (Brooker et al., 2001). The band at 1630 cm<sup>-1</sup> is attributed to the fundamental bending of water molecules (Nakamoto, 1986).

The quantification of the carbonate in the MIR spectra is difficult because the weak carbonate bands are superimposed by the silicate network bands (at 1800 cm<sup>-1</sup> and higher) and by the molecular water band at 1630 cm<sup>-1</sup>. The background features change slightly from experiment to experiment because of changing contents of molecular water and variation in oxygen fugacity, which influences iron speciation. (Although the hydrogen fugacity is approximately constant in the IHPV the oxygen fugacity in the capsule varies due to different water activities.) Thus, a background correction would require carbonate free samples with the same water contents, made at the same oxygen fugacity with the same cooling rate.

The amount of CO<sub>2,mol</sub> was determined from the heights and areas of the baseline corrected absorption band at ~2350 cm<sup>-1</sup>, using a linear baseline. Up to now, no absorption coefficients for the molecular CO<sub>2</sub> band in iron bearing dacitic glasses are available. To estimate the molecular CO<sub>2</sub> contents, I have used the linear molar absorption coefficient of 1066 ± 20 l cm<sup>-1</sup> mol<sup>-1</sup> from Blank (1993) and 1232 ± 36 l cm<sup>-1</sup> mol<sup>-1</sup> from Tamic (2002) for rhyolitic melts and the integral molar absorption coefficient of 16700 ± 1000 l cm<sup>-2</sup> mol<sup>-1</sup> determined by Nowak et al. (2003) for synthetic iron free dacitic glasses. CO<sub>2,mol</sub> values determined with the absorption coefficient of Tamic (2002) and Nowak et al. (2003) are 13,5 % relatively lower and 20 % (in average) higher, respectively, than those determined with the



**Figure 2.1:**

Typical MIR spectra (normed to a thickness of 100 μm) of hydrous and dry CO<sub>2</sub>-bearing dacitic glasses in the range of vibrational bands of CO<sub>2</sub> species.

CO<sub>2</sub> is dissolved both as molecular CO<sub>2</sub> and carbonate.

The upper spectrum is from a nominally dry sample containing 2500 ppm CO<sub>2</sub>, the middle spectrum is from a sample containing 1380 ppm CO<sub>2</sub> and 2.2 wt.% water and the lower spectrum is from the starting glass which is nominally CO<sub>2</sub> and water free.



absorption coefficient of Blank (1993). For graphical presentation I used data calculated with the absorption coefficient from Blank (1993), because these data are intermediate between those calculated after Tamic (2002) and Nowak et al. (2003). These data are listed in table 6. The error on the CO<sub>2,mol</sub> values is high, because I use absorption coefficients for rhyolite, but I am mainly interested in relative variations, where the error due to the absorption coefficient is not so important. In figure 2.7 the contents of CO<sub>2,mol</sub> in the glass measured by IR spectroscopy are combined with the water solubilities. The CO<sub>2,mol</sub> content decreases with increasing water content. The strongest decrease is observed at low water contents.

### ***2.5.4 Determination of CO<sub>2,total</sub> contents with secondary ion mass spectrometry***

#### **2.5.4.1 Evolution of the <sup>12</sup>C/<sup>28</sup>Si ratio with time**

During the measurements on standard and experimental glasses the <sup>12</sup>C/<sup>28</sup>Si ratio (counts of <sup>12</sup>C/counts of <sup>28</sup>Si) did not remain constant with time (10 to 24 % relative difference between highest and lowest <sup>12</sup>C/<sup>28</sup>Si ratio). Four different trends were observed: (1) a continuous drop of the <sup>12</sup>C/<sup>28</sup>Si ratio with time (figure 2.2), (2) the <sup>12</sup>C/<sup>28</sup>Si ratio remained constant for 10-15 cycles and decreased afterwards (figure 2.2), (3) the <sup>12</sup>C/<sup>28</sup>Si ratio increased for 10-15 cycles and subsequently decreased (figure 2.3), (4) in 2 glasses the <sup>12</sup>C/<sup>28</sup>Si ratio firstly increased and then remained constant after approximately 15 cycles. The trends of the <sup>12</sup>C/<sup>28</sup>Si ratio with time seem to be correlated with the CO<sub>2</sub> content of the glasses. Measurements on glasses with more than 2000 ppm show trends (1) and (2), measurements on glasses with less than 1000 ppm CO<sub>2</sub> showed trends (3) and (4). At intermediate CO<sub>2</sub> contents (1000-2000 ppm) trends (1), (2) and (3) were observed. Other parameters such as the pressure of synthesis and the water content which both influence the density of the glass might have an additional effect.

The shape of the experimental curves (<sup>12</sup>C/<sup>28</sup>Si versus time) observed in this study may result from: (1) surface contamination, and/or (2) an electromigration of C caused by charging (Wilson et al., 1989), and/or (3) a preferential sputtering of C from the sample relative to Si (Deloule et al., 1995).

(1) To avoid surface contamination I repolished the samples after the first test measurements with cerium oxide paste. Furthermore the samples were presputtered with a relatively high energy to remove the eventually contaminated sample surface.

It is unlikely that a surface contamination had caused these trends because the behavior of the experimental curves varies systematically with the CO<sub>2</sub> content, and in some samples the <sup>12</sup>C/<sup>28</sup>Si ratio initially increased.

(2) Charging of the sample surface can result from the poor electrical conductivity of the glasses. When the sample charges, a fractionation of <sup>12</sup>C/<sup>28</sup>Si will be produced, which is difficult to quantify for a potential correction. This fractionation can be due to charge-driven diffusion of ionized carbon (or hydrogen) to the surface (note that also enrichment or depletion of H<sub>2</sub>O can have an effect on the <sup>12</sup>C/<sup>28</sup>Si ratio, because of its matrix effect). It is also possible that the secondary-ion beam became unstable due to charge buildup and the intensity dropped because it was partially deflected from the mass spectrometer slits (Hervig et al., 1989).

Sample charging probably can be reduced by using a negative O<sup>-</sup> primary beam instead of a Cs<sup>+</sup> beam. Then positive charging due to the emission of secondary

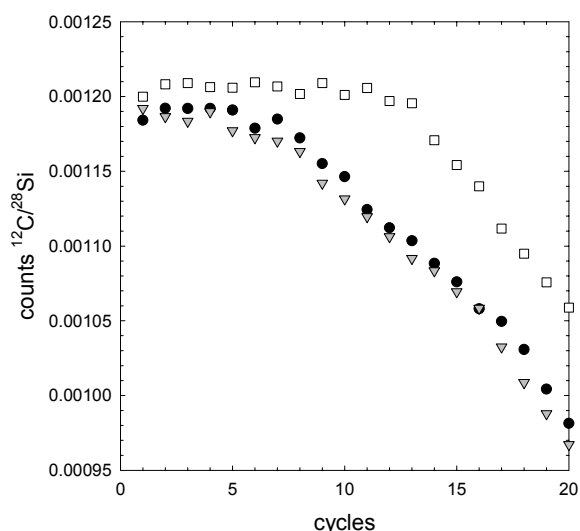


**Figure 2.2:**

Typical evolution of the <sup>12</sup>C/<sup>28</sup>Si ratio (counts <sup>12</sup>C/counts <sup>28</sup>Si) with time for samples with a high CO<sub>2</sub> content (more than 2000 ppm CO<sub>2,total</sub>).

These three trends correspond to a series of three measurements in the same standard glass with 2565 ppm CO<sub>2,total</sub> and 0.5 wt.% water.

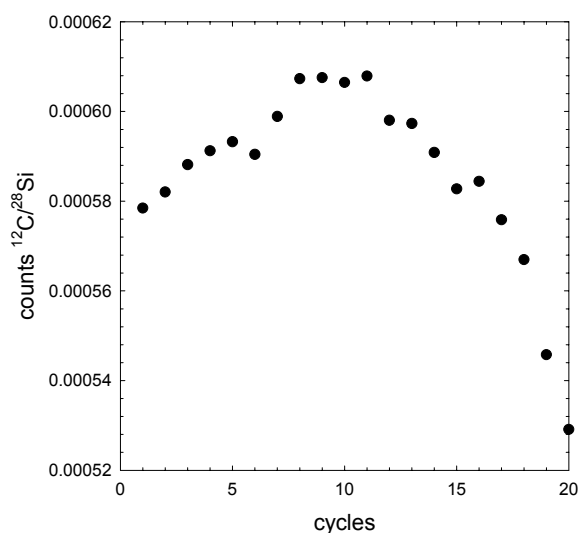


**Figure 2.3:**

Typical evolution of the <sup>12</sup>C/<sup>28</sup>Si ratio (counts <sup>12</sup>C/counts <sup>28</sup>Si) with time for samples with a low CO<sub>2</sub> content (less than 2000 ppm CO<sub>2,total</sub>, here sample 197).

electrons can be neutralized by the incoming negative O<sup>-</sup> ions. Pan et al. (1991) successfully used an O<sup>-</sup> primary beam in their measurements of CO<sub>2</sub> in basaltic glasses. A disadvantage of using a negative ion primary beam is, however, the relatively low sputtering yield of C<sup>-</sup> ions. In the study of Pan et al. (1991) CO<sub>2</sub> contents were in the range of 7000-15000 ppm, so that this has been a minor problem. However, the amounts of CO<sub>2</sub> in my samples are much smaller (down to a few tens ppm of CO<sub>2</sub>).

(3) A preferential sputtering of <sup>12</sup>C relative to <sup>28</sup>Si would increase the <sup>12</sup>C/<sup>28</sup>Si ratio at the beginning of the profile, until the surface layer becomes depleted in <sup>12</sup>C (Deloule et al., 1995). The shape of the experimental curves (<sup>12</sup>C/<sup>28</sup>Si versus time) observed in this study indicate that the dominant effect is a deeper extraction of <sup>12</sup>C than <sup>28</sup>Si (Deloule et al., 1995). This could be the result of degassing of CO<sub>2</sub> under vacuum and high temperature (or electromigration of carbon). If this explanation is right, my <sup>12</sup>C/<sup>28</sup>Si trends would suggest, that the dynamic of deeper extraction of <sup>12</sup>C relative to <sup>28</sup>Si is higher in samples with a higher CO<sub>2</sub> content, because in these samples only the decrease of <sup>12</sup>C/<sup>28</sup>Si is visible which suggests, that the samples are already depleted in <sup>12</sup>C after the 2 minutes of presputtering. In samples with low CO<sub>2</sub> contents the initial increase of the <sup>12</sup>C/<sup>28</sup>Si ratio due to a preferential sputtering still takes place at the beginning of the sample measurements.

#### 2.5.4.2 Calculation of the relative sensitivity factor from standard glasses

Considering the time evolution of the <sup>12</sup>C/<sup>28</sup>Si ratio, I decided to use always the same analytical procedure (2 min presputtering and 20 measurement cycles) and to use the average of the <sup>12</sup>C/<sup>28</sup>Si -ratios corrected for background and deadtime of the electron multiplier to calculate the relative sensitivity factor and the CO<sub>2</sub> contents in the solubility samples.

The relative sensitivity factor (RSF) of C relative to Si is defined by :

$$RSF = \frac{(I_{12C^-} / I_{28Si^-}) \cdot (92.23 / 98.9)}{c_C / c_{Si}} \quad (2.1)$$

where  $I_{12C^-}$  and  $I_{28Si^-}$  are the number of counts on <sup>12</sup>C and <sup>28</sup>Si measured with the ion probe in standard glasses, 92.23 and 98.9 are the relative abundances of the mass <sup>28</sup>Si in natural silicon and <sup>12</sup>C in natural carbon, respectively, and  $c_C$  and  $c_{Si}$  are the

concentrations of carbon and silicon in mol/g measured by independent methods (C by CO<sub>2</sub> titration and Si by electron microprobe).

The relative sensitivity factors depend on the water content of the glasses (see figure 2.4 a and b for two analytical sessions). This shows, that water has a matrix effect on the measurements of carbon by SIMS. The relative sensitivity factor decreases linearly with the water content, e.g. a sample with 5 wt.% water has a 18-20 % lower relative sensitivity factor than a dry sample. Using a linear regression the relative sensitivity factor can be calculated after  $RSF = y_0 + a \cdot c_{water}$ , where  $y_0$  is the relative sensitivity factor for dry glasses and  $a$  is the slope.

### 2.5.4.3 Determination of the C content and uncertainty

The total carbon concentration (in mol/g) in the sample was calculated by

$$c_C = \frac{(I_{12C^-} / I_{28Si^-}) \cdot (92.23 / 98.9)}{RSF / c_{Si}} \quad (2.2)$$

Carbon is dissolved as molecular CO<sub>2</sub> and carbonate (see MIR spectra in figure 2.1). Therefore the carbon concentration is expressed as CO<sub>2</sub> concentration (given in ppm by weight) in the following text.

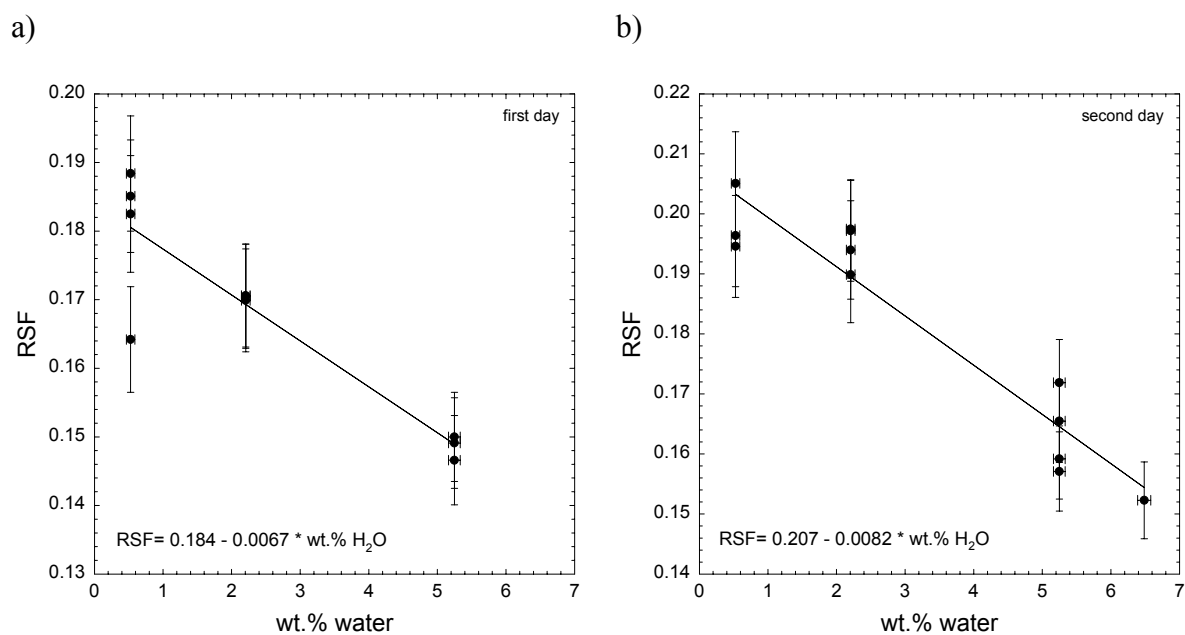


**Figure 2.4:**

Dependence of the relative sensitivity factor (RSF) on the water content for both analytical sessions (a and b).

The error of the carbon concentration which is shown in figure 2.5 is composed of the errors of the <sup>12</sup>C and <sup>28</sup>Si intensities, the error in the CO<sub>2</sub> content of the standards (CO<sub>2</sub> titration), the error of the linear regression of the water dependent relative sensitivity factors and the error due to different trends of counts/time. As most of the standards showed a continuous drop of the <sup>12</sup>C/<sup>28</sup>Si ratio whereas the samples showed an initial constant or increasing <sup>12</sup>C/<sup>28</sup>Si ratio (see chapter 2.5.4.1), I calculated the error of my measurements in considering only that part where the <sup>12</sup>C/<sup>28</sup>Si ratio decreases with time (same shape as in the standards) and extrapolating this curve to 20 cycles. With this procedure I obtain (average) values which are up to 14% relative systematically lower than the (average) values obtained by averaging the first 20 cycles. That means, that the CO<sub>2</sub> contents measured by SIMS can be overestimated by up to 14% relative.

At two analytical sessions 3 and 4 standards were measured. Different points on the same standard had distances of 1-2 mm. The deviation of the CO<sub>2</sub> content in the standard glasses measured by SIMS and by CO<sub>2</sub> titration was up to 4.5 % relative, which is close to the error of CO<sub>2</sub> titration (4 %), except for one point which has a deviation of 9 % relative. On the experimental glasses 1 or 2 points were measured (see table 6). The highest deviation during one day on two points (distance 0.5-1.5 mm) of one sample was 2.5 % relative. On sample 197, one point was analyzed in the first analytical session, and another one in the second analytical session. The calculated CO<sub>2</sub> values of these two points have a deviation of 5 % relative, thus they agree within error. The good agreement of duplicated measurements is a hint on the generally good reproducibility and the good homogeneity of the standards and solubility samples.

Several facts suggest, that the measured data reflect the correct CO<sub>2</sub> content: (1) the measured data have a good reproducibility (2) the average of the <sup>12</sup>C/<sup>28</sup>Si ratios of 20 cycles for two different trends (figure 2.2) agree within 4 % relative and (3) the measured CO<sub>2</sub> contents correlate with the  $x_{CO_2}^{fluid}$  (figure 2.5).

The solubility of total carbon (expressed as CO<sub>2</sub>) in all samples measured with SIMS is shown in figure 2.5. CO<sub>2</sub> solubility increases with increasing pressure and  $x_{CO_2}^{fluid}$  (symbols in figure 2.5). The variation of CO<sub>2,total</sub> solubility with  $x_{CO_2}^{fluid}$  is non-linear. The maximum solubilities at an  $x_{CO_2}^{fluid} \sim 0.8$  are 795±41, 1376±73 and 2949±166 ppm at 100, 200 and 500 MPa, respectively.

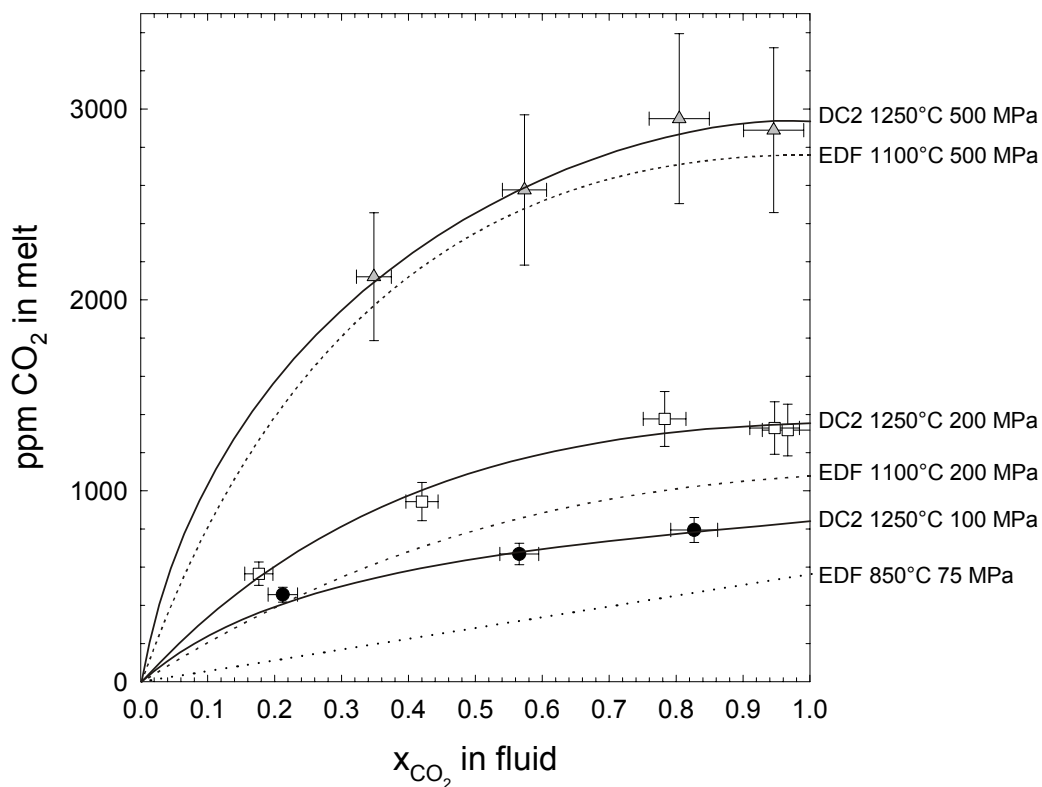


**Figure 2.5:**

Relationship between the mole fraction of CO<sub>2</sub> in the fluid phase and the concentration of total CO<sub>2</sub> dissolved in the melt at 1250°C and various pressures. Solid lines are manually fitted to the data.

Data from Fogel and Rutherford (1990, 850°C, 75 MPa) and Tamic et al. (2001, 1100°C, 200 and 500 MPa) are shown for comparison (dotted lines).

In figure 2.8 all water and CO<sub>2,total</sub> solubilities in dacitic melts (symbols) are combined in one diagram together with the  $x_{H_2O}^{fluid}$  in the corresponding fluid phase. It can be noted, that the CO<sub>2</sub> solubility increases slightly when a small amount of water is added (up to an  $x_{H_2O}^{fluid}$  of ~0.2), and then decreases when more water is present.

## 2.6 Discussion

### 2.6.1 Water solubility

#### 2.6.1.1 Comparison of water solubilities in the dacitic with a rhyolitic composition

I compared my water solubilities in dacitic melts with solubilities in rhyolitic melts investigated by Tamic et al. (2001). Tamic et al. (2001) developed an empirical model for water solubilities in rhyolitic melts as a function of the fluid phase composition, the pressure and the temperature. The basis of this model were solubility experiments at 200 and 500 MPa and 800 and 1100°C and solubility data of Blank et al. (1993) at 75 MPa and 850°C. I extrapolated these data to 1250°C (see figure 2.6) and interpolated them to 100 MPa. The highest error in extrapolating to 1250°C is made at 100 MPa, because data at pressures lower than 200 MPa are from experiments at 850°C only (e.g. the model predicts water solubilities measured at 100 MPa in haplogranitic melts by Holtz et al., 1995, at 800°C within error, but underestimates them by 7 and 10 % relatively at 1200 and 1350°C, respectively).

At 1250°C the solubilities of water at varying  $x_{H_2O}^{fluid}$  are higher in dacitic melts than in rhyolitic melts for water contents lower than ~8 wt.% water (figure 2.6). In contrast, at 500 MPa and water contents higher than ~8 wt.% water, the water solubility is higher in rhyolitic melts than in dacitic melts.

#### 2.6.1.2 Empirical water solubility model

The shape of the water solubility curves as a function of fluid composition is similar for rhyolitic and dacitic compositions. Therefore, at a given pressure and temperature (1250°C), my data plotted in figure 2.6 can be fitted adequately using the same empirical equation as Tamic et al. (2001):

$$C_{\text{water}} (\text{wt.}\%) = Ax^2 + Bx^{2.5} + Cx^{0.5} \quad (2.3)$$

Where  $C_{\text{water}}$  is the total water content of the glass, A, B and C are empirical coefficients and x is the composition of the fluid phase in equilibrium with the melt ( $x = x_{H_2O}^{fluid}$ ). The solid curves in figure 2.6 result from the fit of each data set to equation (2.3).

As Tamic et al. (2001) already mentioned: at low water fugacities the third term in equation (2.3) dominates and water solubilities vary with the square root of  $x_{H_2O}^{fluid}$ . This is consistent with water speciation data, which demonstrate, that water is preferentially incorporated in silicate melts as OH groups at low water contents (e.g. Ihinger et al., 1999; Nowak and Behrens 2001). At high water fugacities, the first and second term in equation (2.3) become increasingly important. This behavior may be related to increasing amounts of molecular H<sub>2</sub>O with increasing water content.

The pressure dependence has been modeled according to Tamic et al. (2001) assuming a second order polynomial dependence of water solubility on pressure. The equation (2.3) can be rewritten as:

$$C_{\text{water}} (\text{wt.}\%) = A_P x^2 + B_P x^{2.5} + C_P x^{0.5} \quad (2.4)$$

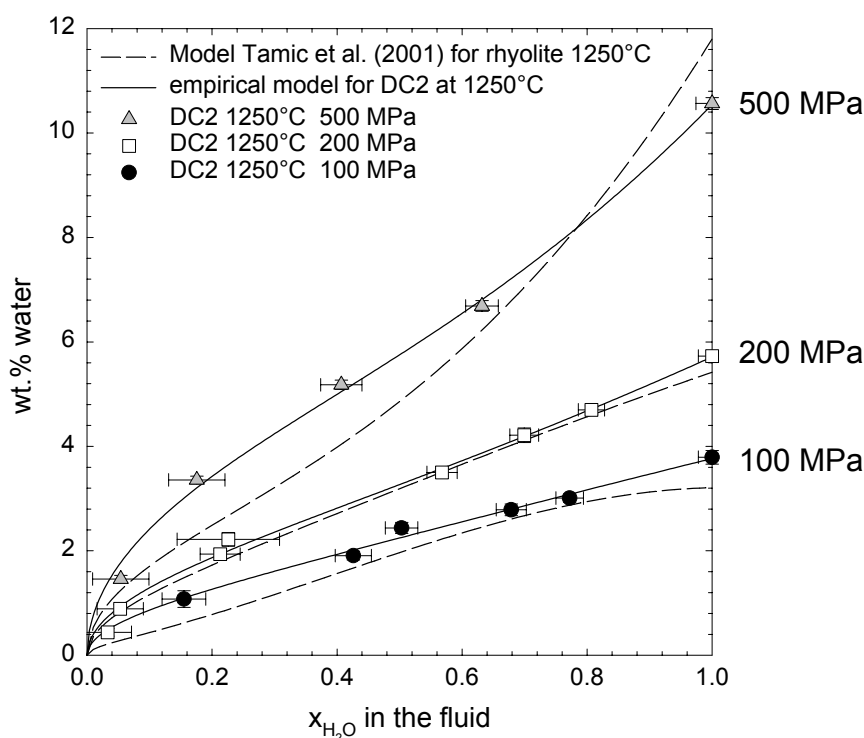


**Figure 2.6:**

Relationship between the mole fraction of H<sub>2</sub>O in the fluid phase and the concentration of total water dissolved in the melt at 1250°C and various pressures.

Solid lines are the fits of the data used for the empirical model developed in this study. For comparison data for rhyolitic melts calculated after the model of Tamic et al. (2001) are shown (dashed lines).



Where

$$A_P = \alpha_a + \beta_a P + \gamma_a P^2 \quad (2.5a)$$

$$B_P = \alpha_b + \beta_b P + \gamma_b P^2 \quad (2.5b)$$

$$C_P = \alpha_c + \beta_c P + \gamma_c P^2 \quad (2.5c)$$

The values of the empirical coefficients  $\alpha_i$ ,  $\beta_i$ ,  $\gamma_i$  are given in table 7. P is given in MPa. Note that only few solubility data (only for 100, 200 and 500 MPa) are available to determine the parameters  $\alpha$ ,  $\beta$  and  $\gamma$ . All experimental data match closely to the fitted curve without any systematic deviation. The maximum deviation between my empirical model and my KFT data is  $\pm 0.31$  wt.% water. The temperature dependence could not be modeled because all solubility experiments were performed at 1250°C.

It is emphasized that this model is valid only between 100 and 500 MPa and at 1250°C. As polynomials are used in the model, an extrapolation out of this range results in a large error (for example, the calculated water solubility at zero MPa and 1250°C is 1 wt.%)

### 2.6.2 *Speciation of CO<sub>2</sub>*

A crucial problem in the evaluation of the IR spectra is the dependence of the speciation of CO<sub>2</sub> on the total water content. In figure 2.7 the contents of CO<sub>2,mol</sub> in the glass measured by IR spectroscopy are plotted versus the water content of the glasses. A very strong decrease of the CO<sub>2,mol</sub> content in the glass when adding a small amount of water can be observed. If the CO<sub>2,mol</sub>/carbonate ratio is independent of the water content, a plot of CO<sub>2,mol</sub> versus the water content (figure 2.7) in the glass should show a similar curvature as a plot of CO<sub>2,total</sub> versus water content (figure 2.8). This is not the case, the curvatures of these plots deviate strongly. Glasses with 4 wt.% water contain almost only carbonate (table 6).

The ratio of CO<sub>2,mol</sub> (measured by IR spectroscopy) to CO<sub>2,total</sub> (measured by SIMS) in the glasses strongly decreases with increasing water content (figure 2.9). This correlation is within error pressure independent. On the other hand, there is no simple pressure independent correlation of the speciation with the total CO<sub>2</sub> content (figure 2.10). For this behavior I have three possible explanations: (1) the absorption coefficient of the CO<sub>2,mol</sub> band decreases with increasing water content, (2) the speciation of CO<sub>2</sub> in the melt is not quenchable, and/or (3) the speciation of CO<sub>2</sub> is

dependent on the water content in the melt. The last two explanations are supported by data of Kohn et al. (1991) who measured the CO<sub>2</sub> speciation in a hydrous and an anhydrous albite glass by NMR spectroscopy. In the hydrous albite glass with 6 wt.% water the overall CO<sub>2,mol</sub>/carbonate ratio is much smaller than in the anhydrous glass.

Fine and Stolper (1985) suggested, that the CO<sub>2</sub> speciation is quenchable. In an IR spectroscopic study on sodium aluminosilicate glasses Fine and Stolper (1985) found that the ratio of CO<sub>2,mol</sub>/carbonate varies only little with total dissolved CO<sub>2</sub> content (0-2%), pressure (1.5-3.3 GPa) or temperature of synthesis (1400-1560°C). Fine and Stolper (1985) assumed, that the speciation of CO<sub>2</sub> measured in their glasses corresponds to the equilibrium speciation in the melt at the experimental conditions. This means that quench rates are supposed to be high enough to preserve the CO<sub>2</sub> speciation during cooling. After Fine and Stolper (1985) the CO<sub>2,mol</sub>/carbonate ratio, however, is a strong function of silicate composition, increasing both with decreasing Na<sub>2</sub>O content along the NaAlO<sub>2</sub>-SiO<sub>2</sub> join and with decreasing Na<sub>2</sub>O content in

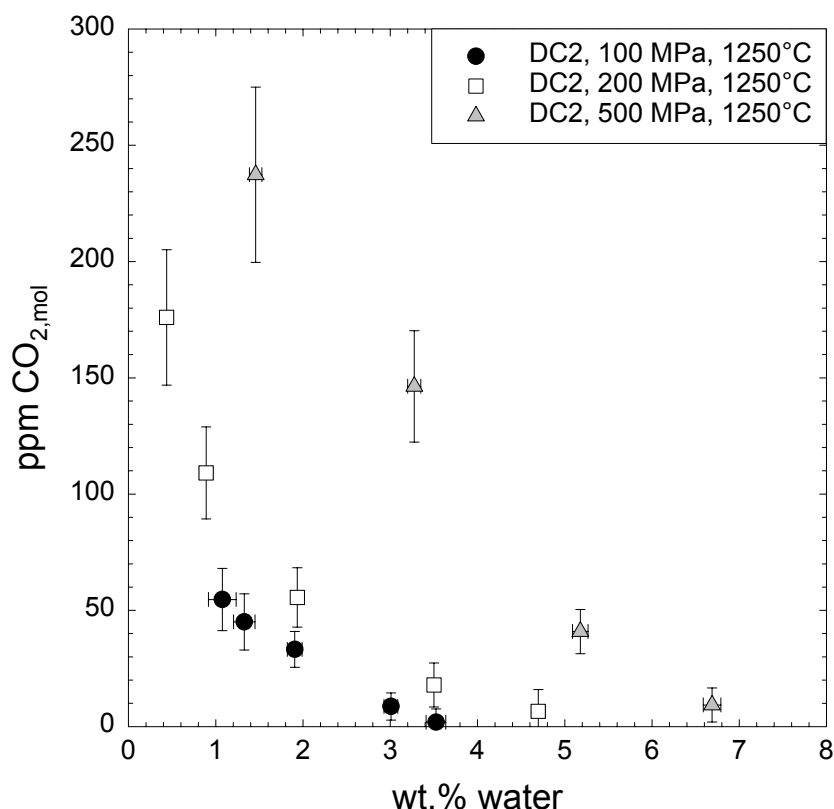


**Figure 2.7:**

Relationship between the molecular CO<sub>2</sub> content and the water content in the dacitic glass at various pressures.

peraluminous compositions of the join. Fine and Stolper (1985) saw no relationship between the ratio of molecular CO<sub>2</sub> to carbonate and the water contents of the samples that they have studied. However, the water contents of their glasses have been low; they suggested, that higher water contents may well influence the speciation of CO<sub>2</sub>.

Also in the recent study of Brooker et al. (1999) on the CO<sub>2</sub> speciation in dry glasses, the authors assume, that the CO<sub>2</sub> speciation can be at least partly preserved during quench. They state that in the case of CO<sub>2</sub> dissolution, the kinetics of the dissolution reactions appear to be virtually decoupled from the structural relaxation time scale, consistent with the growing consensus that CO<sub>2</sub> dissolution may have a limited effect

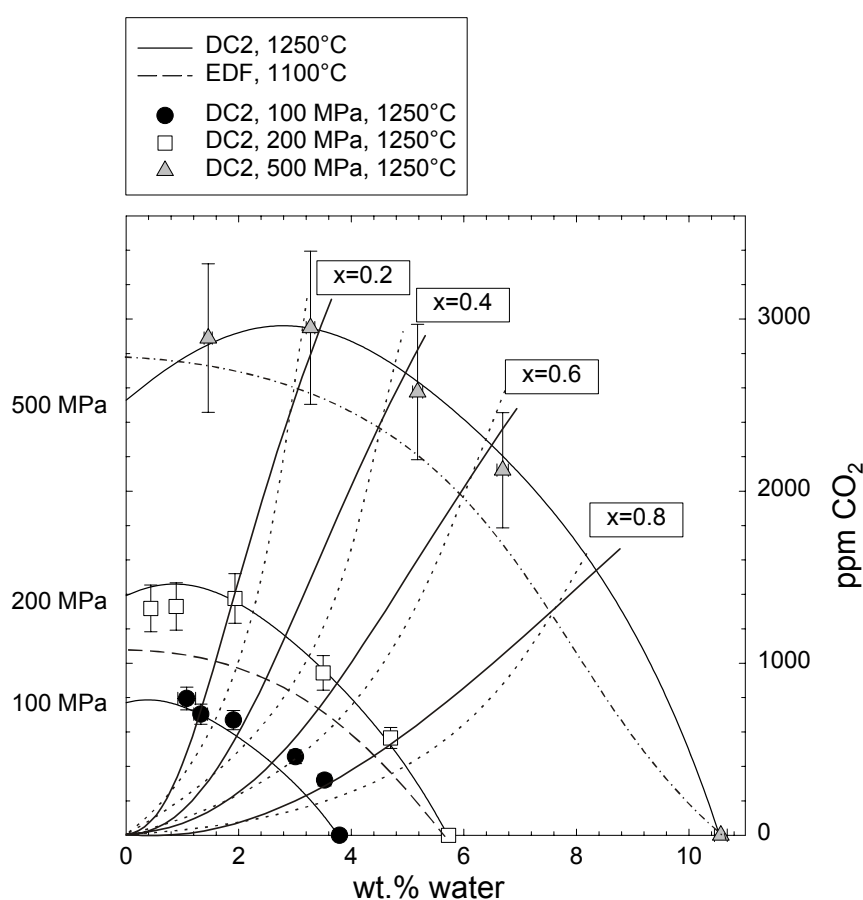


**Figure 2.8:**

Relationship between total water and CO<sub>2</sub> contents dissolved in dacitic (DC2) melts at various pressures and 1250°C. Solubility data from Tamic et al. (2001) in rhyolitic (EDF) melts at 1100°C are shown for comparison (dashed lines).

The solid lines are calculated after the empirical model for water solubilities (chapter 2.6.1.2) and the thermodynamic model for CO<sub>2</sub> solubilities (third model, chapter 2.6.3.3).

on magma viscosity (Lange, 1994), at least for highly polymerized aluminosilicate compositions.

This assumption on CO<sub>2</sub> speciation contrasts with water speciation ( $\text{H}_2\text{O} + \text{O}^{2-} = 2 \text{OH}^-$ ), which changes dramatically during quenching hydrous silicate melts (Nowak and Behrens, 2001). As outlined by Dingwell and Webb (1990), the exchange frequency of bonds between bridging oxygens and tetrahedral cations is a rate controlling step for both water species reaction and structural relaxation. It is hardly to rationalize why the relaxation of the CO<sub>2</sub> speciation reaction should be slower than the relaxation of the silicate network.

My interpretation is, that the CO<sub>2</sub> speciation in water bearing *melts* at a constant temperature may indeed be independent of the water concentration, as shown in the third model in chapter 2.6.3.3, but that the CO<sub>2</sub> speciation cannot be quenched. The CO<sub>2</sub> speciation in the glass reflects the equilibrium speciation at a fictive temperature  $T_f$ , which corresponds to a certain viscosity of the melt (at a certain cooling rate). As an increasing water content lowers the viscosity and thus lowers the fictive

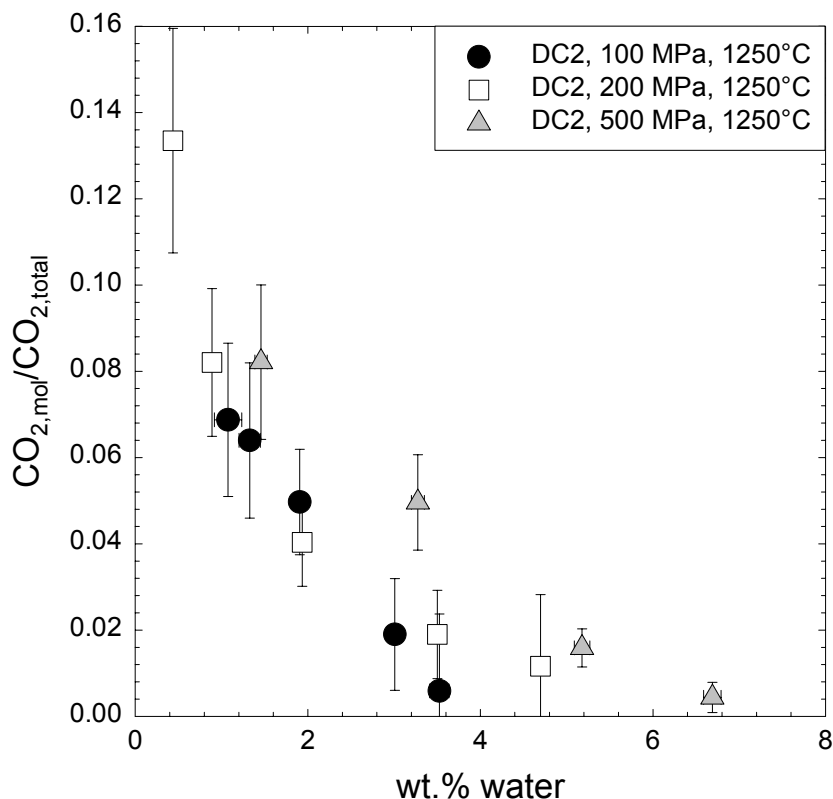


**Figure 2.9:**

Relationship between the  $\text{CO}_{2,\text{mol}}/\text{CO}_{2,\text{total}}$  ratio and the water content in the dacitic glass.

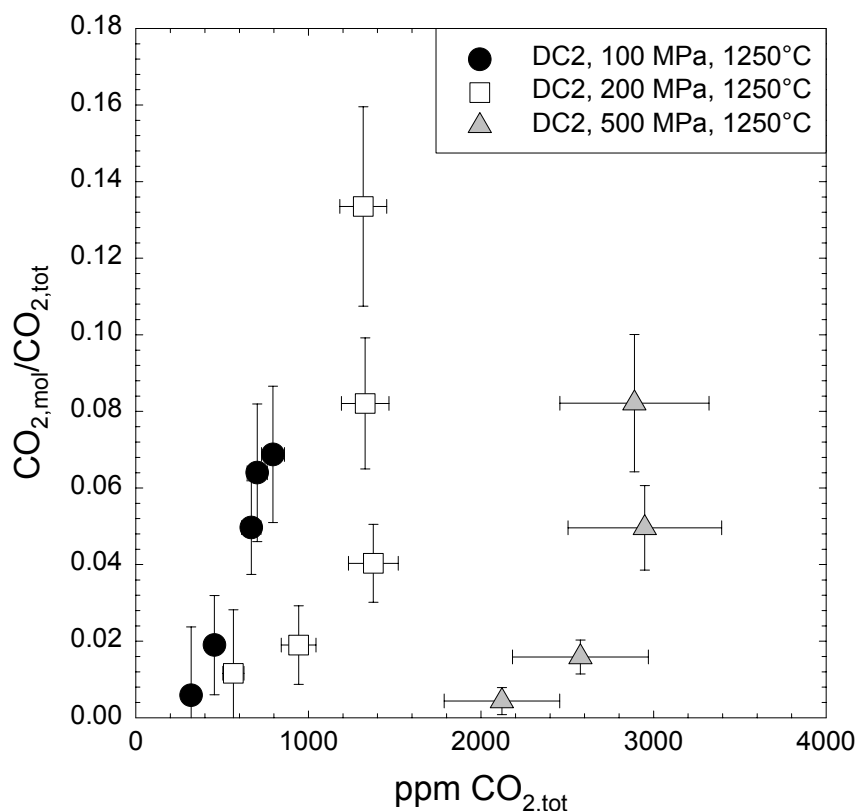


**Figure 2.10:**

Relationship between the  $\text{CO}_{2,\text{mol}}/\text{CO}_{2,\text{total}}$  ratio and the total  $\text{CO}_2$  content in the dacitic glass.

temperature, the  $\text{CO}_2$  speciation measured at ambient conditions is shifted towards carbonate with increasing water content in the glass.

This explanation is supported by data of Nowak et al. (2003) and Morizet et al. (2001). Nowak et al. (2003) have investigated the speciation of  $\text{CO}_2$  in anhydrous albitic and synthetic iron free dacitic glasses after annealing them below the glass transition temperature in the temperature range of 400-700°C at 500 MPa and rapidly quenching. Their results show that the ratio of  $\text{CO}_{2,\text{mol}}/\text{carbonate}$  increases with increasing annealing temperature for both glass compositions. An increase of the  $\text{CO}_{2,\text{mol}}/\text{carbonate}$  ratio with increasing annealing temperature (400-575°C at 0.1 MPa) was also observed by Morizet et al. (2001) in jadeite glasses.

### 2.6.3 $\text{CO}_2$ solubility

In dacitic melts the  $\text{CO}_2$  solubility does not obey Henry's Law, i.e.  $x_{\text{CO}_2,\text{total}}^{\text{melt}}$  is not proportional to  $f_{\text{CO}_2}^{\text{fluid}}$  (see figure 2.11 also for the calculation of  $x_{\text{CO}_2,\text{total}}^{\text{melt}}$  and  $f_{\text{CO}_2}^{\text{fluid}}$ ).

I want to develop a simple thermodynamic model to explain my solubility data. As I do not think, that the speciation of CO<sub>2</sub> is quenchable (see chapter 2.6.2), I do not use my speciation data measured in glasses to describe the melt. I assume that the CO<sub>2</sub> molecules, carbonate groups and oxygen atoms (and OH and H<sub>2</sub>O) mix ideally in the melt (Fine and Stolper, 1985), i.e.  $a_{CO_{2,mol}}^{melt} = x_{CO_{2,mol}}^{melt}$ ,  $a_{CO_3^{2-}}^{melt} = x_{CO_3^{2-}}^{melt}$  and  $a_{O^{2-}}^{melt} = x_{O^{2-}}^{melt}$ , where  $a_i$  and  $x_i$  refer to the activities and mole fractions of CO<sub>2,mol</sub>, carbonate (CO<sub>3</sub><sup>2-</sup>) and oxygens (O<sup>2-</sup>) in the melt. The dissolution of CO<sub>2,total</sub> can be described with two equilibria. The first is the heterogeneous equilibrium between CO<sub>2</sub> in the fluid and CO<sub>2,mol</sub> in the melt:



$$\text{with the equilibrium constant } K_1 = \frac{x_{CO_{2,mol}}^{melt}}{f_{CO_2}^{fluid}}, \quad (2.7)$$

where  $f_{CO_2}^{fluid}$ , the fugacity of CO<sub>2</sub> in the fluid phase was calculated after Aranovich and Newton (1999) using molar volumes and fugacities of pure fluids calculated after Pitzer and Sterner (1994) at the same pressure and temperature.  $x_{CO_{2,mol}}^{melt}$  is defined as

$$x_{CO_{2,mol}}^{melt} = \frac{n_{CO_{2,mol}}^{melt}}{n_{CO_{2,mol}}^{melt} + n_{CO_3^{2-}}^{melt} + n_{water}^{melt} + n_{O^{2-}}^{melt}}, \quad (2.8)$$

where  $n_i$  is the number of moles of the CO<sub>2,mol</sub>, carbonate, water or oxygen in a fixed sample volume (the mole number of oxygen corresponds to (100-wt.% H<sub>2</sub>O-wt.% CO<sub>2</sub>)/(molecular weight of the dacite calculated on one-oxygen basis)).

Secondly the homogeneous speciation reaction in the melt can be described as:



$$\text{with the equilibrium constant } K_2 = \frac{x_{CO_3^{2-}}^{melt}}{x_{CO_{2,mol}}^{melt} \cdot x_{O_r^{2-}}^{melt}}. \quad (2.10)$$

Analog to  $x_{CO_{2,mol}}^{melt}$ ,  $x_{CO_3^{2-}}^{melt}$  is defined as:

$$x_{CO_3^{2-}}^{melt} = \frac{n_{CO_3^{2-}}^{melt}}{n_{CO_{2,mol}}^{melt} + n_{CO_3^{2-}}^{melt} + n_{water}^{melt} + n_{O^{2-}}^{melt}} \quad (2.11)$$

Using these two equilibria, the total CO<sub>2</sub> content can be calculated after:

$$x_{CO_2, total}^{melt} = x_{CO_2, mol}^{melt} + x_{CO_3^{2-}}^{melt} \quad (2.12a)$$

$$= (1 + K_2 \cdot x_{O_r^{2-}}^{melt}) \cdot x_{CO_2, mol}^{melt} \quad (2.12b)$$

$$= (1 + K_2 \cdot x_{O_r^{2-}}^{melt}) \cdot K_1 \cdot f_{CO_2}^{fluid} \quad (2.12c)$$

Several authors consider all oxygens in the melt to be indistinguishable and equally available for the reaction with CO<sub>2,mol</sub> (e.g. Stolper et al., 1987). The highest amount of CO<sub>2,total</sub> measured in this study was  $x_{CO_2, total}^{melt} = 0.0022$ , which is small compared to the  $x_{O_r^{2-}}^{melt} = 1$  for dry glasses. Thus, one can consider  $x_{O_r^{2-}}^{melt}$  to be constant. Assuming that

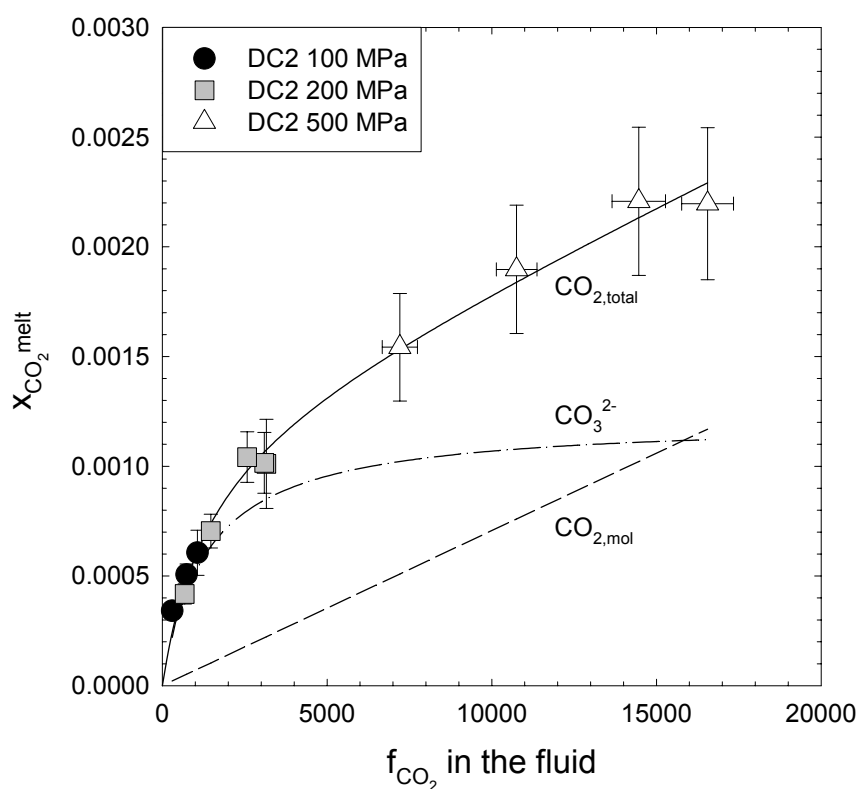


**Figure 2.11:**

CO<sub>2</sub> solubility (expressed as mole fraction  $x_{CO_2, total}^{melt}$ , calculated as  $x_{CO_2, total}^{melt} = n_{CO_2} / (n_{H_2O} + n_{CO_2, mol} + n_{CO_3^{2-}} + n_{O_2})$ , where  $n_i$  is the number of moles of CO<sub>2</sub> ( $n_{CO_2} = n_{CO_2, mol} + n_{CO_3^{2-}}$ ), H<sub>2</sub>O and oxygen) as a function of  $f_{CO_2}^{fluid}$  in the fluid phase in dacitic melts. CO<sub>2</sub> fugacities were calculated after Aranovich and Newton (1999) using molar volumes and fugacities of pure fluids calculated after Pitzer and Sterner (1994) at the same pressure and temperature.

The lines reflect CO<sub>2,total</sub>, CO<sub>2,mol</sub> and carbonate contents calculated after the first thermodynamic model (chapter 2.6.3.1).

$K_1$  and  $K_2$  are independent of the pressure and the water content in the melt, the  $x_{CO_2, total}^{melt}$  in the melt should increase linearly with increasing CO<sub>2</sub> fugacity in the fluid, independently from the speciation of CO<sub>2</sub> in the melt. This is not what my data show. Even at 100 MPa the  $x_{CO_2, total}^{melt}$  increases non-linearly with increasing  $f_{CO_2}^{fluid}$ . The non-linear dependence of the  $x_{CO_2, total}^{melt}$  on  $f_{CO_2}^{fluid}$  (at constant temperature and pressure) can be explained in two ways:

- 1) the oxygens are not indistinguishable, but consist of different kinds of bridging (Si-O-Si or Al-O-Si or Al-O-Al...) and non-bridging oxygens (attached to Si or Al). When not all oxygens are equally available for the reaction with CO<sub>2,mol</sub>, the  $x_{O_r^{2-}}^{melt}$  does not remain constant during reaction (2.9).
- 2)  $K_1$  and  $K_2$  are dependent on the water content of the melt.

### 2.6.3.1 First model

Let us first consider, that the amount of reactive oxygens is so small, that its concentration changes noticeably by reaction with CO<sub>2,mol</sub>. I assume that there is only one type of reactive oxygens O<sub>r</sub><sup>2-</sup>, so that the species reaction can still be described by equation (2.9). The concentration of reactive oxygen  $x_{O_r^{2-}}^{melt}$  can then be calculated as:

$$x_{O_r^{2-}}^{melt} = x_{O_r^{2-}, begin}^{melt} - x_{CO_3^{2-}}^{melt} \quad (2.13)$$

where  $x_{O_r^{2-}, begin}^{melt}$  is the oxygen concentration at the beginning of reaction (2.9) (when no carbonate is formed). For simplicity I assume that the concentration of reactive oxygen is independent of the water content. Inserting equation (2.13) in equation (2.10) I obtain:

$$x_{CO_3^{2-}}^{melt} = \frac{K_2 \cdot x_{CO_2, mol}^{melt} \cdot x_{O_r^{2-}, begin}^{melt}}{1 + K_2 \cdot x_{CO_2, mol}^{melt}} \quad (2.14)$$

and with equation (2.12a):

$$x_{CO_2, total}^{melt} = \frac{K_2 \cdot x_{CO_2, mol}^{melt} \cdot x_{O_r^{2-}, begin}^{melt}}{1 + K_2 \cdot x_{CO_2, mol}^{melt}} + x_{CO_2, mol}^{melt} \quad (2.15a)$$

and with equation (2.7):



$$x_{CO_2, total}^{melt} = \frac{K_2 \cdot K_1 \cdot f_{CO_2}^{fluid} \cdot x_{O_r^{2-}}^{melt}}{1 + K_2 \cdot K_1 \cdot f_{CO_2}^{fluid}} + K_1 \cdot f_{CO_2}^{fluid} \quad (2.15b)$$

$$= \frac{\left( K_1 + K_1 \cdot K_2 \cdot x_{O_r^{2-}}^{melt} \right) \cdot f_{CO_2}^{fluid} + (K_1)^2 \cdot K_2 \cdot \left( f_{CO_2}^{fluid} \right)^2}{1 + K_2 \cdot K_1 \cdot f_{CO_2}^{fluid}} \quad (2.15c)$$

This is an equation of the type

$$y = \frac{a \cdot x + b \cdot x^2}{1 + c \cdot x}$$

with  $y = x_{CO_2, total}^{melt}$ ,  $x = f_{CO_2}^{fluid}$ ,  $a = K_1 + K_1 \cdot K_2 \cdot x_{O_r^{2-}}^{melt}$ ,  $b = (K_1)^2 \cdot K_2$  and  $c = K_2 \cdot K_1$ .

A least squares fit of equation (2.15) to my CO<sub>2,total</sub> solubility data at 1250°C and various P resulted in best fit values of  $K_1 = (7 \pm 3) \cdot 10^{-8}$ ,  $K_2 = 10500 \pm 3800$  and  $x_{O_r^{2-}}^{melt} = 0.0012 \pm 0.0005$  (table 8).

The CO<sub>2,mol</sub> and CO<sub>3<sup>2-</sup></sub> contents calculated using equations (2.7) and (2.14) are shown in figure 2.11. The  $x_{CO_2, mol}^{melt}$  increases linearly with increasing  $f_{CO_2}^{fluid}$ ,  $x_{CO_3^{2-}}^{melt}$  increases strongly at low  $x_{CO_2, total}^{melt}$  and less at higher  $x_{CO_2, total}^{melt}$  and converges to a saturation concentration of  $x_{CO_3^{2-}}^{melt} = 0.0012$ . In contrast to spectroscopic CO<sub>2</sub>-speciation data in the literature (e.g. Fine and Stolper, 1985; Nowak et al., 2003), the CO<sub>2,mol</sub>/carbonate ratio is not independent of the total CO<sub>2</sub> content in this model but increases with increasing total CO<sub>2</sub>. Compared with speciation data of Nowak et al. (2003) in iron free anhydrous dacitic glasses their CO<sub>2,mol</sub>/carbonate ratio at  $x_{CO_2, total}^{melt} \ll 0.0012$  is 60 times higher than in my model, the same CO<sub>2,mol</sub>/carbonate ratio would be reached at an  $x_{O_r^{2-}}^{melt} = 2 \cdot 10^{-5}$  (1/60 of the starting concentration of reactive oxygens). Thus, using the first model, molecular CO<sub>2</sub> is underestimated at low CO<sub>2,total</sub> contents. The concentration of non-bridging oxygens (NBO) in the dry dacitic composition is  $x_{NBO}^{melt} = 0.02$  when all iron is assumed to be network forming (Fe<sup>3+</sup>) and  $x_{NBO}^{melt} = 0.05$  when all iron is assumed to be network modifier (Fe<sup>2+</sup>). ( $x_{NBO}^{melt}$  is defined as  $n_{NBO}/n_{NBO} + n_{BO} = (NBO/T)/4$ , NBO = non-bridging oxygen, BO = bridging oxygen, T= tetrahedral cation). These values are 17-42 times larger than the starting concentration of reactive oxygens determined in this model ( $x_{O_r^{2-}}^{melt} = 0.0012$ ). That would mean that only a part

of the non-bridging oxygens (e.g. only those connected to Al<sup>3+</sup>) react with CO<sub>2,mol</sub> to carbonate.

This model describes very well the trend of my data. The standard deviation between predicted and measured CO<sub>2,total</sub> contents is ±10 % relative. However, the values for K<sub>2</sub> and  $x_{O_r,begin}^{melt}$  do not fit with data in the literature as discussed above.

In addition, former studies showed, that K<sub>1</sub> is not pressure independent, but decreases with increasing pressure, i.e. for a constant temperature:

$$K_1 = K_1' \cdot \exp\left(\frac{-\bar{V}^m_{CO_2,mol}(P - P_0)}{RT}\right), \quad (2.16)$$

where K<sub>1</sub>' is the equilibrium constant at a reference pressure P<sub>0</sub>,  $\bar{V}^m_{CO_2,mol}$  is the partial molar volume of molecular CO<sub>2</sub>, T is the temperature and R is the general gas constant (Holloway and Blank, 1994).

Spera and Bergman (1980) determined the partial molar volume of total dissolved CO<sub>2</sub> at 1450-1650°C in a wide range of melt compositions (albite, jadeite, nepheline, andesite, tholeiite and olivine melilite) for which CO<sub>2</sub> solubility data were available. The average of their values for  $\bar{V}^m_{CO_2,total}$  was 33.4±0.4 cm<sup>3</sup>/mol. Similar values of  $\bar{V}^m_{CO_2,mol}$  = 33.04±0.78 cm<sup>3</sup>/mol and  $\bar{V}^m_{CO_3^{2-}} - \bar{V}^m_{O^{2-}}$  = 33.0±0.5 cm<sup>3</sup>/mol were obtained for a rhyolitic and basaltic melts, respectively (Fogel and Rutherford, 1990; Stolper and Holloway, 1988,  $\bar{V}^m_{CO_3^{2-}} - \bar{V}^m_{O^{2-}}$  is the effective partial molar volume of total CO<sub>2</sub> dissolved as carbonate in the melt), whereas Blank et al. (1993) determined a value of  $\bar{V}^m_{CO_2,total}$  = 28±2 cm<sup>3</sup>/mol in hydrous rhyolitic melts.

In my first model the effect of pressure and water content are not included, i.e. I assume, that either both effects are negligible or both effects neutralize each other. The main arguments against this model are (1) the discrepancy of resulted CO<sub>2</sub> speciation between this model and data of Nowak et al. (2003) and (2) that the effect of pressure is not included in this model. Equation (2.15c) is already very complex, it is not possible to fit a pressure dependence with this approach.

### 2.6.3.2 Second model

To include the effect of pressure and water concentration in a thermodynamic model I fall back on equation (2.12c). I assume, that the concentration of reactive oxygens is equal to the concentration of non-bridging oxygens.  $x_{NBO}^{melt}$  was calculated without considering the iron in the glass composition and including OH groups formed by reaction of H<sub>2</sub>O with bridging oxygen, assuming that the speciation of water is equal to the speciation in haplogranitic melts which was determined by Nowak and Behrens (2001) using in situ NIR spectroscopy. For example at 1250°C and for 2, 4 and 6 wt.% water content in the melt 92, 86 and 80 %, respectively, of the water is dissociated to OH. The concentration of NBO is 27-400 times higher than the concentration of total CO<sub>2</sub>, so that it is a good approximation when I consider  $x_{NBO}^{melt}$  to be constant during reaction (2.9). Additionally I assume that the partial molar volume of CO<sub>2,mol</sub> is positive and constant with pressure and that K<sub>2</sub> is independent on pressure, i.e. reaction (2.9) is not accompanied by a volume change ( $\bar{V}_{CO_2,mol}^m = \bar{V}_{CO_3^{2-}}^m - \bar{V}_{O^{2-}}^m$ ). Combining equations (2.7) and (2.16) gives:

$$x_{CO_2,mol}^{melt} = f_{CO_2}^{fluid} \cdot K'_1 \cdot \exp\left(-\bar{V}_{CO_2,mol}^m \cdot \frac{P - P_0}{RT}\right), \quad (2.17)$$

and equation (2.10) can be rewritten to:

$$K'_2 = \frac{x_{CO_3^{2-}}^{melt}}{x_{CO_2,mol}^{melt} \cdot x_{NBO}^{melt}} \quad (2.18a)$$

$$x_{CO_3^{2-}}^{melt} = K'_2 \cdot x_{NBO}^{melt} \cdot x_{CO_2,mol}^{melt}, \quad (2.18b)$$

$$= K'_2 \cdot x_{NBO}^{melt} \cdot f_{CO_2}^{fluid} \cdot K'_1 \cdot \exp\left(-\bar{V}_{CO_2,mol}^m \cdot \frac{P - P_0}{RT}\right) \quad (2.18c)$$

The concentration of the total CO<sub>2</sub> content can therefore be calculated as:

$$x_{CO_2,total}^{melt} = \left(1 + K'_2 \cdot x_{NBO}^{melt}\right) \cdot f_{CO_2}^{fluid} \cdot K'_1 \cdot \exp\left(-\bar{V}_{CO_2,mol}^m \cdot \frac{P - P_0}{RT}\right). \quad (2.19)$$

A least squares fit to equation (2.19) using a reference pressure of zero bar and my CO<sub>2,total</sub> solubility data at 1250°C and given P,  $f_{CO_2}^{fluid}$  and  $x_{NBO}^{melt}$  resulted in best fit values of  $K'_1 = (4.5 \pm 0.5) \cdot 10^{-7}$ ,  $K'_2 = 13 \pm 3$  and  $\bar{V}_{CO_2,mol}^m = 46.6 \pm 2.1 \text{ cm}^3/\text{mol}$  (table 9). The

resulting CO<sub>2,total</sub>, CO<sub>2,mol</sub> and carbonate contents are shown in figure 2.12. The value of K'<sub>1</sub> compares well with K'<sub>1</sub>=2.5\*10<sup>-7</sup> with a reference pressure of 1 bar and at 1250°C calculated after the model of Blank et al. (1993) and K'<sub>1</sub>=7,09\*10<sup>-7</sup> with a reference pressure of zero bar and at 1250°C calculated after the model of Fogel and Rutherford (1990) in rhyolitic melts.

Stolper and Holloway (1988) determined the equilibrium constant

$$K_{S\&H} = \frac{x_{CO_3^{2-}}^{melt}}{x_{CO_2,mol}^{fluid} \cdot x_{O^{2-}}^{melt}}$$

in dry basaltic melts, with a reference pressure of 100 MPa and at 1200°C which can be compared with my model when multiplying K'<sub>1</sub> (which is 3.1\*10<sup>-7</sup> when a reference pressure of 100 MPa is used), K'<sub>2</sub> and  $x_{NBO}^{melt}$  in the dry dacitic melt. The

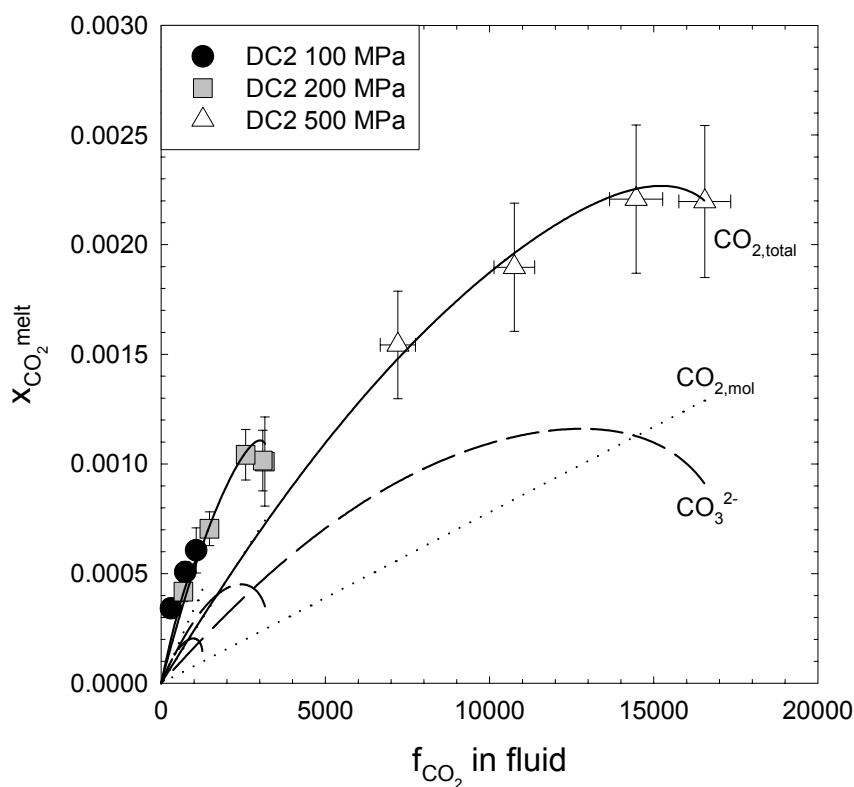


**Figure 2.12:**

CO<sub>2</sub> solubilities (expressed as mole fraction  $x_{CO_2,total}^{melt}$ ) as a function of  $f_{CO_2}^{fluid}$ . The solid lines reflect the total CO<sub>2</sub> solubilities at various pressures calculated after the second thermodynamic model for CO<sub>2</sub> solubilities.

Dashed lines are carbonate contents, and dotted lines CO<sub>2,mol</sub> contents calculated after the second thermodynamic model.

value of the equilibrium constant of Stolper and Holloway (1988) is  $K_{S\&H}=(2.63\pm 0.15)*10^{-7}$  which is in good agreement with  $K_{S\&H}=K'_1(100\text{MPa})*K'_2*x_{NBO}^{melt}=(1.28\pm 0.46)*10^{-7}$  determined by my model.

The value of  $K_2$  at 1250°C calculated using the reaction enthalpy and reaction entropy determined by Nowak et al. (2003) in iron free anhydrous dacitic glasses which were heated below the glass transition temperature is  $K_2=0.21$ . Nowak et al. (2003) assume that the oxygen concentration is constant and  $x_{O^{2-}}^{melt}=1$ . Therefore, their  $K_2$  value can be compared with my  $K'_2$  value, when dividing it with  $x_{NBO}^{melt}$ . The corrected value for the  $x_{NBO}^{melt}=0.0277$  of their melt is  $K'_2=7.6$ , which is also in a good agreement with my value of  $K'_2=13.3$ .

The partial molar volume of CO<sub>2,mol</sub> (which is the partial molar volume of total CO<sub>2</sub>, since  $\bar{V}_{CO_2,mol}^m$  is assumed to be equal to  $\bar{V}_{CO_3^{2-}}^m - \bar{V}_{O^{2-}}^m$ ) of 46.6 cm<sup>3</sup>/mol is a bit high compared to partial molar volumes of total CO<sub>2</sub> of ~33 cm<sup>3</sup>/mol determined by Fogel and Rutherford, (1990) in rhyolitic melts, Stolper and Holloway (1988) in basaltic melts and Spera and Bergman (1980) in a wide range of melt compositions (albite, jadeite, nepheline, andesite, tholeiite and olivine melilite). (I do not compare with values determined by species concentrations in glasses because the species concentration cannot be quenched). This deviation might result from the calculation of  $f_{CO_2}^{fluid}$ . I calculated  $f_{CO_2}^{fluid}$  after Aranovich and Newton (1999) using molar volumes and fugacities of pure fluids calculated after Pitzer and Sterner (1994) at the same pressure and temperature. Blank et al. (1993) and Stolper and Holloway (1988) used a modified Redlich-Kwong (Holloway, 1977) equation, Fogel and Rutherford (1990) the hard sphere modified Redlich Kwong model of Kerrick and Jacobs (1981). Pan et al. (1991) recalculated data from Stolper and Holloway (1988) with a Saxena and Fei (1987) equation which resulted in a change of  $\bar{V}_{CO_3^{2-}}^m - \bar{V}_{O^{2-}}^m$  from 33.0 to 27.7 cm<sup>3</sup>/mol.

The second model predicts my data only slightly less precise than the first model. The standard deviation between predicted and measured  $x_{CO_2,total}^{melt}$  data is 13 % relative. At 100 MPa this model systematically underestimates the CO<sub>2</sub> solubility (see figure 2.12). At 200 and 500 MPa the deviation between predicted and measured data is not

systematic. The deviation at 100 MPa can be due to a pressure dependence of the partial molar volume.

It is remarkable, that a decrease of the CO<sub>2,total</sub> solubility at  $x_{CO_2}^{fluid} > 0.8$  can be described by my second model (see figure 2.5 and 2.12). It predicts a very strong decrease of CO<sub>2</sub> solubilities in melts with  $x_{CO_2}^{fluid}$  higher and thus water contents lower than in my samples (see figure 2.8). This strong decrease is consistent with CO<sub>2</sub> solubility data of King and Holloway (2002) and Mysen et al. (1976). King and Holloway (2002) found an increase of CO<sub>2</sub> solubility in hydrous andesitic melts by about 600 ppm per wt.% water (from 3100 ppm to 5800 ppm) at 1 GPa and 1300°C and up to 3.4 wt.% water. Mysen et al. (1976) measured CO<sub>2</sub> solubilities in albite, jadeite and nepheline compositions. The highest CO<sub>2</sub> solubility were not found for the pure CO<sub>2</sub> fluid but at  $x_{CO_2}^{fluid} < 1$ . However, as discussed by Blank and Brooker (1994), there may be substantial errors with the <sup>14</sup>C β-track autoradiography which was used by Mysen et al. (1976) as the analytical method for carbon determination. On the other hand this strong decrease contrasts with CO<sub>2</sub> solubility data by Tamic et al. (2001) in rhyolitic melts. I do not recommend to use this model at  $x_{CO_2}^{fluid} > 0.95$ . Nevertheless, the good agreement of my fit parameters to values in the literature shows, that my model is a good approximation.

After this model the CO<sub>2,mol</sub>/carbonate ratio in the melt decreases with increasing  $x_{NBO}^{melt}$  and thus with increasing water concentration in the melt. The carbonate concentration in the melt decreases especially at high  $x_{CO_2}^{fluid}$  (with increasing  $x_{CO_2}^{fluid}$  and thus decreasing water concentration), because in this region the linear dependence of the water solubility on  $x_{CO_2}^{fluid}$  (and thus  $x_{H_2O}^{fluid}$ ) turns over to a square root dependence (figure 2.6). This is the reason why a slightly decreasing CO<sub>2</sub> solubility is observed at  $x_{CO_2}^{fluid} > 0.8$  (figure 2.5 and 2.8).

If this model is true and also applicable to melts with other dry compositions, I would expect to measure carbonate in hydrous rhyolitic melts and glasses, which were synthesized at high enough pressures to obtain high water contents at simultaneously high  $x_{CO_2}^{fluid}$ . (The CO<sub>2</sub> speciation shifts towards carbonate during quench (see chapter 2.6.2), so that carbonate should be also visible in quenched glasses). The same NBO/T

in a hydrous rhyolitic melt as in a dry dacitic melt is reached at a water content of only ~1.5 wt.% water. However, Tamic et al. (2001) did not observe any carbonate bands in hydrous rhyolitic glasses which were synthesized at pressures up to 500 MPa (glasses with more than 2000 ppm CO<sub>2</sub> contained up to 5.2 wt.% water).

### 2.6.3.3 Third model

In the second model I assumed the incorporation of carbonate (and thus K<sub>2</sub>) to be dependent on the water content, because water enhances the concentration of NBO. It is also possible, that water can stabilize the incorporation of CO<sub>2,mol</sub> (and thus influences K<sub>1</sub>), e.g. water can expand the silicate network and therefore can produce additional sites for the incorporation of CO<sub>2,mol</sub>.

In the third model I consider the CO<sub>2,mol</sub>/carbonate ratio to be independent of the water content in the melt. Instead I assume, that the amount of total CO<sub>2</sub> (and thus K<sub>1</sub>) is dependent on the concentration of water in the melt. K<sub>2</sub> is according to this model only dependent on the dry composition of the melt, the fact that carbonate cannot be detected in rhyolitic melts can be explained by a equilibrium constant K<sub>2</sub> which is very small.

I consider all oxygens to be equally available for the reaction with CO<sub>2,mol</sub>. Thus, the concentration of reactive oxygens can be treated to be constant because the highest amount of CO<sub>2,total</sub> in this study was  $x_{CO_2,total}^{melt} = 0.0022$ , which is small compared to the  $x_{O^{2-}}^{melt} = 1$ . I assume like in the second model, that reaction (2.9) is not accompanied by a volume change ( $\bar{V}_{CO_2,mol}^m = \bar{V}_{CO_3^{2-}}^m - \bar{V}_{O^{2-}}^m$ ). The dependence of K<sub>1</sub> on the water content is described by an exponential relationship ( $K_1'' = K_1' \cdot \exp(k \cdot x_{water}^{melt})$ ). The explanation for this empirical approach is that kinetic properties (such as diffusivity) often were found to vary exponentially with compositional parameters (e.g. Ar diffusion in rhyolitic melts, Behrens and Zhang, 2001).

Equation (2.17) can be rewritten to:

$$x_{CO_2,mol}^{melt} = f_{CO_2}^{fluid} \cdot K_1'' \cdot \exp(k \cdot x_{water}^{melt}) \cdot \exp\left(-\bar{V}_{CO_2,mol}^m \cdot \frac{P - P_0}{RT}\right), \quad (2.20)$$

where  $x_{water}^{melt}$  is the mole fraction of water in the melt which was calculated as:

$$x_{\text{water}}^{\text{melt}} = \frac{n_{\text{water}}^{\text{melt}}}{n_{\text{water}}^{\text{melt}} + n_{\text{O}^{2-}}^{\text{melt}}}$$

(the CO<sub>2</sub> content in the melt was neglected for this calculation).

With equation (2.10) the carbonate content is then:

$$x_{\text{CO}_3^{2-}}^{\text{melt}} = K_2 \cdot x_{\text{O}^{2-}}^{\text{melt}} \cdot x_{\text{CO}_2, \text{mol}}^{\text{melt}}, \quad (2.21a)$$

$$= K_2 \cdot x_{\text{O}^{2-}}^{\text{melt}} \cdot f_{\text{CO}_2}^{\text{fluid}} \cdot K_1'' \cdot \exp(k \cdot x_{\text{water}}^{\text{melt}}) \cdot \exp\left(-\bar{V}_{\text{CO}_2, \text{mol}}^m \cdot \frac{P - P_0}{RT}\right) \quad (2.21b)$$

The concentration of total CO<sub>2</sub> content can be calculated as:

$$x_{\text{CO}_2, \text{total}}^{\text{melt}} = \left(1 + K_2 \cdot x_{\text{O}^{2-}}^{\text{melt}}\right) \cdot f_{\text{CO}_2}^{\text{fluid}} \cdot K_1'' \cdot \exp(k \cdot x_{\text{water}}^{\text{melt}}) \cdot \exp\left(-\bar{V}_{\text{CO}_2, \text{mol}}^m \cdot \frac{P - P_0}{RT}\right) \quad (2.22)$$

I constrained the ratio of CO<sub>2,mol</sub>/carbonate to be the same, as determined by Nowak et al. (2003) in iron free dacitic glasses. The value of K<sub>2</sub> at 1250°C calculated (and extrapolated) using the reaction enthalpy and entropy determined in the by Nowak et al. (2003) temperature range 400-700°C is K<sub>2</sub>=0.21.

Using my solubility data in dacitic melts at 1250°C and given P,  $f_{\text{CO}_2}^{\text{fluid}}$  and with K<sub>2</sub>=0.21, I have obtained the values  $K_1''=(5.6\pm 0.4)*10^{-7}$ ,  $k=5.3\pm 0.6$  and  $\bar{V}_{\text{CO}_2, \text{mol}}^m=45.7\pm 2.1$  cm<sup>3</sup>/mol for the unknown parameters in equation (2.22) by least squares (table 10). The values of  $K_1' = K_1'' / \exp(k \cdot x_{\text{water}}^{\text{melt}})$  which ranges between  $5.4*10^{-7}$  and  $2.2*10^{-7}$  for the range of water contents in this study and  $\bar{V}_{\text{CO}_2, \text{mol}}^m$  are similar as in the second model. The standard deviation between measured and predicted data is ± 14.5 % relative. Both the second and the third model are good approximations. The resulting fittings curves of  $x_{\text{CO}_2, \text{total}}^{\text{melt}}$  versus  $f_{\text{CO}_2}^{\text{fluid}}$  are similar for both the second and the third model (figures 2.12 and 2.13).

Thus, if only the total CO<sub>2</sub> concentration is known, thermodynamic modeling cannot be used to predict the CO<sub>2</sub> species concentration at run temperature. There are no in situ measurements of the CO<sub>2</sub> speciation in water bearing melts in the literature, which would make it possible to state whether the ratio of CO<sub>2,mol</sub>/carbonate changes with the water content in the melt or not.



The fact that carbonate cannot be detected in CO<sub>2</sub> bearing hydrous glasses can also be attributed to the fact that the absorption coefficients and thus the intensities of the carbonate bands are too small to resolve these bands. In fact, the absorption coefficients of CO<sub>2,mol</sub> and carbonate bands in glasses on the NaAlO<sub>2</sub>-SiO<sub>2</sub> join decrease with increasing SiO<sub>2</sub> content (Brooker et al., 1999). For example the absorption coefficient of the carbonate band at 1600 cm<sup>-1</sup> in nepheline (Na<sub>2</sub>O-Al<sub>2</sub>O<sub>3</sub>-2SiO<sub>2</sub>) is 282±20 l mol<sup>-1</sup> cm<sup>-1</sup>, in the 1 bar eutectic silica-albite composition (Na<sub>2</sub>O-Al<sub>2</sub>O<sub>3</sub>-8SiO<sub>2</sub>) it is 155 l mol<sup>-1</sup> cm<sup>-1</sup>, and in pseudorhyolite (Na<sub>2</sub>O-Al<sub>2</sub>O<sub>3</sub>-12SiO<sub>2</sub>) it is about 30 l mol<sup>-1</sup> cm<sup>-1</sup>. Additionally the carbonate bands are superimposed by the water attributed band at 1630 cm<sup>-1</sup>. Thus, it is possible, that CO<sub>2,total</sub> in hydrous rhyolitic melts has to be present in concentrations higher than 2000 ppm before carbonate may be detected by IR spectroscopy.

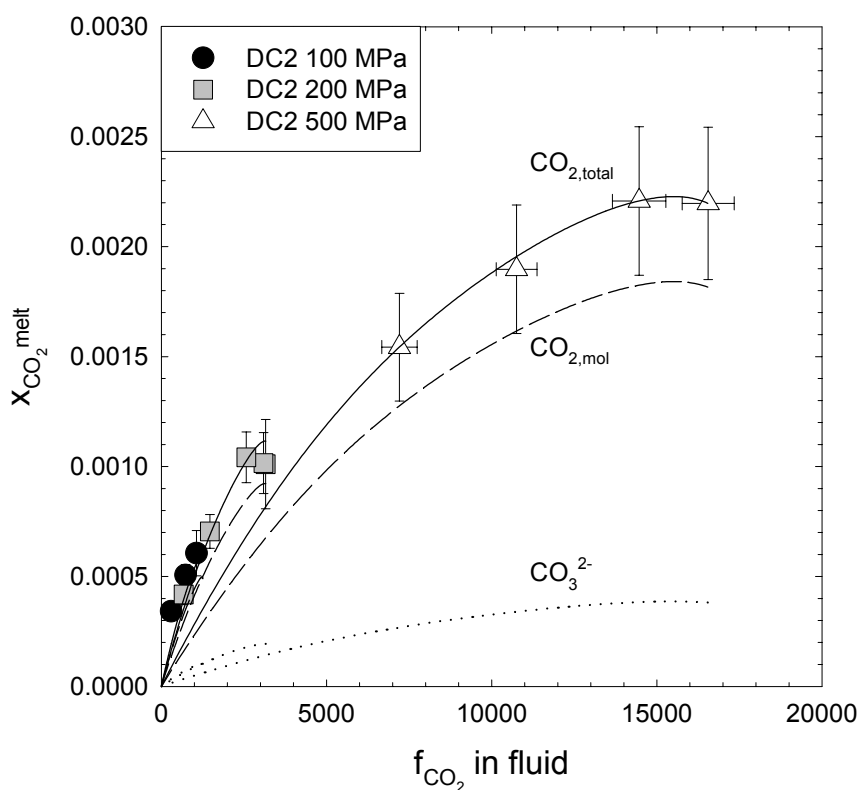


**Figure 2.13:**

CO<sub>2</sub> solubilities (expressed as mole fraction  $x_{CO_2,total}^{melt}$ ) as a function of  $f_{CO_2}^{fluid}$ . The solid lines reflect the total CO<sub>2</sub> solubilities at various pressures and water contents calculated after the third thermodynamic model for CO<sub>2</sub> solubilities. Dashed lines are carbonate contents, and dotted lines CO<sub>2,mol</sub> contents calculated after the third thermodynamic model.

### 2.6.3.4 Comparison of CO<sub>2</sub> solubilities in the dacitic with a rhyolitic composition

In figure 2.5 solubility data of total CO<sub>2</sub> at various  $x_{CO_2}^{fluid}$  in dacitic melts at 1250°C are compared with data in rhyolitic melts at 1100°C (200 and 500 MPa, Tamic et al., 2001) and 850°C (75 MPa, Blank et al., 1993). At 500 and 200 MPa (and also for interpolation to 100 MPa) the solubility of CO<sub>2</sub> is higher in dacitic than in rhyolitic melts. Note however, that I compare solubility data in dacite at 1250°C with solubility data in rhyolite at 1100°C. At 200 MPa Tamic et al. (2001) observed no obvious effect of temperature between 800 and 1100°C on the CO<sub>2</sub> solubility. At 500 MPa they found an increase of the CO<sub>2</sub> solubility from 800 to 1100°C. At an  $x_{CO_2}^{fluid} = 0.5$  and 500 MPa the CO<sub>2</sub> solubility increases in rhyolitic melts by 330 ppm with increasing temperature from 800 to 1100°C (Tamic et al., 2001). If I assume a linear temperature dependence of the CO<sub>2</sub> solubility, the value for 1250°C at an  $x_{CO_2}^{fluid} = 0.5$  would be ~2500 ppm. That means the solubilities of CO<sub>2</sub> in dacitic and rhyolitic melts at 1250°C would be approximately the same at 500 MPa. Thus, at 200 MPa the CO<sub>2</sub> solubility is higher in dacite than in rhyolite, whereas at 500 MPa the CO<sub>2</sub> solubility is similar in rhyolite and dacite.

The data of Tamic et al. (2001) shows only a constant, but not a decreasing CO<sub>2</sub> solubility at low water contents and thus low  $x_{H_2O}^{fluid}$ . I do not have enough data points to be sure whether this decrease of CO<sub>2</sub> solubility at low water contents, which is predicted by my second and third model is real or not.

## 2.7 Implication (Degassing)

My C-H-O solubility data shown in figure 2.8 can be used to determine the total pressure at which dacitic melts with given concentrations of CO<sub>2</sub> and H<sub>2</sub>O would be fluid saturated (and start to degas) at 1250°C and to determine the fluid composition ( $x_{H_2O}^{fluid}$ ) of the coexisting fluid with such a melt at equilibrium. A dacitic melt containing for example 1000 ppm CO<sub>2</sub> and 4 wt.% water would be saturated at 200 MPa (see figure 2.8). The composition of the degassing fluid phase would be  $x_{H_2O}^{fluid} = 0.6$ .

In figure 2.8 the combined CO<sub>2</sub> and water solubilities in dacitic melts at 1250°C are compared with solubilities in rhyolitic melts at 1100°C. The values for water solubilities in CO<sub>2</sub> free melts are the same for rhyolitic and dacitic melts at 200 and 500 MPa (contrary to data shown in figure 2.6), because data for dacite at 1250°C are

compared with data for rhyolite at 1100°C. At 500 MPa and 1250°C the water solubility in rhyolite is higher than in dacite (see figure 2.6), because of a positive temperature dependence of the water solubility in rhyolitic melts (Tamic et al., 2001). At 200 MPa the water solubility in rhyolite is slightly lower than in dacite, because of a negative temperature dependence.

The values for CO<sub>2</sub> solubilities in dacitic melts (1250°C) are higher than in rhyolitic melts (1100°C) at (100,) 200 and 500 MPa. The temperature dependence of the CO<sub>2</sub> solubility in rhyolitic melts is positive at 500 MPa and small and slightly negative at 200 MPa (Tamic et al., 2001). Hence, at 500 MPa and 1250°C the compositional dependence of the CO<sub>2</sub> solubility is small, whereas at 200 MPa a compositional dependence clearly exists. An explanation for this is, that the dissolved water content which is higher at 500 MPa than at 200 MPa compensates the effect of the dry composition.

A rhyolitic melt containing the same CO<sub>2</sub> and water contents as in the example above (1000 ppm CO<sub>2</sub> and 4 wt.% water) would be saturated at 1100°C at a pressure of approximately 250 MPa (see figure 2.8). The composition of the degassing fluid phase would be around  $x_{H_2O}^{fluid}=0.5$ .

Typically the temperature in magma chambers is lower than 1250°C (800-1000°C). I expect the same trend (compositional dependence) at lower temperatures, because I expect the temperature dependence of water and CO<sub>2</sub> solubility to be the same in dacitic melts as in rhyolitic melts. One argument for this is, that I have quench bubbles in samples synthesized at 500 MPa, which indicates a positive temperature dependence of the CO<sub>2</sub>-H<sub>2</sub>O solubility at 500 MPa similar to rhyolitic melts. At 100 and 200 MPa I observed no quench bubbles, which indicates no or a negative temperature dependence.

Hence, a rhyolitic melt is saturated at higher depths than dacitic melts and the fluid coexisting to rhyolitic melts contains more CO<sub>2</sub> when compared to fluids coexisting with dacitic melts. Degassing of dacitic melts containing CO<sub>2</sub> and water can be triggered both by decompression and by crystallization which shifts the composition of the melt towards rhyolitic composition and increases the volatile content of the melt.

### **3 THE EFFECT OF THE COMPOSITION ON THE WATER SOLUBILITY AND APPLICATIONS TO DEGASSING**

#### **3.1 Introduction**

The third chapter is an extension of the second chapter. Thus, see chapter 2 for a detailed introduction. In this study I investigated the effect of the glass composition on the water solubility in rhyolitic to basaltic melts.

The solubilities of H<sub>2</sub>O and CO<sub>2</sub> and the nature of their mixing behavior have been determined in a dacitic liquid (composition of the Unzen volcano, Japan) at 1250°C and 100 to 500 MPa, see chapter 2. One application of the experimental results presented in chapter 2 and 3 is the quantification of the behavior of volatiles during degassing. In this study I present a method for determining the pressure of equilibration between vapor and melt and the composition of a vapor phase that could coexist with a given dacitic melt. I also present new forward degassing models that can be used to predict melt and vapor compositions and vesicularity as a function of pressure and pre-eruptive volatile contents of dacitic magmas.

#### **3.2 Experimental and analytical**

For the investigation of water solubilities eight natural compositions characteristic for the differentiation from basalt to rhyolite were used (figure 3.1, table 1). The compositions used in this study were B1 (averaged MOR basalt, Berndt, 2002), PU (Pre-Unzen andesite, Chen et al., 1993), DC (dacite of the Unzen volcano, Chen et al., 1993), DC2 a newly synthesized glass with a composition close to DC, GMS (the rhyodacitic groundmass of the Unzen volcano, Sato et al., 1997), EGL (the residual melt of a crystallization experiment with DC, 6 wt.% water at 850°C, 200 MPa, Sierralta, personnel communication), EDF (Erevan Dry Fountain, Armenia, Bagdassov and Dingwell, 1993; Withers and Behrens, 1999; Tamic et al., 2001), and IGL (interstitial glass, residual melt of the Unzen magma, Nakada and Motomura, 1995).

Water solubility experiments were performed using the same procedure described in chapter 2.3.2. Small glass pieces were loaded with excess water and oxalic acid in Au or Au<sub>80</sub>Pd<sub>20</sub> capsules which were subsequently welded shut. Experiments were

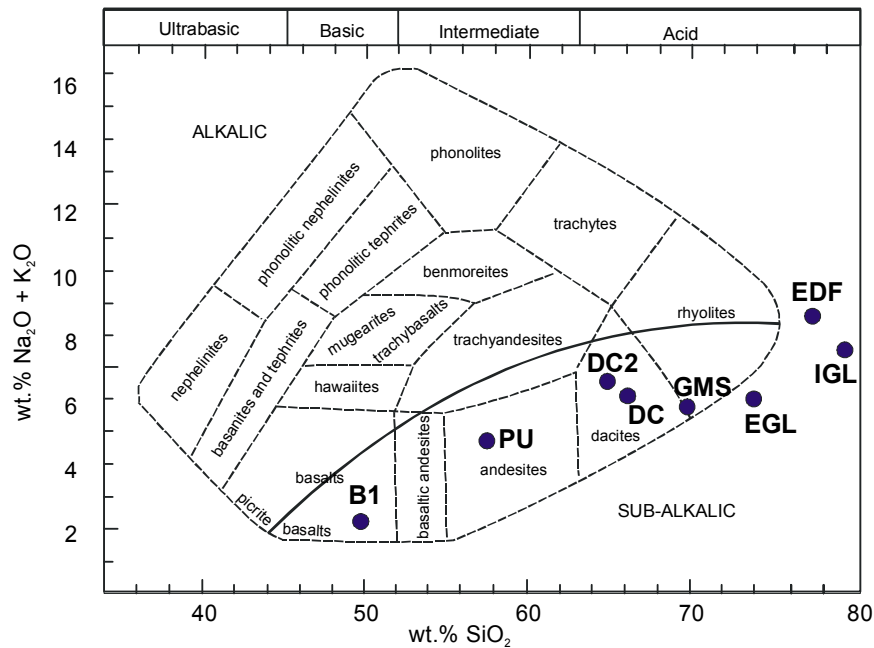


**Figure 3.1:**

Starting glasses (see also table 1) range from basaltic to rhyolitic compositions.

performed at 1000 - 1250°C and 50 - 500 MPa for 15-334 h (see table 11) at intrinsic oxygen fugacity in internally heated pressure vessels equipped with a rapid-quench device (quench rate  $\sim 150^\circ\text{C}/\text{s}$ , see chapter 2), except for experiments at 1000°C which were quenched by switching off the furnace, resulting in an initial cooling rate of  $\sim 200^\circ\text{C}/\text{min}$ , decreasing to  $\sim 100^\circ\text{C}/\text{min}$  around the glass transition. See chapter 2.3 for more details.

The analytical techniques were described in chapter 2. The fluid composition after the experiment was determined by gravimetry (chapter 2.4.1). Karl-Fischer Titration (KFT, chapter 2.4.2) was used to measure the water content in samples which were equilibrated with pure water. GMS samples which were equilibrated with a mixed  $\text{H}_2\text{O}-\text{CO}_2$  fluids were additionally analyzed by NIR spectroscopy (chapter 2.4.4).

### 3.3 Results and Discussion

#### 3.3.1 Description of run products

Due to a slower quench rate ( $\sim 200^\circ\text{C}/\text{min}$ ) in the experiments performed at 1000°C, samples 24-28 have quench crystals. Usually crystallization would lead to an oversaturation of the melt and therefore degassing. As the time scale of crystallization

### 3. The effect of the composition on the water solubility and applications to degassing

---

is short, diffusion of water out of the sample is negligible. Therefore water contents which are measured in the glass with Karl-Fischer Titration are believed to be equal to the water contents dissolved in the melt.

All the other samples which were quenched rapidly from higher temperature are bubble- and crystal-free.

#### 3.3.2 *NIR spectroscopic determination of water contents*

NIR spectroscopy was used to determine the water content in the GMS glasses. The concentrations of H<sub>2</sub>O and OH were determined from the heights of the baseline corrected absorption bands at ~5200 and ~4500 cm<sup>-1</sup>, respectively by using the Lambert-Beer law.

Densities of rhyodacitic glasses (GMS) were assumed to be intermediate between rhyolitic (EDF, Tamic et al., 2001) and dacitic (DC, chapter 1.3.2) glasses and were calculated assuming a linear relationship between densities and the content of the SiO<sub>2</sub> component in the compositional range from rhyolitic to dacitic at a given water content. The resulting relationship for densities (in g/l) in rhyodacitic glasses is:

$$\rho = -12.9 \cdot c_{\text{water}} + 2421 ,$$

where  $c_{\text{water}}$  is the water content in the glass in wt.%. This relationship is consistent with the density measurement in a rhyodacitic glass sample with 5.8 wt.% water which deviates only by 0.2 % relative.

I used the combination of two gaussians fitted to the iron-related band at ~5700 cm<sup>-1</sup> and the water-related band at ~4000 cm<sup>-1</sup> as a baseline (see chapter 1 for more detail). I fit a gaussian at ~5700 cm<sup>-1</sup> without fixing the peak position as described in chapter 2.

I determined linear absorption coefficients for the H<sub>2</sub>O band at ~5200 cm<sup>-1</sup> and the OH band at ~4500 cm<sup>-1</sup> by using peak heights measured in five samples with known water contents (measured by KFT) and assuming, that the ratio of  $\epsilon_{\text{H}_2\text{O}}/\epsilon_{\text{OH}}$  is identical to that determined by Withers and Behrens (1999), as it is also for dacitic to basaltic compositions investigated in this study, see chapter 1 for more detail. The determined absorption coefficients are  $\epsilon_{\text{H}_2\text{O}} = 1.30 \text{ l mol}^{-1} \text{ cm}^{-1}$  and  $\epsilon_{\text{OH}} = 1.48 \text{ l mol}^{-1} \text{ cm}^{-1}$ , respectively.

### 3. The effect of the composition on the water solubility and applications to degassing

---

These absorption coefficients are 4.8 % relatively higher than those calculated after the absorption coefficient - SiO<sub>2</sub> content relationship given in chapter 1.5.1. This deviation is consistent with observations for the dacitic composition and is attributed to the modifications of the IR spectrometer during this work (see chapter 1.5.3 for more detail).

Supplementary effects might be because GMS has a lower Na<sub>2</sub>O + K<sub>2</sub>O content than the compositions used for the calibration in chapter 1 (the latter compositions lie on a straight line in a diagram of wt.% Na<sub>2</sub>O and K<sub>2</sub>O versus wt.% SiO<sub>2</sub> (see figure 3.1)). But also other compositional parameters can have an effect on the absorption coefficients, e.g. the ratio of Na/K, the excess of alkali to aluminum or the concentration of alkaline earth elements (e.g. Stolper, 1982; Silver et al., 1990; Behrens et al., 1996). The densities were not directly measured but calculated. The new calibrated absorption coefficients can counterbalance the error made due to the density calculation.

The highest deviation between water contents measured with KFT and IR spectroscopy using the new calibration is 2.8 % relative (in the five samples used for the calibration).

#### 3.3.3 *Water solubilities, $x_{H_2O}^{fluid} = 1$*

Water solubilities increase with increasing pressure (figure 3.2, table 11). Water solubility increases from the rhyolitic to the dacitic composition but decreases from the dacitic to the basaltic composition in the pressure range of 50 - 200 MPa. At 200 MPa a negative temperature dependence is observed in rhyolitic to dacitic compositions between 1200°C and 1000°C.

At 500 MPa and 1250°C the water solubilities in dacitic and rhyodacitic melts are lower than in rhyolitic melts (figure 3.3). In this figure the water solubility in the rhyolitic melt at 1250°C is calculated after an empirical model developed by Tamic et al. (2001), but also the water solubility measured at 1100°C in rhyolitic melt (Tamic et al., 2001) is higher than the solubility in dacitic and rhyodacitic melts.

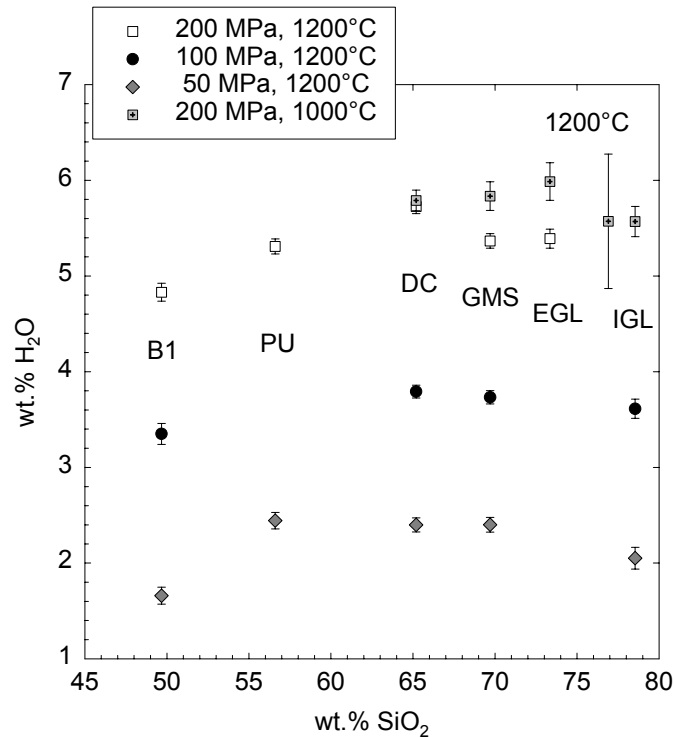


**Figure 3.2:**

Water solubilities of basaltic to rhyolitic melts equilibrated with pure water at 50 - 200 MPa and 1000 - 1200°C. Solubility experiments in the basaltic (B1) composition were performed by Berndt (2002).

### 3.3.4 Water solubilities $0 \leq x_{H_2O}^{fluid} \leq 1$

Water solubilities of GMS glasses which were equilibrated with mixed H<sub>2</sub>O-CO<sub>2</sub> fluids at 100 and 200 MPa and 1250°C are equal to corresponding solubility data in dacitic melts within error (figure 3.3). At 500 MPa and  $x_{H_2O}^{fluid}$  lower than ~0.8 (corresponding to 8 wt.% water) the solubility increases from the rhyolitic over the rhyodacitic to the dacitic composition whereas at  $x_{H_2O}^{fluid}$  higher than ~0.8 the water solubility is higher in rhyolitic than in rhyodacitic and dacitic melts.

## 3.4 Discussion

The maximum of the water solubility ( $x_{H_2O}^{fluid} = 1$ ) around the dacitic composition shows, that opposing effects influence the water solubility.

From the rhyolitic composition to the basaltic composition the amount of non-bridging oxygens (NBO) increases, the concentration of monovalent cations ( $M^+ = Na, K$ )



### 3. The effect of the composition on the water solubility and applications to degassing

decreases and the concentration of divalent cations ( $M^{2+} = \text{Ca, Mg, Fe}$ ) increases (figure 3.4).

One could argue, that the incorporation of water is favored with an increasing amount of NBO, because molecular water reacts with non-bridging oxygens to form hydroxyl groups. Indeed, the OH/H<sub>2</sub>O ratio in quenched glasses increases from the rhyolitic and dacitic to the andesitic and basaltic composition (chapter 1.5.4), but this behavior was explained by a lower glass transition temperature in hydrous rhyolitic (and dacitic) than in hydrous andesitic (and basaltic) melts (chapter 1.5.4). The fictive temperatures could be calculated for rhyolitic and andesitic melt compositions for which the viscosity in dependence of the temperature and the water content is known (Ohlhorst et al., 2000). The resulting data show, that at a given (fictive) temperature the OH/H<sub>2</sub>O

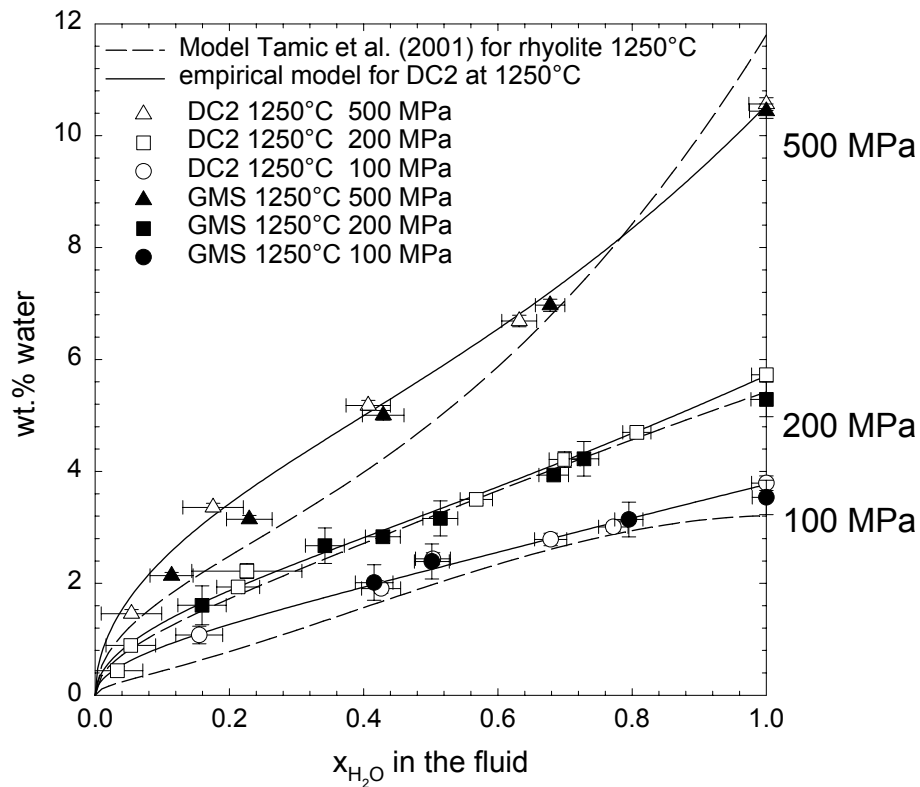


**Figure 3.3:**

Relationship between the mole fraction of H<sub>2</sub>O in the fluid phase and the concentration of total water dissolved in dacitic to rhyolitic melts at 1250°C and various pressures.

Solid lines are the fits of the solubility data in the dacitic composition used for the empirical model developed in this study (chapter 2.6.1.2). For comparison data for rhyolitic melts calculated after the model of Tamic et al. (2001) are shown (dashed lines).

### 3. The effect of the composition on the water solubility and applications to degassing

ratio is similar in rhyolitic and andesitic melts. It should be mentioned, that the composition of andesite is different in the viscosity and in the water speciation study.

An additional explanation is that the water solubility is influenced by the ratio of monovalent cations to divalent cations. Due to a higher ionic field strength ( $z/r^2$  by Dietzel, 1942;  $z$ =cation charge,  $r$ =ionic radius) divalent cations form stronger complexes with OH groups, H<sub>2</sub>O molecules and bridging or non-bridging oxygens than monovalent cations (see figure 3.4 for concentrations of mono- and divalent cations). This favors the incorporation of water until the coordination sphere is saturated with hydrous species (or oxygens). Thus, at low water fugacities (low pressures and/or low  $x_{H_2O}^{fluid}$ ) the water solubility increases with increasing  $M^{2+}/M^+$  ratio from the rhyolitic to the dacitic composition.

Because of the higher ionic field strength of divalent cations compared to monovalent cations the network is more contracted, which results in a decrease of the ionic

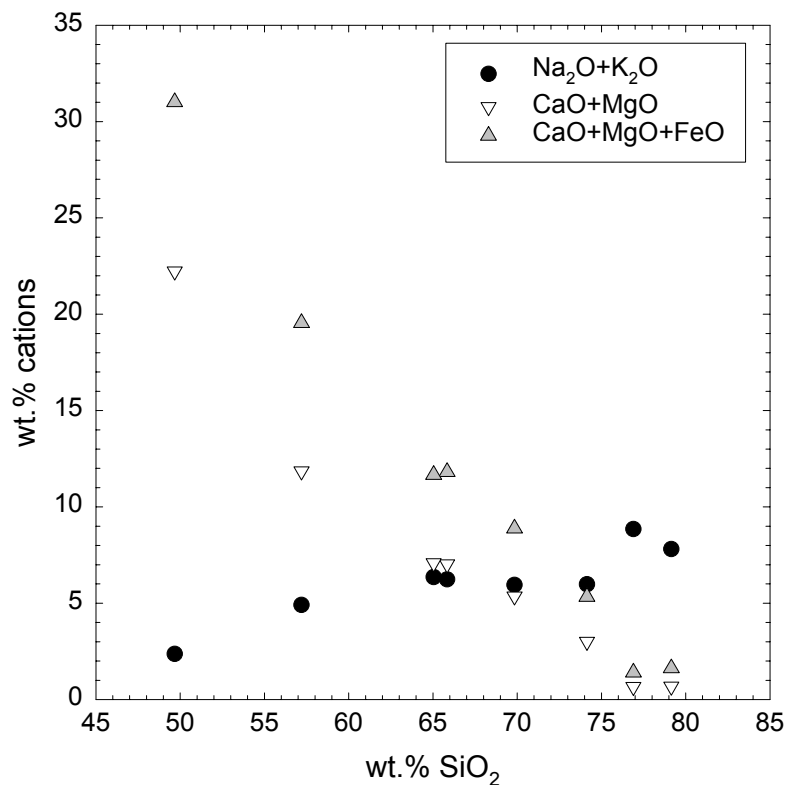


**Figure 3.4:**

The variation of the concentration of monovalent (K, Na) and divalent (Ca, Mg, Fe) cations in basaltic to rhyolitic compositions used in this study.

Compositions from left to right: B1, PU, DC2, DC, GMS, EGL, EDF, IGL. See table 1 and figure 3.1 for more compositional detail.

porosity in the melt. A decrease of ionic porosity can also be observed in the glasses (calculated after Dowty (1980) from chemical composition and density of the anhydrous glasses). It decreases from 54.6% (EDF) to 53.8% (DC) to 52.4% (PU) to 50.4 (B1), but the glass state and the melt state might not be comparable. An increasing contraction of the network results in a decrease of the water solubility at higher water fugacities (higher pressures and higher  $x_{H_2O}^{fluid}$ ) or in more depolymerized melts in which the coordination shell around the cations is filled with non-bridging oxygens so that it is saturated at lower water contents.

This explanation is supported by data of Grams and Behrens (1996) who measured the water solubility in fully polymerized melts of tonalitic composition (system Qz-Ab-An) at 1200°C. At low pressures (e.g. 30 MPa) the water solubility increases with an increase of the An component, whereas at higher pressures (e.g. 500 MPa) the water solubility increases with a decreasing An content (Grams and Behrens, 1996). Along the Qz<sub>100</sub> - Ab<sub>50</sub>An<sub>50</sub> join Grams and Behrens (1996) observed a maximum of the water solubility in the intermediate composition Qz<sub>50</sub>Ab<sub>25</sub>An<sub>25</sub> at 500 MPa.

Most of my water solubilities were measured at 1200-1250°C. At 1000°C and 200 MPa the same trend of an increasing water solubility from the rhyolitic to the dacitic composition is observed. On the other hand Tamic et al. (2001) observed a dramatic temperature effect between 1100°C and 800°C at 500 MPa. The solubility curve in dependence of the  $x_{H_2O}^{fluid}$  in the rhyolitic melt at 800°C is similar to that in the dacitic melt at 1250°C. To be able to make generally valid statements more temperature dependent experiments are necessary.

## 3.5 Implications

### 3.5.1 Pre-eruptive volatile contents

My CO<sub>2</sub>-H<sub>2</sub>O- $x_{H_2O}^{fluid}$  solubility relations determined in chapter 2 and 3 can be used to determine the pressure at which a dacitic liquid with given concentrations of CO<sub>2</sub> and water would be vapor saturated and the composition ( $x_{H_2O}^{fluid}$ ) of the vapor coexisting with such a liquid at equilibrium. Water solubilities in dependence of  $x_{H_2O}^{fluid}$  and pressure are calculated using the empirical model described in chapter 2.6.1.2. The CO<sub>2</sub> solubilities in dependence of the pressure,  $f_{CO_2}^{fluid}$  and the water content in the melt

### 3. The effect of the composition on the water solubility and applications to degassing

are calculated using the third thermodynamic model (chapter 2.6.3.3). H<sub>2</sub>O and CO<sub>2</sub> solubilities for selected pressures are shown in figure 3.5.

My solubility data can be directly applied to the degassing history of the Unzen volcano in Japan. For this intention it is necessary to know more about pre-eruptive P-T conditions, volatile contents and melt compositions.

Previous studies on magmas of the Unzen volcano (e.g., Nakada and Fujii, 1993; Nakamura, 1995; Nakada and Motomura, 1999, Holtz et al., revised) have shown that magma mixing of ~35 wt.% of a nearly aphyric andesitic high-temperature (~1050°C) magma and ~65 wt.% of a phenocryst-rich low-temperature magma (at ~775°C) with

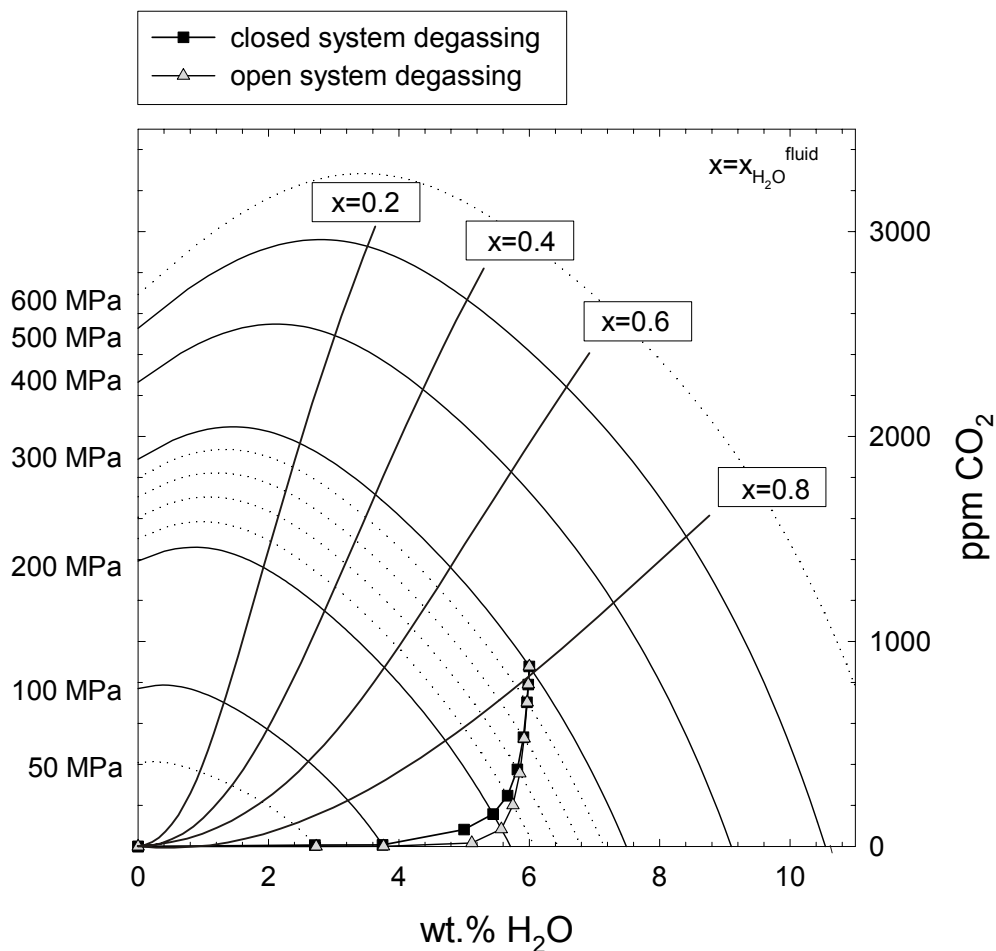


**Figure 3.5:**

Relationship between total water and CO<sub>2</sub> contents dissolved in dacitic melts calculated after the empirical model for water solubility (chapter 2.6.1.2) and the third thermodynamic model for CO<sub>2</sub> solubility (chapter 2.6.3.3) at various pressures and 1250°C. Note that dotted curves for 50 and 600 MPa are extrapolated and may be not reliable.

Symbols refer to results from open (triangles) and closed (squares) system degassing. See text for more details.

### 3. The effect of the composition on the water solubility and applications to degassing

---

a rhyolitic residual melt took place before the eruption of the dacitic magma. The proportions of the rhyolitic residual melt of the low temperature magma and phenocrysts incorporated to the mixed magma are 35-40% and 25-30%, respectively (Holtz et al., revised). Phase relations at 300 MPa and above 870°C, which are conditions assumed to be representative of the main magma chamber after mixing, show that the main phenocrysts (orthopyroxene, plagioclase, hornblende) only coexist at reduced water activity (5 - 7 wt.% water, Holtz et al., revised). These authors attributed this water content ( $6 \pm 1$  wt.%) to the postmixing melt. The investigation of glass inclusions suggests that the water content of the rhyolitic residual melt in the low temperature magma prior to mixture could be as high as 8 wt.% water (Holtz et al., revised).

Thus, the water contents in the premixing and postmixing melts are fairly well known. But the CO<sub>2</sub> content is not well constrained. No analyses of CO<sub>2</sub> from glass inclusions are available and CO<sub>2</sub> contents can be only estimated by the comparison of discharge rates of CO<sub>2</sub> in fumaroles and the amount of erupted magma. For example the average discharge rate of CO<sub>2</sub> and SO<sub>2</sub> from May to December 1992 were 330 and 120 ton/day, respectively (Hirabayashi et al., 1995). Hirabayashi et al. (1995) converted the amount of degassed sulfur to a concentration of  $150 \pm 80$  ppm S as SO<sub>2</sub> in the pre-eruptive magma. Thus, assuming that sulfur and CO<sub>2</sub> were exclusively derived from degassing of the postmixing melt, the pre-eruptive CO<sub>2</sub> content can be calculated to be 830 ppm CO<sub>2,total</sub>.

The water solubility in a rhyolitic melt at 780°C and 3 kb is 7.6 wt.% calculated after Tamic et al. (2001). Thus, assuming that 8 wt.% water was dissolved in the residual melt of the premixing low temperature magma, this melt was saturated in fluid. In addition, because of the high water content, the  $a_{H_2O}^{fluid}$  must have been close to 1, i.e. almost no CO<sub>2,total</sub> was dissolved in this melt.

Holtz et al. (revised) deduced that the andesitic premixing high temperature magma contained approximately 4 wt.% water. Solubility data of water and CO<sub>2</sub> are not available for andesitic melts close to 300 MPa. Using my H<sub>2</sub>O-CO<sub>2</sub> solubility data determined in dacitic melts at 1250°C as a approximation, melts with 4 wt.% water can have a CO<sub>2,total</sub> content of up to 1600 ppm CO<sub>2,total</sub> at 3 kb (figure 3.5). Thus, assuming that 50 wt.% of the andesitic high temperature melt mixed with 50 wt.% of

### 3. The effect of the composition on the water solubility and applications to degassing

---

the rhyolitic low temperature residual melt (Holtz et al., revised), the  $\text{CO}_{2,\text{total}}$  in the postmixing melt would be up to 800 ppm.

The  $\text{CO}_{2,\text{total}}$  solubility at 3 kb of dacitic melts containing 6 wt.% water at 1250°C is approximately 880 ppm (see figure 3.5), for rhyolitic melts approximately 650 ppm. The maximum  $\text{CO}_{2,\text{total}}$  content in the postmixing rhyodacitic residual melt is therefore between ~880 and ~650 ppm  $\text{CO}_2$ . Hence, the estimated (maximal)  $\text{CO}_{2,\text{total}}$  contents from the discharge rates of  $\text{CO}_2$  and the solubility data are in good agreement.

However, the maximal  $\text{CO}_2$  content estimated from solubility data may range from 1300 to 300 ppm  $\text{CO}_{2,\text{total}}$  if the water content after mixing varies between 5 to 7 wt.%.

#### **3.5.2 Degassing of ascending magma**

In this work combined  $\text{CO}_2\text{-H}_2\text{O}$  solubility data have been only obtained for the dacitic composition at 1250°C. These data can be used to model roughly possible degassing paths of the pre-eruptive melt of the Unzen volcano. The effect of the composition (the “real” melt was rhyodacitic) and temperature (the “real” temperature was around 900°C) will be discussed. In my degassing models I assume, that the melt is dacitic and does not change its composition and its temperature (1250°C) during ascent.

Degassing is calculated for a closed and an open system. In the open system degassing, the vapor phase is removed from the melt after each pressure step. Applied to a magma this means, that bubbles grow in equilibrium with the melt and step by step bubbles separate from the melt. In closed system degassing, the vapor phase remains in contact and equilibrium with the melt, increasing in amount and changing in composition after each increment of volatile loss from the liquid.

The starting point of the calculation was a fluid-saturated dacitic melt at 300 MPa (6 wt.% water and 880 ppm  $\text{CO}_{2,\text{total}}$  in equilibrium with an infinitely small amount of fluid with an  $x_{\text{H}_2\text{O}}^{\text{fluid}} = 0.79$ ). Degassing during decompression is modeled in successive isobaric steps. The  $\text{H}_2\text{O-CO}_2$  content in the melt in equilibrium with the  $x_{\text{H}_2\text{O}}^{\text{fluid}}$  in the fluid phase was calculated using the empirical model for water solubility (chapter 2.6.1.2) and the third thermodynamic model for  $\text{CO}_2$  solubility (chapter 2.6.3.3) after following procedure:

### 3. The effect of the composition on the water solubility and applications to degassing

---

At each pressure the water and CO<sub>2</sub> solubility was calculated for the  $x_{H_2O}^{fluid}$  determined from the previous step. The composition of the new fluid was determined from mass balance and calculated iteratively. The pressure is then decreased incrementally, leading again to a supersaturated melt, and the calculation is repeated. Pressure steps varied between 10 and 70 MPa.

Figure 3.5 shows the variation of water and CO<sub>2</sub> in the melt during open and closed system degassing, figure 3.6 shows variation of the  $x_{H_2O}^{fluid}$  in the corresponding fluid phases. The curves between the calculated pressures are interpolated linearly. To calculate the CO<sub>2</sub> and water contents in the melt at a given pressure for the closed system degassing the size of the pressure steps do not matter. On the hand for the open system degassing the size of the pressure steps predetermine the water and CO<sub>2</sub> values at a given pressure. In both, the open and the closed system CO<sub>2</sub> is partitioned strongly into the fluid (figure 3.5 and 3.6). The CO<sub>2,total</sub> content in the melt decreases dramatically from 300 to 200 MPa (to 160 ppm for closed system degassing and 90 ppm for open system degassing), whereas the decrease of water content is only minor (to 5.4 wt.% and 5.6 wt.% for closed and open system degassing, respectively). As a consequence, the water activity in the fluid increases and is close to unity at 200 MPa ( $x_{H_2O}^{fluid}=0.95$  and  $0.97$  for closed and open system degassing, respectively). For smaller pressure steps in the open system degassing, the decrease of CO<sub>2</sub> in the melt would be even more dramatic, because CO<sub>2</sub> which partitions into the fluid is more effectively removed from the melt.

In a rhyodacitic melt with the same initial water and CO<sub>2,total</sub> content the calculated water (5.3 wt.%) and CO<sub>2,total</sub> contents (20 ppm) for the closed system at 200 MPa are lower than for the dacitic composition, but the  $x_{H_2O}^{fluid}$  is approximately the same ( $x_{H_2O}^{fluid}=0.95$ ). The water solubility increases with the temperature and the CO<sub>2,total</sub> solubility is independent of the temperature in rhyolitic melts at 200 MPa (Tamic et al., 2001). The same negative temperature dependence of water solubility is observed in rhyodacitic melts in this study. Thus, for a rhyodacitic melt at lower temperature the same or even a stronger partitioning of CO<sub>2</sub> into the fluid phase is expected.

### 3. The effect of the composition on the water solubility and applications to degassing

A decompression of a crystal-bearing magma with an almost constant water content will lead to decompression melting due to increasing water activity (Johannes and Holtz, 1996). In a P-T-diagram (e.g., for AOQ-minimum melt compositions in figure 2.25 in Johannes and Holtz, 1996) the liquidus curves for constant (minimum) water contents in the melt have negative slopes. As a consequence a magma with a constant water content has a lower melt fraction at a higher pressure.

These considerations are supported by phase relations determined by Holtz and coworkers (revised): At 850°C and 300 MPa a dacitic magma (composition of the Unzen magma) with a melt containing 6 wt.% water has a melt fraction of approximately 50 wt.%. At 200 MPa, the same temperature and water content in the melt, the melt fraction is approximately 70 wt.%. During melting, the water and  $\text{CO}_{2,\text{total}}$  content decreases (when anhydrous minerals are melting). Because supersaturation will be reached at lower pressure melting leads to a delayed degassing.

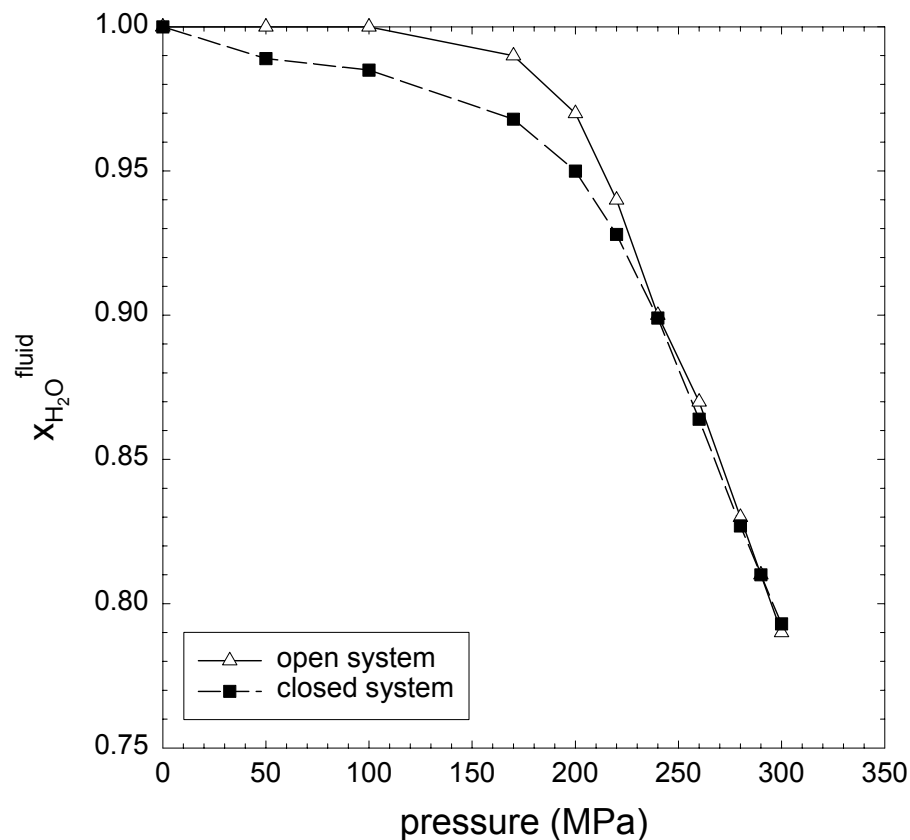


**Figure 3.6:**

Variation of the fluid composition calculated for open (triangles) and closed (squares) system degassing during decompression. See text for more details.



---

#### 4 REFERENCES

- Aranovich L.Y., Newton R.C. (1999) Experimental determination of CO<sub>2</sub>-H<sub>2</sub>O activity-composition relations at 600-1000°C and 6-14 kbar by reversed decarbonation and dehydration reactions. *American Mineralogist*, **84**, 1319-1332.
- Bagdassarov N.S., Dingwell D.B. (1993) Frequency-dependent rheology of vesicular rhyolite. *Journal of Geophysical Research*, **98**, 6477-6487.
- Barclay J., Carroll M.R., Houghton B. F., Wilson C.J.N. (1996) Pre-eruptive volatile content and degassing history of an evolving peralkaline volcano. *Journal of Volcanology and Geothermal Research*, **74**, 75-87.
- Bartholomew R.F., Butler B.L., Hoover H.L., Wu C.K. (1980) Infrared spectra of a water-containing glass. *Journal of the American Ceramic Society*. **63**, 481-485.
- Becker A., Holtz F., Johannes W. (1998) Liquid temperatures and phase compositions in the system Qz-Ab-Or at 5 kbar and very low water activities. *Contributions to Mineralogy and Petrology*, **130**, 213-224.
- Behrens H. (1995) Determination of water solubilities in high-viscosity melts: An experimental study on NaAlSi<sub>3</sub>O<sub>8</sub> and KAlSi<sub>3</sub>O<sub>8</sub> melts. *European Journal of Mineralogy*, **7**, 905-920.
- Behrens H., Jantos N. (2001) The effect of anhydrous composition on water solubility in granitic melts. *American Mineralogist*, **86**, 14-20.
- Behrens H., Romano C., Nowak M., Holtz F., Dingwell D.B. (1996) Near-infrared spectroscopic determination of water species in glasses of the system MAlSi<sub>3</sub>O<sub>8</sub> (M=Li,Na,K): an interlaboratory study. *Chemical Geology*, **128**, 41-63.
- Behrens H., Schmidt M.O. (1998) Infrared spectroscopy of hydrous silicic glasses at temperatures up to 600°C and implications for the incorporation and dynamics of water in glasses. *Neues Jahrbuch der Mineralogie, Abhandlungen*, **172**, 203-226.

- Behrens H., Zhang X (2001) Ar diffusion in hydrous silicic melts: implications for volatile diffusion mechanisms and fractionation *Earth and Planetary Science Letters*, **192**, 377-388.
- Berndt J. (2002) Differentiation of MOR Basalt at 200 MPa: Experimental Techniques and Influence of H<sub>2</sub>O and *f*O<sub>2</sub> on Phase Relations and Liquid Line of Descent. Ph.D. thesis. Institut für Mineralogie, Universität Hannover, p. 118.
- Berndt J., Liebske C., Holtz F., Freise M., Nowak M., Ziegenbein D. Hurkuck W., Koepke J. (2002) A combined rapid-quench and H<sub>2</sub>-membrane setup for internally heated pressure vessels: Description and application for water solubility in basaltic melts. *American Mineralogist*, **87**, 1717-1730.
- Blank J.G. (1993) An experimental investigation of the behavior of carbon dioxide in rhyolitic melt. Ph.D. thesis, California Institute of Technology, Pasadena, CA.
- Blank J.G., Brooker R.A. (1994) Experimental studies of carbon dioxide in silicate melts: solubility, speciation and stable isotope behavior. In: Carroll M.R., Holloway J.R. (eds.) Volatiles in Magmas, *Reviews in Mineralogy*, **30**, 157-186.
- Blank J.G., Stolper E.M., Carroll M.R. (1993) Solubilities of carbon dioxide and water in rhyolitic melt at 850°C and 750 bars. *Earth and Planetary Science Letters*, **119**, 27-36.
- Botcharnikov R., Holtz F., Behrens H., Sato H., Koepke J. (2002) Experimental study of sulfur and chlorine solubility in rhyodacite and andesite melts of Unzen volcano, Japan, *Journal of Conference Abstracts*, **7**, 17.
- Brenan J.M., Shaw H.F., Ryerson F.J., Phinney D.L. (1995) Experimental determination of trace-element partitioning between pargasite and a synthetic hydrous andesitic melt. *Earth and Planetary Science Letters*, **135**, 1-11.
- Brey, G. (1976) CO<sub>2</sub> solubility and solubility mechanisms in silicate melts at high pressures. *Contributions to Mineralogy and Petrology*, **57**, 215-221.
- Brooker R.A., Kohn S.C., Holloway J.R., McMillan P.F. (2001) Structural controls on the solubility of CO<sub>2</sub> in silicate melts. Part II: IR characteristics of carbonate groups in silicate glasses. *Chemical Geology*, **174**, 241-254.

- Brooker R.A., Kohn S.C., Holloway J.R., McMillan P.F., Carroll M.R. (1999) Solubility, speciation and dissolution mechanisms for CO<sub>2</sub> in melts on the NaAlO<sub>2</sub>-SiO<sub>2</sub> join. *Geochimica et Cosmochimica Acta*, **63**, 3549-3565.
- Bureau H., Pineau F., Métrich N., Semet M.P., Javoy M. (1998) A melt and fluid inclusion study of the gas phase at Piton de la Fournaise volcano (Réunion Island). *Chemical Geology*, **147**, 115-130.
- Burns R.G. (1993) *Mineralogical Application of Crystal Field Theory*. 2<sup>nd</sup> Edition Cambridge University Press, p. 551.
- Carroll M.R., Holloway J.R. (eds.) (1994) Volatiles in magmas. *Reviews in Mineralogy*, **30**, p. 517.
- Cashman K.V. (1992) Groundmass crystallization of Mount St. Helens dacite, 1980-1986: a tool for interpreting shallow magmatic processes. *Contributions to Mineralogy and Petrology*, **109**, 431-449.
- Chen C.-H., DePaolo D.J., Nakada S., Shieh Y.-N. (1993) Relationship between eruption volume and neodymium isotopic composition at Unzen volcano. *Nature*, **362**, 831-834.
- Deloule E., Paillat O., Pichavant M., Scaillet B. (1995) Ion microprobe determination of water in silicate glasses: methods and applications. *Chemical Geology*, **125**, 19-28.
- Dietzel A. (1942) Die Kationenfeldstärken und ihre Beziehungen zu Entglasungsvorgängen, zur Verbindungsbildung und zu den Schmelzpunkten von Silikaten. *Zeitschrift der Elektrochemie*, **49**, 9-23.
- Dingwell D.B., Webb S.L. (1990) Relaxation in silicate melts. *European Journal of Mineralogy*, **2**, 427-447.
- Dixon J.E., Stolper E.M., (1995) An experimental study of water and carbon dioxide solubilities in mid-ocean ridge basaltic liquids. Part II: Applications to degassing. *Journal of Petrology*, **36**, 1633-1646.
- Dixon J.E., Stolper E.M., Holloway J.R. (1995) An experimental study of water and carbon dioxide solubilities in mid-ocean ridge basaltic liquids. Part I: Calibration and solubility models. *Journal of Petrology*, **36**, 1607-1631.

- Dowty E. (1980) Crystal-chemical factor affecting the mobility of ions in minerals. *American Mineralogist*, **65**, 174-182.
- Eccles A.J. (1989) SIMS instrumentation. *In*: Vickerman J.C., Brown A., Reed N.M. (eds.) Secondary Ion Mass Spectrometry – Principles and Applications. International Series of Monographs on Chemistry, Clarendon Press Oxford, p 73.
- Finch A.A., Shaw P.A., Weedon G.P., Holmgren K. (2001) Trace element variation in speleothem aragonite: potential for palaeoenvironmental reconstruction. *Earth and Planetary Science Letters*, **186**, 255-267.
- Fine G., Stolper E. (1985) The speciation of carbon dioxide in sodium aluminosilicate glasses. *Contributions to Mineralogy and Petrology*, **91**, 105-121.
- Fogel R.A., Rutherford M.J. (1990) The solubility of carbon dioxide in rhyolitic melts: A quantitative FTIR study. *American Mineralogist*, **75**, 1311-1326.
- Grams M., Behrens H. (1996) Water solubility in tonalitic melts, TERRA abstracts supplement.
- Hamilton D.L., Burnham C.W., Osborn E.F. (1964) The solubility of water and effects of oxygen fugacity and water content on crystallization in mafic magmas. *Journal of Petrology*, **5**, 21-39.
- Harte B., Fitzsimons I.C.W., Harris J.W., Otter M.L. (1999) Carbon isotope ratios and nitrogen abundances in relation to cathodoluminescence characteristics for some diamonds from the Kaapvaal Province, S. Africa. *Mineralogical Magazine*, **63**, 829-856.
- Hervig R.L., Thomas R.M., Williams, P. (1989) Charge neutralization and oxygen isotopic analysis of insulators with the ion microprobe. *In*: Shanks, W.C.III, Criss, R.E. (eds.) New frontiers in stable isotopic research; laser probes, ion probes, and small-sample analysis. *U. S. Geological Survey Bulletin*, 137-143.
- Hess K.U., Dingwell D.B. (1996) Viscosities of hydrous leucogranitic melts: A non-Arrhenian model. *American Mineralogist*, **81**, 1297-1300.
- Hirabayashi J., Ohba T., Nogami K., Yoshida M. (1995) Discharge rate of SO<sub>2</sub> from Unzen volcano. Kyushu, Japan. *Geophysical Research Letters*, **22**, 1709-1715.

- Holloway J.R., Blank J.G. (1994) Application of Experimental Results to C-O-H Species in Natural Melts *In: Carroll, M.R., Holloway, J.R. (eds.) Volatiles in Magmas. Reviews in Mineralogy, 30*, 187-230.
- Holloway J.R. (1976) Fluids in the evolution of granitic magmas; consequences of finite CO<sub>2</sub> solubility. *Geological Society of America Bulletin, 87*, 1513-1518.
- Holloway J.R. (1977) Fugacity and activity of molecular species in supercritical fluids. *In: Fraser D. (ed.), Thermodynamics in Geology*, 161-181. Reidel.
- Holtz F., Sato H., Lewis, J. Experimental phase relations and phase chemistry of the 1991-1995 Unzen dacite and implications for the crystallisation conditions of phenocrysts in mixed magmas. *Journal of petrology*. (revised).
- Holtz F., Behrens H., Dingwell D.B., Johannes W. (1995) H<sub>2</sub>O solubility in haplogranitic melts: Compositional, pressure, and temperature dependence. *American Mineralogist, 80*, 94-108.
- Ihinger P.D., Zhang Y., Stolper E.M. (1999) The speciation of dissolved water in rhyolitic melt. *Geochimica et Cosmochimica Acta, 63*, 3567-3578.
- Ihinger, P. D., Hervig R. L., McMillan P. F. (1994) Analytical methods for volatiles in glasses. *In: Carroll, M.R., Holloway, J.R. (eds.) Volatiles in Magmas. Reviews in Mineralogy, 30*, 67-121.
- Jakobsson S. (1997) Solubility of water and carbon dioxide in an icelandite at 1400°C and 10 kilobars. *Contributions to Mineralogy and Petrology, 127*, 129-135.
- Jaupart C., Allegre C. (1991) Gas content, eruption rate and instabilities of eruption regime in silicic volcanoes. *Earth and Planetary Science Letters, 102*, 413-429.
- Jendrzewski N., Javoy M., Trull T. (1996) Mesures quantitatives de carbones et d'eau dans les verres basaltiques naturels par spectroscopie infrarouge. Partie II : l'eau. *C.R. Acad. Sci. Paris, 322*, 735-742.
- Johannes W., Holtz, F. (1996) Petrogenesis and experimental petrology of granitic rocks, Springer, Heidelberg, p. 335.
- Johnson M.C. Anderson Jr. A.T., Rutherford M.J. (1994) Preeruptive volatile contents of magmas. *In: Carroll M.R., Holoway, J.R. (eds.) Volatiles in magmas. Reviews in Mineralogy, 30*, 281-323.

- Kerrick D.M., Jacobs G.K. (1981). A modified redlich-kwong equation for H<sub>2</sub>O, CO<sub>2</sub>, and H<sub>2</sub>O-CO<sub>2</sub> mixtures at elevated pressures and temperatures. *American Journal of Science*, **281**, 735-767.
- King P.L. Holloway, J.R. (2002) CO<sub>2</sub> solubility and speciation in intermediate (andesitic) melts: The role of H<sub>2</sub>O and composition, *Geochemica et Cosmochemica Acta*, **66**, 1627-1640.
- Kohn S.C., Brooker R.A. (1994) The effect of water on the solubility and speciation of CO<sub>2</sub> in aluminosilicate glasses along the join SiO<sub>2</sub>-NaAlO<sub>2</sub>. *Mineralogical Magazine*, **58A** 489-490.
- Kohn S.C., Brooker R.A., Dupree R. (1991) <sup>13</sup>C MAS NMR: A method for studying CO<sub>2</sub> speciation in glasses. *Geochimica et Cosmochimica Acta*, **55**, 3879-3884.
- Kohn, S.C. (2000) The dissolution mechanisms of water in silicate melts; a synthesis of recent data. *Mineralogical Magazine*, **64**, 389-408.
- Lange R..A. (1994) The effect of H<sub>2</sub>O, CO<sub>2</sub> and F on the density and viscosity of silicate melts. In: Carroll M.R., Holloway J.R. (eds.) Volatiles in magmas, *Reviews in Mineralogy*, **30**, 387-396.
- McKeegan K.D., Walker R.M., Zinner E. (1985) Ion microprobe isotopic measurements of individual interplanetary dust particles. *Geochimica et Cosmochimica Acta*, **49**, 1971-1987.
- McMillan P.F.(1994) Water solubility and speciation models. In: Carroll M.R., Holloway J.R. (eds.) Volatiles in magmas, *Reviews in Mineralogy*, **30**, 131-156.
- Moore G., Vennemann T., Carmichael I.S.E. (1998) An empirical model for the solubility of H<sub>2</sub>O in magmas to 3 kilobars. *American Mineralogist*, **83**, 36-42.
- Morizet Y., Brooker R.A., Kohn S.C. (2002) CO<sub>2</sub> in haplo-phonolite melt; solubility, speciation and carbonate complexation. *Geochimica et Cosmochemica Acta*, **66**, 1809-1820.
- Morizet Y., Kohn S.C., Brooker R.A. (2001) Annealing experiments on CO<sub>2</sub>-bearing jadeite glass: an insight into the true temperature dependence of CO<sub>2</sub> speciation in silicate melts, *Mineralogical Magazine*, **65**, 701-707.

- Mysen B.J., Eggler D.H., Seitz M.G., Holloway J.R. (1976) Carbon dioxide in silicate melts and crystals. Part I. Solubility measurements. *American Journal of Science*, **276**, 455-479.
- Mysen B.O. (1976) The role of volatiles in silicate melts: solubility of carbon dioxide and water in feldspar, pyroxene, and feldspathoid melts to 30 kbar and 1625°C. *American Journal of Science*, **276**, 969-996.
- Mysen B.O., Seitz M.G., Frantz J.D. (1974) Measurements of the solubility of carbon dioxide in silicate melts utilizing maps of carbon-14 beta activity. *Carnegie Institute of Washington Yearbook*, **73**, 224-226.
- Mysen B.O., Virgo D. (1980a) Solubility mechanisms of carbon dioxide in silicate melts: a Raman spectroscopic study. *American Mineralogist*, **65**, 885-899.
- Mysen B.O., Virgo D. (1980b) The solubility behavior of CO<sub>2</sub> in melts on the join NaAlSi<sub>3</sub>O<sub>8</sub>-CaAl<sub>2</sub>Si<sub>2</sub>O<sub>8</sub>-CO<sub>2</sub> at high pressure and temperature: a Raman spectroscopic study. *American Mineralogist*, **65**, 1166-1175.
- Nakada S., Fujii, T. (1993) Preliminary report on the activity at Unzen volcano (Japan), November 1990-November 1991: dacite lava domes and pyroclastic flows. *Journal of Volcanology and Geothermal Research*, **54**, 319-333.
- Nakada S., Motomura Y., (1995) Manner of magma ascent at Unzen volcano (Japan), *Geophysical Research Letters*, **22**, 567-570.
- Nakada S., Motomura Y. (1999) Petrology of the 1991-95 eruption at Unzen: effusion pulsation and groundmass crystallization. *Journal of Volcanology and Geothermal Research*, **89**, 183-196.
- Nakada S., Motomura Y., Shimizu, H. (2002) Aim of conduit drilling at Unzen volcano. Unzen Workshop 2002, 26-29 January 2002 Shimabara, Nagasaki, Japan, 21-24.
- Nakamura M. (1995) Continuous mixing of crystal mush and replenished magma in the ongoing Unzen eruption. *Geology*, **23**, 807-810.
- Newman S., Stolper E.M., Epstein S. (1986) Measurement of water in rhyolitic glasses: Calibration of an infrared spectroscopic technique. *American Mineralogist*, **71**, 1527-1541.

- Nowak M., Behrens H. (1995) The speciation of water in haplogranitic glasses and melts determined by in situ near-infrared spectroscopy. *Geochimica et Cosmochimica Acta*, **59**, 3445-3450.
- Nowak M., Behrens H. (2001) Water in rhyolitic magmas: getting a grip on a slippery problem. *Earth and Planetary Science Letters*, **184**, 515-522.
- Nowak M., Porbatzki D., Dietrich O. (2003) Carbon dioxide speciation in silicate melts: A restart. *Earth and Planetary Science Letters*. **207**, 131-139.
- Ohlhorst S., Behrens H., Holtz F., Schmidt B.C. (2000) Water speciation in aluminosilicate glasses and melts. In Rammlmair D., Mederer J., Oberthür Th., Heimann R.B. and Pentinghaus H. (eds.) Applied Mineralogy in Research, Economy, Technology and Culture. Proceedings of the 6th ICAM, A.A. Balkema, Rotterdam, 193-196.
- Oxtoby S., Hamilton, D.L. (1978a) The discrete association of water with Na<sub>2</sub>O-Al<sub>2</sub>O<sub>3</sub>-SiO<sub>2</sub> in NaAl silicate melts. *Contributions to Mineralogy and Petrology*, **66**, 185-188.
- Oxtoby S., Hamilton, D.L. (1978b) Solubility of water in melts of Na<sub>2</sub>O-Al<sub>2</sub>O<sub>3</sub>-SiO<sub>2</sub> and K<sub>2</sub>O-Al<sub>2</sub>O<sub>3</sub>-SiO<sub>2</sub> systems. In: Mackenzie W.S. (ed.) Progress in experimental petrology, Natural Environment Research Council, Manchester, **4**, 33-36
- Pallister J.S., Hoblitt, R.P., Reyes, A.G. (1992) A basalt trigger for the 1991 eruptions of Pinatubo volcano? *Nature*, **356**, 426-428.
- Pan V., Holloway J.R., Hervig R.L. (1991) The pressure and temperature dependence of carbon dioxide solubility in tholeiitic basalt melts. *Geochimica et Cosmochimica Acta*, **55**, 1587-1595.
- Pandya N., Muenow D., Sharma S.K. (1992) The effect of bulk composition on the speciation of water in submarine volcanic glasses. *Geochimica et Cosmochimica Acta*. **56**, 1875-1883.
- Papale P. (1999) Modeling of the solubility of a two-component H<sub>2</sub>O + CO<sub>2</sub> fluid in silicate liquids. *American Mineralogist*, **84**, 477-492.



- Pawley A.R., Holloway J.R., McMillan P.F. (1992) The effect of oxygen fugacity on the solubility of carbon-oxygen fluids in basaltic melts. *Earth and Planetary Science Letters*, **110**, 213-225.
- Pitzer K.S., Sterner S.M. (1994) Equation of state valid continuously from zero to extreme pressures for H<sub>2</sub>O and CO<sub>2</sub>. *Journal of Chemical Physics*, **102**, 3111-3116.
- Reed S.J.B. (1989) Ion microprobe analysis - A review of geological applications. *Mineralogical Magazine*, **53**, 3-24.
- Richet P., Lejeune A.M., Holtz F., Roux J., 1996. Water and the viscosity of andesitic melts. *Chemical Geology*, **128**, 185-197.
- Romano C., Dingwell D.B., Behrens H. (1995) The temperature dependence of the speciation of water in NaAlSi<sub>3</sub>O<sub>8</sub>-KAlSi<sub>3</sub>O<sub>8</sub> melts: an application of fictive temperatures derived from synthetic fluid inclusions. *Contributions to Mineralogy and Petrology*, **122**, 1-10.
- Rossmann G.R. (1988) Optical spectroscopy. In: Hawthorne F.C. (editor), *Spectroscopic Methods in Mineralogy and Geology. Reviews in Mineralogy*, **18**, 207-243.
- Roux J., Lefèvre, A. (1992) A fast-quench device for internally heated pressure vessels. *European Journal of Mineralogy*, **4**, 279-281.
- Sato H., Fujii T., Nakada S., (1992) Crumbling of dacite dome lava and generation of pyroclastic flows at Unzen volcano. *Nature*, **366**, 664-666.
- Sato H., Nakada S., Fujii T., Nakamura M., Kamata K.S. (1997) Groundmass amphibole in the 1991-1995 dome dacite of Unzen volcano: Experimental equilibrium studies and volcanological implications. *Proceedings of the Unzen International Workshop: Decade Volcano and Scientific Drilling*, **C12**, 88-90.
- Saxena F.J., Fei Y. (1987) High pressure and high temperature fluid fugacities. *Geochimica et Cosmochimica Acta*, **51**, 783-791.
- Scherer G.W. (1984) Use of the Adam-Gibbs equation in the analysis of structural relaxation. *Journal of the American Ceramic Society*, **67**, 504-511.

- 
- Schmidt, B.C., Behrens, H., Riemer, T., Kappes, R., Dupree, R. 2001. Quantitative determination of water in aluminosilicate glasses: A comparative NMR and IR spectroscopic study. *Chemical Geology*, **174**, 195-208.
- Scholze H. (1960) Zur Frage der Unterscheidung zwischen H<sub>2</sub>O-Molekeln und OH-Gruppen in Gläsern und Mineralien. *Naturwissenschaften*, **47**, 226-227.
- Scholze H. (1966) Gases and water in glasses. *Glass Industry*, **47**, (546-551), 622-628.
- Shen A., Keppler H. (1995) Infrared spectroscopy of hydrous silicate melts to 1000°C and 10 kbar: Direct observations of H<sub>2</sub>O speciation a diamond anvil cell. *American Mineralogist*, **80**, 1335-1338.
- Sierralta M. Nowak M. Keppler H. (2002) The influence of bulk composition on the diffusivity of carbon dioxide in sodium aluminosilicate melts *American Mineralogist*, **87**, 1710-1716.
- Silver L.A., Ihinger P.D., Stolper E. (1990) The influence of bulk composition on the speciation of water in silicate glasses. *Contributions to Mineralogy and Petrology*, **104**, 142-162.
- Spera F.J., Bergman S.C. (1980) Carbon dioxide in igneous petrogenesis: I. Aspects of the dissolution of CO<sub>2</sub> in silicate liquids. *Contributions to Mineralogy and Petrology*, **74**, 55-66.
- Stolper E. (1982) Water in silicate glasses: An infrared spectroscopic study. *Mineralogy and Petrology*, **81**, 1-17.
- Stolper E., Fine G., Johnson T., Newman S. (1987) Solubility of carbon dioxide in albitic melt. *American Mineralogist*, **72**, 1071-1085.
- Stolper E., Holloway J.R. (1988) Experimental determination of the solubility of carbon dioxide in molten basalt at low pressure. *Earth and Planetary Science Letters*, **87**, 397-408.
- Storms H.A., Brown K.F., Stein J.D. (1977) Evaluation of a cesium positive ion source for secondary ion mass spectrometry. *Analytical Chemistry*, **49**, 2023-2030.
- Tamic N. (2002) Solubility of H<sub>2</sub>O and CO<sub>2</sub> and diffusion of CO<sub>2</sub> in rhyolitic melts: an experimental study. Ph.D. thesis, Institut für Mineralogie, Universität Hannover. p 96.

- Tamic N., Behrens H., Holtz F. (2001) The solubility of H<sub>2</sub>O and CO<sub>2</sub> in rhyolitic melts in equilibrium with a mixed CO<sub>2</sub>-H<sub>2</sub>O fluid phase. *Chemical Geology*, **174**, 333-347.
- Vickermann J.C. (1989) The SIMS phenomenon – the experimental parameters. In: Vickerman J.C., Brown A., Reed N.M. (eds.) Secondary Ion Mass Spectrometry – Principles and Applications. *International Series of Monographs on Chemistry*, Clarendon Press Oxford, p 341.
- Wiedenbeck M., Rocholl A., Koepke J. (2001) Water - A Source of systematic error in quantitative SIMS analyses of hydrous glasses. Eos Transactions. AGU Meeting Supplement.
- Wilke M., Behrens H. (1999) The dependence of the partitioning of iron and europium between plagioclase and hydrous tonalitic melt on oxygen fugacity. *Contributions to Mineralogy and Petrology*, **137**, 102-114.
- Wilson R.G., Stevie F.A., Magee C.W. (1989) Secondary ion mass spectrometry: A practical handbook for depth profiling and bulk impurity analysis. *Wiley-Interscience Publication*, New York
- Withers A.C., Behrens H. (1999) Temperature induced changes in the NIR spectra of hydrous albitic and rhyolitic glasses between 300 and 100 K. *Physics and Chemistry of Minerals*, **27**, 119-132.
- Yamashita S., Kitamura T., Kusakabe M. (1997) Infrared spectroscopy of hydrous glasses of arc magma compositions. *Geochemical Journal*, **31**, 169-174.
- Yamashita S. (1999) Experimental study of the effect of temperature on water solubility in natural rhyolite melt to 100 MPa, *Journal of Petrology*, **40**, 1497-1507.
- Zhang Y. (1999) H<sub>2</sub>O solubility in rhyolitic glasses and melts: measurement, speciation, solubility, and diffusion. *Reviews of Geophysics*, **37**, 493-516.
- Zhang Y., Belcher R., Ihinger P.D., Wang L., Xu Z., Newman S. (1997) New calibration of infrared measurement of dissolved water in rhyolitic glasses. *Geochimica et Cosmochimica Acta*, **61**, 3089-3100.
- Zhang Y., Stolper E.M., Ihinger, P.D. (1997) Kinetics of reaction H<sub>2</sub>O + O = 2OH in rhyolitic glasses: Preliminary results. *American Mineralogist*, **80**, 593-612.

- Zhang Y., Xu Z., Behrens H. (2000) Hydrous species geospeedometer in rhyolite; improved calibration and application. *Geochimica et Cosmochimica Acta*, **64**, 3347-3355.
- Zinner E., Ming T., Anders E. (1989) Interstellar SiC in the Murchison and Murray meteorites: isotopic composition of Ne, Xe, Si, C and N. *Geochimica et Cosmochimica Acta*, **53**, 3273-3290.

## APPENDIX

**Table 1:** Normalized composition of the starting materials.

	<b>B1</b>	<b>PU</b>	<b>DC</b>	<b>DC2</b>	<b>GMS</b>	<b>EGL</b>	<b>EDF</b>	<b>IGL</b>
	<b>basalt</b>	<b>andesite</b>	<b>dacite</b>	<b>dacite</b>	<b>rhyodacite</b>	<b>rhyolite</b>	<b>rhyolite</b>	<b>rhyolite</b>
<b>SiO<sub>2</sub></b>	49.67	57.21	65.84	65.04	69.85	74.14	76.90	79.14
<b>TiO<sub>2</sub></b>	0.87	0.84	0.66	0.70	0.51	0.32	0.11	0.35
<b>Al<sub>2</sub>O<sub>3</sub></b>	16.08	17.50	15.44	16.24	14.81	14.22	12.74	11.06
<b>FeO</b>	8.64	7.58	4.73	4.50	3.40	2.25	0.68	0.93
<b>MnO</b>	0.15	0.11	0.07	0.08	0.12	0.09	0.07	0.03
<b>MgO</b>	9.78	4.27	2.14	1.94	1.44	0.30	0.08	0.05
<b>CaO</b>	12.45	7.59	4.89	5.14	3.92	2.71	0.58	0.62
<b>Na<sub>2</sub>O</b>	2.28	3.31	3.68	3.75	3.32	3.03	4.06	3.14
<b>K<sub>2</sub>O</b>	0.08	1.60	2.55	2.60	2.63	2.95	4.78	4.67

Notes: The composition was determined by electron microprobe analysis, using a Cameca microprobe, with 15 kV accelerating voltage, 5 nA beam current and a defocused beam with 10-30  $\mu\text{m}$  in diameter.

B1 = averaged primitive MOR basalt (Berndt 2002)

PU = Pre - Unzen andesite (age: 500 000 years, Chen et al., 1993)

DC = total composition of the Unzen eruption 1992 (Chen et al., 1993)

DC2 = total composition of the Unzen eruption 1992 (second glass)

GMS = microcrystalline groundmass of the Unzen (1991-95, Sato et al., 1997)

EGL = (experimental glass) residue melt of a crystallization experiment with DC and 6 wt.% H<sub>2</sub>O at 850°C and 2kb

EDF = rhyolite from Armenia (Bagdassov and Dingwell, 1993; Withers and Behrens, 1999, Tamic et al., 2001)

IGL = (interstitial glass) residue melt of the Unzen (1991, Nakada and Motomura, 1995).

**Table 2:** Experimental results and spectroscopic data.

sample	type	P (MPa)	T (°C)	Duration (h)	c <sub>water</sub> (wt.%)	thickness (cm)	density (g/l)	A <sub>OH</sub> (GG)	A <sub>H<sub>2</sub>O</sub> (GG)	A* <sub>OH</sub> (GG) (cm <sup>-1</sup> )	A* <sub>H<sub>2</sub>O</sub> (GG) (cm <sup>-1</sup> )
DC 55A	a	500	1296	1.0	1.39 ± 0.12	0.0474	2502	0.078	0.025	17.6	4.0
DC 55B	a	500	1296	1.0	1.53 ± 0.13	0.0471	2502	0.082	0.029	18.3	4.5
DC 56A	a	500	1303	1.0	2.11 ± 0.11	0.0465	2492	0.099	0.057	22.0	10.1
DC 56B	a	500	1303	1.0	2.15 ± 0.10	0.0460	2492	0.101	0.057	22.3	10.5
DC 57A	a	500	1300	1.0	2.77 ± 0.11	0.0468	2493	0.114	0.086	25.1	14.5
DC 57B	a	500	1300	1.0	2.71 ± 0.11	0.0472	2493	0.114	0.086	24.9	14.6
DC 58A	a	500	1300	1.0	3.06 ± 0.09	0.0454	2480	0.114	0.099	24.6	17.2
DC 58B	a	500	1300	1.0	3.05 ± 0.09	0.0463	2480	0.117	0.109	24.9	18.7
DC 77A	a	500	1300 <sup>3)</sup>	4.0	5.38 ± 0.15	0.0279	2449	0.085	0.148	18.8	23.3
DC 77B	a	500	1300 <sup>3)</sup>	4.0	5.82 ± 0.15	0.0275	2449	0.086	0.161	18.9	27.0
DC 84	b	200	1207	47.4	5.73 ± 0.11	0.0489	2448 <sup>1)</sup>	0.152	0.279	31.7	49.3
DC 88	b	100	1223	52.4	3.79 ± 0.13	0.0460	2470 <sup>1)</sup>	0.127	0.138	26.9	23.4
PU 70A	a	500	1313	0.5	1.82 ± 0.10	0.0289	2622	0.051	0.015	13.0	2.6
PU 70B	a	500	1313	0.5	1.96 ± 0.08	0.0279	2622	0.050	0.018	11.8	3.6
PU 71A	a	500	1306	0.6	2.87 ± 0.07	0.0277	2607	0.061	0.036	14.5	7.0
PU 71B	a	500	1306	0.6	2.80 ± 0.07	0.0273	2607	0.061	0.034	14.5	6.4
PU 72A	a	500	1339	0.5	3.67 ± 0.07	0.0280	2624	0.074	0.056	17.3	9.9
PU 72B	a	500	1339	0.5	3.62 ± 0.07	0.0284	2624	0.077	0.053	19.5	8.8
PU 73A	a	500	1292	0.5	3.29 ± 0.07	0.0277	2594	0.069	0.048	15.9	9.0
PU 73B	a	500	1292	0.5	3.26 ± 0.07	0.0289	2594	0.075	0.048	18.2	8.3
PU 74	a	500	1300	0.5	4.36 ± 0.09	0.0281	2578	0.082	0.072	19.7	12.4
PU 75A	a	500	1253	4.0	5.75 ± 0.08	0.0277	2550	0.089	0.124	20.6	20.7
B1 28	b	50	1200	15.0	1.66 ± 0.14	0.0456	2784 <sup>2)</sup>	0.061	0.015	13.9	3.6
B1 24	b	100	1200	20.0	3.35 ± 0.16	0.0459	2749 <sup>2)</sup>	0.099	0.054	22.5	12.4
B1 23	b	200	1200	24.0	4.83 ± 0.14	0.0453	2719 <sup>2)</sup>	0.111	0.105	23.7	25.4
B1 27	b	300	1200	22.0	6.29 ± 0.16	0.0453	2688 <sup>2)</sup>	0.126	0.149	27.7	34.6

In the sample notation A and B refer to pieces from opposite ends of one large sample. Total water (c<sub>water</sub>) was determined by pyrolysis and subsequent Karl - Fischer titration. A<sub>OH,H<sub>2</sub>O</sub> denotes absorbance and A\*<sub>OH,H<sub>2</sub>O</sub> integrated intensity. GG indicate that the baseline is composed of two gaussians (see text). Errors are: thickness - 0.0002 cm; density - 1 % for dacite and andesite and 2 % for basalt; absorbance - 0.003 for the OH peak and 0.002 for the H<sub>2</sub>O peak; integrated intensity - 1 cm<sup>-1</sup> for the OH peak and 0.7 cm<sup>-1</sup> for the H<sub>2</sub>O peak.

Type of experiment: a - synthesis with water contents lower than the solubility under experimental conditions, b - water solubility experiments.

<sup>1)</sup> densities calculated by the density - total water relationship ( $\rho = -18.4 * c_{\text{water}} + 2661$ ) derived for andesitic samples in our study,

<sup>2)</sup> densities of basaltic glasses are calculated using the equation  $\rho = -20.8 * c_{\text{water}} + 2819$  derived from data of Yamashita et al. (1997),

<sup>3)</sup> temperature oscillation of  $\pm 25^\circ\text{C}$  during the experiment,

**Table 3:** Molar absorption coefficients for OH and H<sub>2</sub>O combination bands for a variety of hydrous glasses.

Composition	SiO <sub>2</sub> (wt.%)	Range (wt.% H <sub>2</sub> O)	Baseline	$\epsilon_{\text{OH}}$ (l mol <sup>-1</sup> cm <sup>-1</sup> )	$\epsilon_{\text{H}_2\text{O}}$ (l mol <sup>-1</sup> cm <sup>-1</sup> )	$\epsilon^*_{\text{OH}}$ (l mol <sup>-1</sup> cm <sup>-2</sup> )	$\epsilon^*_{\text{H}_2\text{O}}$ (l mol <sup>-1</sup> cm <sup>-2</sup> )	Source of data
Dacite	65.19	1.5-5.9	GG	1.12(3)	1.14(3)	252(11)	188(8)	this study
			GG <sub>par</sub>	1.07(7)	1.21(10)	239(22)	198(15)	
			TT	0.97(4)	1.11(5)	175(14)	188(15)	
			TT <sub>par</sub>	0.96(6)	1.13(9)	185(21)	179(16)	
Andesite	56.80	1.9-6.3	GG	0.82(5)	1.01(7)	216(11)	153(8)	this study
			GG <sub>par</sub>	0.85(8)	0.96(10)	203(21)	168(15)	
			TT	0.68(2)	0.86(3)	135(8)	148(9)	
			TT <sub>par</sub>	0.70(4)	0.83(7)	145(16)	140(12)	
Basalt	49.64	1.6-6.3	GG	0.66(2)	0.65(2)	154(3)	143(3)	this study
			GG <sub>par</sub>	0.62(6)	0.71(8)	163(17)	135(15)	
			TT	0.56(5)	0.56(5)	123(26)	116(24)	
			TT <sub>par</sub>	0.52(6)	0.61(8)	121(27)	117(23)	
Rhyolite	77.04	1.0-6.2	GG	1.52(8)	1.72(6)	310(17)	257(10)	Withers and Behrens (2000)
			TT	1.41(7)	1.66(5)	246(14)	238(8)	
			FC	1.48(8)	1.68(5)	271(16)	246(9)	
Rhyolite	77.58	0.1-1.8	FC	1.73(2)	1.61(5)	341(25)	248(24)	Newman et al. (1986)
Rhyolite	unknown	unknown	FC	1.50(5)	1.86(5)	-	-	Ihinger et al. (1994)
Dacite	65.42	1.4-3.0	Two gaussians	0.94(6)	1.6(3)	-	-	Yamashita et al. (1997)
Islandite	54.55	1.2-8.7	devol.glass	0.95(10)	1.25(5)	230(25)	190(15)	Jakobsson (1997)
High-Al basalt/ tholeiite basalt	51.84	1.1-3.7	Two gaussians	0.85(7)	0.84(6)	-	-	Yamashita et al. (1997)
	53.59							
MORB basalt	50.72	0.4-2.5	Five gaussians	0.67(3)	0.62(7)	-	-	Dixon et al. (1995)

Notes:

Error in the last decimal is given in parenthesis

For explanation of GG, TT, FC see text.

GG<sub>par</sub> and TT<sub>par</sub> are fitted with a constant  $\epsilon_{\text{H}_2\text{O}}/\epsilon_{\text{OH}}$  ratio (for details see text)

Devol.glass: the baseline consists of a spectrum of a devolatilized glass

**Table 4:** Parameters to calculate the molar absorption coefficients for glasses with rhyolitic to basaltic compositions

	<b>a</b>	<b>b</b>	<b>r<sup>2</sup></b>
$\epsilon_{\text{OH}} \text{GG}_{\text{par}}$	0.00	0.000255	0.999
$\epsilon_{\text{H}_2\text{O}} \text{GG}_{\text{par}}$	0.00	0.000290	0.998
$\epsilon^*_{\text{OH}} \text{GG}_{\text{par}}$	63	0.0417	0.998
$\epsilon^*_{\text{H}_2\text{O}} \text{GG}_{\text{par}}$	52	0.0346	0.998
$\epsilon_{\text{OH}} \text{TT}_{\text{par}}$	-0.13	0.000257	0.999
$\epsilon_{\text{H}_2\text{O}} \text{TT}_{\text{par}}$	-0.15	0.000304	0.999
$\epsilon^*_{\text{OH}} \text{TT}_{\text{par}}$	29	0.0366	0.999
$\epsilon^*_{\text{H}_2\text{O}} \text{TT}_{\text{par}}$	28	0.0354	0.999

Absorption coefficients can be calculated by  $\epsilon = a + b x^2$  with  $x = \text{wt.}\% \text{SiO}_2$ .  $\epsilon$  values are given in  $\text{l mol}^{-1} \text{cm}^{-1}$  and  $\epsilon^*$  values in  $\text{l mol}^{-1} \text{cm}^{-2}$ ;  $r^2$  is the coefficient of determination and characterizes the goodness of fit.



**Table 5:** Experimental conditions.

sample	P [MPa]	T [°C]	t [h]	x <sub>H2O</sub> before	x <sub>H2O</sub> after	comments
DC 95	500	1250	120	0.685	0.054 ±0.045	-
DC 101	500	1250	137	0.720	0.179 ±0.045	bubbles
DC 102	500	1250	137	0.807	0.415 ±0.033	bubbles
DC 103	500	1250	137	0.863	0.645 ±0.026	bubbles
DC 104	500	1250	137	1.000	1.000 ±0.026	?
DC 84	200	1200	47.4	1.000	1.000 ±0.022	
DC 199	200	1250	114.6	0.000	0.033 ±0.038	
DC 198	200	1250	114.6	0.330	0.053 ±0.037	
DC 135	200	1250	68	0.434	0.231 ±0.082	
DC 197	200	1250	114.6	0.626	0.217 ±0.032	
DC 133	200	1250	68	0.738	0.713 ±0.023	
DC 196	200	1250	114.6	0.810	0.580 ±0.024	
DC 195	200	1250	114.6	0.910	0.825 ±0.021	
DC 88	100	1200	52.4	1.000	1.000 ±0.022	
DC 156	100	1250	95.3	0.164	0.155 ±0.035	x <sub>H2O</sub> after by GC
DC 155	100	1250	95.3	0.239	- -	
DC 130	100	1250	72	0.561	0.513 ±0.026	small crystals
DC 154	100	1250	95.3	0.610	0.434 ±0.029	-
DC 129	100	1250	72	0.726	0.692 ±0.024	small crystals
DC 153	100	1250	95.3	0.868	0.788 ±0.022	-
DC 152	100	1250	95.3	1.000	- -	-

Notes: Error on temperature (variation along the capsules): less than 20°C

Error on pressure ±5 MPa

GC = gas chromatography

**Table 6:** Results from water and CO<sub>2</sub> solubility experiments

Sample	P [MPa]	T [°C]	c <sub>water</sub> (KFT) [wt%] in Ar	c <sub>water</sub> (KFT) [wt%] in dried air	c <sub>water</sub> (NIR) [wt%]	c <sub>OH</sub> (NIR) [wt%]	c <sub>H<sub>2</sub>O</sub> (NIR) [wt%]	CO <sub>2,total</sub> (SIMS) [ppm]	CO <sub>2,mol</sub> Blank [ppm]
DC 95	500	1250	*1.46 ±0.07		1.44 ±0.08	1.01 ±0.05	0.42 ±0.03	2920 ±436 2859 ±427	237
DC 101	500	1250	3.36 ±0.08		3.34 ±0.08	1.69 ±0.05	1.65 ±0.04	2949 ±445 2949 ±445	146
DC 102	500	1250	5.18 ±0.09		5.13 ±0.10	1.97 ±0.05	3.17 ±0.05	2557 ±391 2596 ±397	38
DC 103	500	1250	6.69 ±0.10		6.69 ±0.11	2.05 ±0.05	4.64 ±0.06	2119 ±335 2124 ±335	9
DC 104	500	1250	10.57 ±0.11		-	-	-	-	-
DC 84	200	1200	*5.73 ±0.11		5.51 ±0.09	1.92 ±0.04	3.58 ±0.05	-	-
DC 199	200	1250	*0.44 ±0.08		0.55 ±0.07	0.49 ±0.04	0.06 ±0.03	1317 ±136 1319 ±136	176
DC 198	200	1250	*0.89 ±0.08		0.88 ±0.07	0.70 ±0.04	0.18 ±0.03	1346 ±139 1312 ±136	109
DC 135	200	1250	-		-	-	-	-	-
DC 197	200	1250	*1.94 ±0.07	1.83 ±0.08	1.93 ±0.07	1.17 ±0.04	0.76 ±0.03	1408 ±147 1344 ±141	56
DC 133	200	1250	-		-	-	-	-	-
DC 196	200	1250	*3.50 ±0.07	3.53 ±0.07	3.63 ±0.08	1.64 ±0.05	1.99 ±0.04	943 ±101 945 ±101	18
DC 195	200	1250	*4.70 ±0.08	4.71 ±0.08	4.76 ±0.09	1.73 ±0.05	3.03 ±0.04	568 ±61 564 ±61	7
DC 88	100	1200	3.79 ±0.13		-	-	-	-	-
DC 156	100	1250	*1.08 ±0.16		1.32 ±0.10	1.05 ±0.06	0.27 ±0.04	795 ±66	55
DC 155	100	1250	*1.33 ±0.12		1.63 ±0.10	1.19 ±0.06	0.45 ±0.04	698 ±58 709 ±59	43
DC 130	100	1250	-		-	-	-	-	-
DC 154	100	1250	*1.91 ±0.08		1.92 ±0.11	1.26 ±0.06	0.67 ±0.04	669 ±56	32
DC 129	100	1250	-		-	-	-	-	-
DC 153	100	1250	*3.01 ±0.08		2.99 ±0.11	1.59 ±0.06	1.40 ±0.05	456 ±39	7
DC 152	100	1250	*3.53 ±0.11		3.49 ±0.11	1.66 ±0.07	1.83 ±0.05	320 ±28	2

\*These water contents measured by KFT were used for NIR calibration.

When two points were measured with SIMS, both data are given in this table.

Error on CO<sub>2,mol</sub>: ±15%

**Table 7:** Fit parameters of Equation (2.5)

	<b>a</b>	<b>b</b>	<b>c</b>
$\alpha_i$	2.3946	-1.9846	1.2430
$\beta_i$	1.8831e-4	7.1235e-3	0.0147
$\gamma_i$	-1.9320e-5	1.4608e-5	-3.6775e-6

**Table 8:** Fit parameters of Equation (2.15), first model.

$K_1$	$7 \cdot 10^{-8}$	$\pm 3 \cdot 10^{-8}$
$K_2$	10500	$\pm 3800$
$x_{O_2,begin}^{melt}$	0.0012	$\pm 0.0005$

**Table 9:** Fit parameters of Equation (2.19), second model.

$P_0$	0 MPa	
$T$	1250 °C	
$K'_1$	$4.5 \cdot 10^{-7}$	$\pm 0.5 \cdot 10^{-7}$
$K'_2$	13	$\pm 3$
$\bar{V}_{CO_2,mol}^m$	46.6 cm <sup>3</sup> /mol	$\pm 2.1$ cm <sup>3</sup> /mol

**Table 10:** Fit parameters of Equation (2.22), third model.

$P_0$	0 MPa	
$T$	1250 °C	
$K_2$	0.21	(Nowak et al., 2003)
$K''_1$	$5.6 \cdot 10^{-7}$	$\pm 0.4 \cdot 10^{-7}$
$k$	5.3	$\pm 0.6$
$\bar{V}_{CO_2,mol}^m$	45.7 cm <sup>3</sup> /mol	$\pm 2.1$ cm <sup>3</sup> /mol

**Table 11:** Experimental conditions and results from water solubility experiments.

Sample		P [MPa]	T [°C]	t [h]	C <sub>water</sub> (KFT) [wt%]		C <sub>water</sub> (NIR) [wt%]		X <sub>H2O</sub>	comments
IGL	90	50	1200	36	2.05	±0.11	-	-	1.000 ±0.030	-
GMS	91	50	1200	36	2.40	±0.08	-	-	1.000 ±0.030	-
DC	92	50	1200	36	2.40	±0.07	-	-	1.000 ±0.030	-
PU	93	50	1200	36	2.44	±0.09	-	-	1.000 ±0.030	-
B1*	28	50	1200	15	1.66	±0.14	-	-	1.000 ±0.030	-
IGL	86	100	1200	52	3.61	±0.10	-	-	1.000 ±0.030	-
GMS	87	100	1200	52	3.73	±0.07	-	-	1.000 ±0.030	-
DC	88	100	1200	52	3.79	±0.07	-	-	1.000 ±0.030	-
B1*	24	100	1200	20	3.35	±0.16	-	-	1.000 ±0.030	-
GMS	126	100	1250	115	-	-	2.01	±0.21	0.416 ±0.039	-
GMS	125	100	1250	115	-	-	2.39	±0.20	0.502 ±0.036	-
GMS	123	100	1250	115	-	-	3.15	±0.20	0.795 ±0.023	-
GMS	122	100	1250	115	-	-	3.53	±0.20	1.000 ±0.026	-
DC	24b	200	1000	72	5.79	±0.11	-	-	1.000 ±0.030	crystals
EGL	25	200	1000	72	5.99	±0.20	-	-	1.000 ±0.030	crystals
GMS	26	200	1000	72	5.83	±0.15	-	-	1.000 ±0.030	crystals
EDF	27	200	1000	72	5.57	±0.70	-	-	1.000 ±0.030	crystals
IGL	28	200	1000	72	5.57	±0.16	-	-	1.000 ±0.030	crystals
GMS	83	200	1200	47	5.37	±0.08	-	-	1.000 ±0.030	-
DC	84	200	1200	47	5.73	±0.08	-	-	1.000 ±0.030	-
PU	85	200	1200	47	5.31	±0.08	-	-	1.000 ±0.030	-
B1*	23	200	1200	24	4.83	±0.09	-	-	1.000 ±0.030	-
GMS	141	200	1250	92	-	-	1.59	±0.26	0.159 ±0.055	-
GMS	140	200	1250	92	-	-	2.66	±0.21	0.342 ±0.035	-
GMS	119	200	1250	334	2.83	±0.07	2.77	±0.22	0.429 ±0.033	-
GMS	139	200	1250	92	-	-	3.32	±0.20	0.514 ±0.035	-
GMS	120	200	1250	334	3.94	±0.07	-	-	0.683 ±0.024	-
GMS	138	200	1250	92	-	-	4.22	±0.20	0.728 ±0.025	-
GMS	137	200	1250	92	-	-	5.22	±0.20	1.000 ±0.035	-
GMS	111	500	1250	145	2.14	±0.06	2.13	±0.23	0.114 ±0.045	-
GMS	113	500	1250	168	3.15	±0.07	-	-	0.230 ±0.052	-
GMS	114	500	1250	168	5.00	±0.09	4.92	±0.21	0.429 ±0.048	-
GMS	115	500	1250	168	6.97	±0.11	-	-	0.678 ±0.025	-
GMS	116	500	1250	168	10.44	±0.13	9.19	±0.21	1.000 ±0.044	-

Notes:

\* Solubility experiments in the basaltic composition (B1) were performed by Berndt (2002).

Error on temperature (variation along the capsules): less than 20°C

Error on pressure ± 5 MPa

## LEBENS LAUF

### Personalien

---

Name	Susanne Ohlhorst
Anschrift	Bennostr. 3 30451 Hannover
Email	Susanne.Ohlhorst@gmx.de
Geburtstag	15.04.1971
Geburtsort	Braunschweig
Familienstand	ledig

### Schulischer Werdegang

---

1977 - 1981	Grundschule Braunschweig
1981 - 1983	Orientierungsstufe Braunschweig
1983 - 1990	Gymnasium Braunschweig, Abschluss Abitur

### Wissenschaftlicher Werdegang

---

10/90 - 06/97	Studium der Mineralogie an der Universität Hannover Erlangung des Grades einer Diplom - Mineralogin  Thema der Diplomarbeit: <i>„Synthese und Charakterisierung von eisenhaltigem Anorthit“</i>
07/97 - 03/01	Wissenschaftliche Mitarbeiterin am Institut für Mineralogie, Universität Hannover im Rahmen des Internationalen Kontinentalen Tiefbohr Programms ICDP (Projekt Ho 1337/3-1) der Deutschen Forschungsgemeinschaft
07/97 - 06/02	Promotion am Institut für Mineralogie, Universität Hannover